NONLINEAR MODELING OF FLEXIBILITY EFFECTS IN MANIPULATOR DESIGN

By

GANAPATHY NAGANATHAN

Bachelor of Engineering (Honours)
University of Madras
Madras, India
1978

Master of Science
Clarkson University
Potsdam, New York, U.S.A.
1981

Submitted to the Faculty of the
Graduate College of the
Oklahoma State University
in partial fulfillment of
the requirements for
the Degree of
DOCTOR OF PHILOSOPHY
December, 1986

To my dear Parents

Kamalam & Ganapathy Sastri

NONLINEAR MODELING OF FLEXIBILITY

EFFECTS IN MANIPULATOR DESIGN

Thesis Approved:

[illegible]

Thesis Advisor

Richard L. Lowery

[illegible]

Donald W. Grace

Norman N. Durham

Dean of the Graduate College

ACKNOWLEDGEMENTS

I take this opportunity to express my most sincere thanks to my thesis adviser, Dr. A.H. Soni for his excellent guidance, encouragement, and friendship throughout my stay at Oklahoma State University. It is a privilege to have been associated with him as a member of his team. I want to thank the other members of my committee, Dr. R.L. Lowery, Dr. L. Zirkle, and Dr. D. Grace for their most valuable input during the course of this study. Their thorough criticisms have greatly helped to enhance the scope of this study. My sincere appreciation to Dr. Lowery who has been most kind to spend much time in helping me with the experimental aspects of this study. Dr. V. Srinivasan of IBM Thomas Watson Research Center, has greatly contributed to the success of this study. I thank him for his dear friendship and support. My colleagues at OSU have provided a tremendous source of support and inspiration for me -- Dev, Ram & Vani, Saeed, Gary, Jim, Amir, Fu, Mohan, Dr. Tsai, Dr. Ting, Jay, Dan, and many others. I am thankful to them for their friendship and their contribution.

Special gratitude is expressed to my parents, brothers, and sisters for their warm affection, encouragement, and support over the years. My wife Kasturi deserves a special recognition for being most patient and caring and helping me in every way possible.

The financial support provided by the National Science Foundation via Grant MEA83-08395 and the National Institutes of Health via Grant AM # 27855 are gratefully acknowledged.

TABLE OF CONTENTS

Chapter		Page

LIST OF TABLES

LIST OF FIGURES

Figure Page

Figure Page

CHAPTER I

INTRODUCTION

Flexible automation has for many years provided an attractive alternative to fixed automation. However, the state-of-the-art in manipulator technology severely restricts its implementation in complex tasks. This restriction is either due to the inadequacy of the manipulator to meet the requirements of a complex task (as in a miniature assembly or an environment wherein random disturbances are possible) or the manipulator being capable of providing the required level of sophistication at very low speeds only. The latter in particular, is in direct conflict with the motivation for the increased implementation of these manipulators in industries.

With the need for higher productivity in industries, the operating speeds of these manipulators are being continually upgraded. In such a situation, other issues relating to the manipulator's performance described in terms of end-effector precision, repeatability, accuracy, payload, control, etc., come under close scrutiny. However, the concept that regulates all these issues is the manipulator's dynamics. Under low operating speeds, the manipulators can be treated as multi-rigid body systems. On the other hand, the assumption of rigidity may not be quite appropriate when the operating speeds are increased. At higher speeds, the deflections and bearing loads are dynamically amplified. These problems are currently being tackled either by settling for a conservatively-rigid design or by 'stiffening' the system by a closed-loop, feed-back control system. Both of these methods have their drawbacks in that the former results in a very bulky design. Very often, this is the factor that limits the response of the system due to increased inertia effects. However sophisticated the control system may be, the physical inertia of the components may allow little or no improvement in the response time of the system. Further, the effect of inertia increases the nonlinearity of the response. The latter approach of 'pseudo-stiffening' by feedback correction has the inherent drawback of increased computational time and prolonged transient behavior. Hence, there is a strong need to design manipulators with reduced inertia effects (light-weight manipulators). This in turn would lead to a parallel concern for the effects of link and joint flexibilities in the system, particularly at higher operating speeds. Therefore, more accurate and efficient analytical methods must be developed to predict the effects of the distributed mass and elasticity on the dynamic positioning characteristics of the manipulators. Sophisticated control systems may then be devised to improve the manipulator's performance. Prompted by functional incentives (both technical and economic), investigators over the last decade have increasingly shifted their attention to systems that include flexible components.

Literature Survey

Investigations on manipulator dynamics belong to the classical branch of multibody dynamics. The last two decades have seen significant strides in these analyses due to the availability of superior computing power. The existing literature relating to multibody dynamics in engineering has emerged mainly from two fields - simulation of spacecraft with flexible appendages and analysis of planar and spatial mechanisms in machinery design. The knowledge derived from these fields has been successfully applied in the area of manipulators. This literature can be classified into two categories--modeling of gross spatial motions of rigid body systems and structural behavior of general flexible systems with spatial motion. A brief review of this literature follows:

Spacecraft Simulation

Since the early sixties, considerable attention has been paid to the studies on the simulation of spacecraft. With the increasing sophistication of spacecraft technology, more computationally efficient schemes for the simulation of complex spacecraft have been developed. Hooker and Margulies [40] and Roberson and Wittenberg [80] developed the augmented body method to analyze a system of rigid bodies in a topological chain. They observed that certain inertia-like terms appear in combination, in the individual equations of motion of each of the rigid bodies in the set. These combinations admit of physical interpretations as the inertia dyadics of abstractions called 'augmented bodies'. In this, the i^{th} augmented body consists of the i^{th} body of the set together with all masses attached to each of the joints of that body. If there are 'r' number of constraint equations for this set, then the final system of equations is a set of '6n+r' first order differential equations. These studies were followed by Velman [101] and Russell [81], who adopted the 'nested body methods' wherein subsets of rigid bodies (nested bodies) in a n-body system of bodies were analyzed. Though the Newton-Euler approach was used, the formulation eliminated the constraint torques from the final set of equations. Kane and Wang [53] introduced the generalized force method which is under the framework of Lagrangian equations. Kane's equations have the advantage of automatically eliminating the 'non-working' internal constraint forces, without the introduction of tedious, often unwieldy, differentiation of scalar energy functions and other similar calculations. Euler parameters were used to define the system orientation. They provided for the computational efficiencies and for the avoidance of analytical singularities which are sometimes encountered with Euler angles. The use of generalized speeds also decouples the equations involving the joint force and moment components. Further, Kane's method is applicable to some nonholonomic systems also. Likins et al.[55] developed the hybrid-coordinate method. The earlier developments analyzed a multibody system wherein flexible bodies were attached to a central rigid body. In the hybrid-coordinate method, separate coordinates were used to describe the large, rigid body motions and small (linearly) elastic deformations. This technique has been extended to a description of large flexible motion of a system of arbitrary number of hinge connected rigid bodies.

Planar and Spatial Mechanisms

There has been a contemporary development of literature in multibody dynamics in the field of mechanisms and machinery design. Significant amount of work has been done on the dynamic modeling of rigid planar and spatial closed-loop kinematic chains. Flexible planar linkages have also been analyzed in detail. A wide variety of mathematical tools were used in the investigations such as matrix methods, vector approach, screw calculus, dual vectors, etc. Sheth and Uicker [86] used the matrix approach to analyze multiloop, spatial mechanisms with multiple degrees of freedom. Chace [21] developed a vector technique to analyze three dimensional kinematic chains. Soni [89], Freudenstein [113], and others have promoted the screw calculus based approach while Yang [114] used a dual number approach.

Further to analyzing these rigid systems, flexible planar systems have also been extensively studied. The basic methodology has been to freeze the mechanism at each position and analyze the resulting instantaneous structure. Finite element based schemes using beam like elements have been developed. Bahgat and Willmert [8] used a line geometry and hermite polynomials, to analyze the vibratory behavior of flexible planar mechanisms. Variable length finite elements were introduced for the first time to model links with moving sliders. Naganathan and Willmert [67] developed special finite elements to quasi-statically analyze planar chains. More recently, Dado and Soni [24] have presented comprehensive forward and inverse analysis methodologies for planar elastic linkages.

The literature addressing elastic, closed-loop kinematic chains, executing spatial motion are comparatively limited. Winfrey [112] used simple beam elements along with a 4 X 4 matrix approach to analyze flexible Bennett mechanism. Spatial chains with single closed-loops have also been analyzed by Maatuk [57] and Sunada [93,94]. Bagci, et al.[7] used a matrix displacement, direct element method to analyze simple, spatial mechanisms with straight links. Some of the above schemes are capable of analyzing open-loop (serial) spatial manipulators also. The literature involving the dynamics of manipulators are discussed in detail in the following section.

Manipulator Dynamics

The configurations of the commercially available robotic manipulators can be classified into two categories as open-loop chains (serial configurations) and mixed-loop chains (parallel configurations), as shown in figure 1. In the former, the links of the manipulator are arranged in an open chain form, while in the latter, closed-loop kinematic chains (usually parallelogram chains) are added to the open-loop configurations. The adjacent links of the manipulators are normally connected by single degree of freedom kinematic pairs. These joints can be either revolute or prismatic, and are actuated by electric, or hydraulic motors. In order to control the motion of the manipulators, the required values of forces/torques at these actuators must be computed repetitively, for a prescribed set of joint motions. This sampling rate is usually of the order of 60 Hertz or more. Therefore, efficient mathematical representation of manipulator dynamics is essential for the real time control of manipulator systems. For the purpose of dynamic modeling, the links of the manipulators are usually assumed to be rigid, while some of the formulations accommodate flexibility in the links.

The existing literature in manipulator dynamics deals almost exclusively with the open-loop chains. The problem in manipulator dynamics is classified into two kinds. The first problem is the 'inverse dynamics problem' wherein the

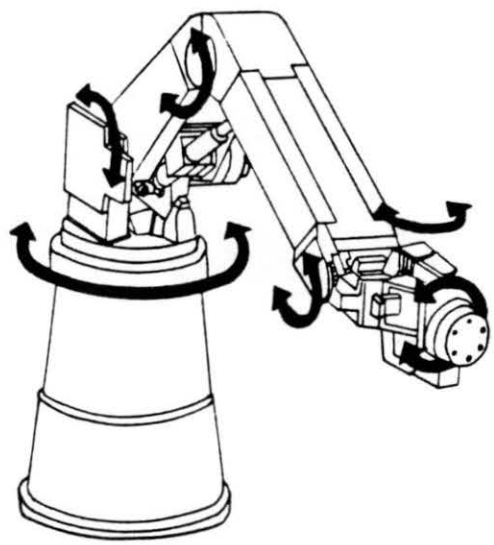

a) Open-Loop (Serial) Manipulator

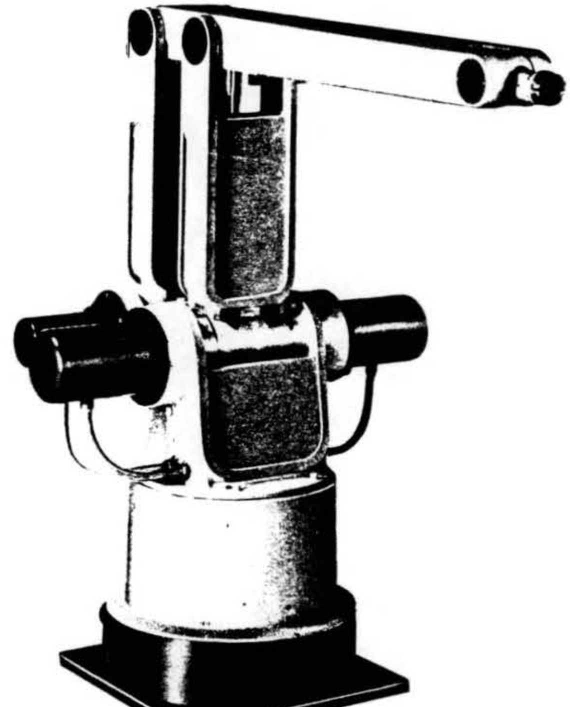

b) Mixed-Loop (Parallel) Manipulator

Figure 1. Manipulator Configurations

motion at the joints are known and we are interested in computing the required actuator forces or torques. This is normally the case while the manipulator is controlled, to execute a predetermined motion. The second problem is commonly referred to as the 'forward dynamics problem'. In this case, the actuator forces are known, and we would like to determine the joint kinematics (displacements, velocities, and accelerations of the joints). This situation may arise during such applications as simulation studies. The various dynamic formulations relevant to manipulator dynamics may be classified as below:

* Tabular reference or memory schemes
* Lagrangian formulations
* Newton-Euler formulations
* Kane's method of generalized speeds
* Dynamic formulations including system flexibilities.

In the following sections each of the above formulations is briefly reviewed.

<u>Tabular Reference/Memory Schemes</u>. Tabular references were initially sought after as possible solutions for real time computation of manipulator dynamics. Albus [2,3] indexed his table as a function of the n-dimensional vectors of displacements, velocities and accelerations. The actuator forces were derived by interpolating the contents of the table for given values of joint motion parameters. Raibert [78] eliminated the acceleration dimension, by storing position and velocity dependent terms in the memory.

This scheme was further revised by Horn and Raibert [43]. They proposed the 'Configuration Space Method' with a reformulation of the Lagrangian equation. The control forces/torques were written as a function of the gravity compensation terms, inertial terms, and coriolis coefficients. For manipulators with less than 9 joints, this formulation has been found to be more efficient than the recursive Newton-Euler scheme of Luh, et al.[56] Despite the saving in computational burden, the tabular methods have the disadvantage of requiring a large memory size for a fine enough search along the various dimensions of the table. Further, the table entries are valid only for a particular end-effector loading condition.

Lagrangian Formulations. Lagrangian formulation has long been recognized as a very powerful dynamic analysis tool. The basic advantage of this formulation is the automatic elimination of internal joint reaction forces. For a prescribed set of joint motions, this method directly yields the desired set of joint actuator forces. Bejczy, et al.[12,13] derived these forces as a function of 'Dynamic Projection Functions'. Some of these terms are functions of partial derivatives of the elements of the transformation matrix with respect to the generalized coordinates. The presence of these numerical differentiations was the main hurdle to the computational efficiency on digital computers. Several reformulations have been proposed since, aiming at improving the computational efficiency of the Lagrangian based schemes.

Mahil [58,59] proposed an application of the Lagrangian approach to an open-loop manipulator with single degree of freedom revolute joints. Generalized Inertia Matrices which depend on the instantaneous configurations of the manipulator were developed. Several theorems have been derived which replace the numerical differentiation of the Generalized Inertia Matrix by a series of vector operations. However, no numerical evaluation of the computational efficiency has been cited. One of the earlier Lagrangian formulations of manipulator dynamics was by Kahn.[50] The number of multiplications and additions had a n^4 dependency, where, 'n' is the number of joints of the manipulator. Bejczy and Paul [13] observed that at low speeds, the coriolis and the centrifugal terms in equation (1.1), do not contribute significantly to the manipulator dynamics and they could be ignored in order to improve the computational efficiency of the algorithm. However, Raibert [78] pointed out that these terms were quite dominant at higher speeds. Errors due to ignoring these terms were found to exceed the limits of feedback correction.

Recursive schemes have since been proposed to take advantage of the serial configurations of the industrial manipulators. In the forward recursive scheme, the analysis proceeds from the end-effector of the manipulator to the base of the manipulator. In backward recursion, the analysis proceeds from the base to the end-effector. Waters

[110] observed that an n^2 dependency can be achieved for the arithmetic operations by adopting a backward recursion while evaluating the manipulator kinematics. Hollerbach [37] achieved a linear dependency by adopting a forward recursion to determine the generalized forces. He further improved the efficiency of the algorithm by preferring 3 X 3 rotation matrices instead of the 4 X 4 homogeneous transformations. An improvement of more than 50% was observed in terms of the number of arithmetic operations. The number of arithmetic operations required for the various schemes has been tabulated by Hollerbach [37], and Cvetkovic and Vukobratovic [23]. Wang and Kohli [109] have proposed an alternate Lagrangian formulation starting from Silver's [87] form of the Lagrangian equations. This method is shown to be as efficient as the most efficient Newton-Euler scheme of Luh, et al.[56]. Thomas and Tesar [97] have developed a quasi-rigid link model of an open-loop manipulator using dynamic influence coefficients. The arm's dynamic properties were modeled by their effective values at the actuators. The influence coefficients necessary for the analysis were presented in a simple tabular form.

Newton-Euler Formulations. Apart from the studies cited under spacecraft simulation, the Newton-Euler scheme has gained popularity for applications in the real time evaluation of manipulator dynamics. Vukobratovic, et al. [102-105] used the kinetostatic approach to determine the dynamics of articulated chains that include locomotion mechanisms. The generalized forces were expressed in the base frame (inertial frame). This approach yielded a set of n-dimensional algebraic equations relating joint actuator forces and joint kinematics. Orin, et al.[69] suggested that the computational efficiency may be improved by referring the forces and torques to the local coordinate systems. Luh, Walker, and Paul [56] have proposed a backward recursive scheme to determine the system kinematics and a forward recursion to determine the actuator forces. This method has been observed to be the most computationally efficient scheme in terms of the number of arithmetic operations. In this formulation, the linear and angular velocities of the links were also represented in the local link coordinates. An accelerated algorithm based on the Newton-Euler scheme has been proposed by Cvetkovic and Vukobratovic [23]. Walker and Orin [108] solved the forward dynamics problem using a Newton-Euler approach. Featherstone [31] utilized the concept of 'articulated body inertias' in solving the forward problem for an open-loop manipulator with a spherical wrist. This algorithm was found to be more efficient than that of Walker and Orin, when the number of joints was less than or equal to 12.

Pennock and Yang [75] presented an analytical technique based on screw-calculus and dual number matrices. The formulation aims at deriving closed-form expressions for joint forces and torques. The technique is demonstrated for the case of open-loop three degree of freedom chains. Use of the algebraic manipulation program (REDUCE) has been suggested for manipulators with general configurations. Silver [87] pointed out that both Newton-Euler and Lagrangian schemes have no fundamental difference in their computational efficiency. His work proved that with a proper choice of representation, the computational effort for both the schemes could be identical.

Horak [42] used both the Lagrangian and Newton-Euler techniques in improving the efficiency of the computation. The formulation is particularized to specific manipulator configurations wherein the positional and the orientational structures can be isolated. The equations were derived in closed-form using the Lagrangian approach for the position structure, and the Newton-Euler scheme for the orientational structure. The algorithm proved to be five times faster than the recursive Newton-Euler scheme. The efficiency was further doubled by using a second microprocessor in the computer architecture.

Kane's Method of Generalized Forces. Huston, et al. [45-48] utilize Kane's dynamical equations to derive the governing equations. Kane's dynamical equations have the advantage of automatically eliminating the 'non-working' internal constraint forces, but without the introduction of tedious, often unwieldy differentiation of scalar energy functions. Each of the bodies was considered to be connected to the adjacent body through a spheric pair and Euler parameters were adopted to define the relative orientations of adjacent members. Kane and Levinson [51] choose to promote the discipline of formulations particularized to the system that is being analyzed. The concept of Kane's generalized speeds is used in deriving coefficients of the system equations in an explicit form. It is shown that such a formulation is more efficient than the recursive Newton-Euler scheme.

Dynamics of Flexible Manipulators. The literature on dynamics of flexible manipulators is comparatively limited. Book, et al.[20] discussed feedback control schemes for a two-beam, two link planar open-loop systems. The links were assumed to be Euler-Bernoulli beams with distributed flexibility. A fixed-free type of an elastic deformation was assumed for each of the links. The dynamical equations were derived in an explicit form. Beazley [11] developed a method using transfer matrices for a quasi-static vibrational analysis of a slowly moving teleoperator. Maatuk [57] used beam-like links to analyze open-loop manipulators. A Lagrangian based scheme along with a normal mode synthesis technique was used to study the elastic deformations. The perturbed motion due to elasticity was considered small enough to admit Euler-Bernoulli beam theory. The equations of motion were derived for a particular three degrees of freedom open loop manipulator. The method was restricted to manipulators with rotational degrees of freedom only. Hopkins [41] presented a generalized finite element based scheme to investigate open chains with screw joints. However, the application of the method has not been demonstrated for practical configurations. Sunada [94,95] presented a method to investigate manipulators with links of complex geometry. The kinematics and dynamics of the manipulator were expressed using 4 X 4 transformation matrices. The distributed flexibility and mass properties of the links were obtained using the commercially available NASTRAN software, at each instantaneous position of the manipulator. Component mode synthesis procedure was applied to simplify the final set of equations for numerical integration. The method is restricted to robotic manipulators with revolute joints only. Huston and Kelly [46] used a modified form of Kane's equations to investigate flexible open loop chains. Bagci, et al.[6,7] proposed flexural line elements to estimate the end-effector position and orientation errors of planar and spatial manipulators. A case study of a robot with planar configuration was presented. Singh and Likins [88] developed a scheme to study a general, flexible open loop chain. The bodies of this open-loop chain were considered to be connected together by kinematic pairs which permit kinematic constraints, control, or relative motion with six degrees of freedom. Kane's method has been extended to include elastic bodies in the chain. Truckenbrodt [98,99] developed a scheme based on Hamilton's principle using hybrid coordinates to study moving flexible structures. The resulting nonlinear, differential equations were linearized with respect to a reference motion. The method was demonstrated for the case of a manipulator with one link only. Recently a modal control model has been proposed by Book [14] to simulate flexible open-loop manipulators with revolute joints.

Apart from the kinematic and link compliant effects, the compliance at the actuators have been known to influence the dynamic performance of a manipulator with servo-drives. The significance of these interactions have been cited in the previous works of various investigators. The basic methodology of modeling the actuator dynamics involves the identification of their inertia, stiffness, and damping parameters. Asada [5] has described in detail the design of a direct drive arm and the methodolgy to identify the design parameters of the control system, such as the position and velocity gains, servo stiffness, etc. Sunada and Dubowsky [94,95] used contant position and rate gains while modeling the interactions of the control system and the link flexibilities to augment the system equations. For the case of the indirect drive, Ahmad [1] has presented a comprehensive description of the second order, nonlinear kinematic effects associated with a typical actuator and the gear drives. Book, Majette, and Ma [18,19] presented a frequency domain analysis of the space shuttle arm and its payloads. Majette [60] discussed a modal state variable control model for a 2-arm planar manipulator with point compliances at the joints.

Existing literature reports very few experimental investigations on the performance of flexible manipulators. Good et al.[32] experimentally investigated the flexibility effects in the actuator linkages of an industrial manipulator and developed a 4 degree of freedom nonlinear model. Hastings and Book [33] have recently reported a linear state-space model for a single link flexible arm, together with experimental results on the performance of this arm.

From the above survey, it appears that much remains to be done in order to be able to predict and control the complete performance of a flexible manipulator. There is a strong need to develop a comprehensive model that would predict the performance of a flexible manipulator in the presence of all perturbive effects, namely kinematic effects, link compliance and joint compliance.

Significance of the Study

The modeling procedures for studies on flexible manipulator dynamics cited in the previous section have often evolved from research efforts in the areas of structural dynamics, spacecraft, and mechanisms. The usual procedure is to freeze the manipulator at a particular instant of time and apply basic principles of structural dynamics to this instantaneous structure. However, a manipulator is typically different either from a structure, or a spacecraft in that we command the different joints of the manipulator to undergo gross motions. These motions are mutually independent and are time dependent. This being the case, the natural question would be, to what extent does this typical nature influence its positioning characteristics? Further, the interactions between the gross motions and system flexibilities are expected to be nonlinear in nature. How does this nonlinear interaction affect the performance of the manipulator? Instead of making empirical judgements on these issues, a comprehensive analytical model is developed in this study to critically examine the nonlinear interactions of the system gross motions with the flexibilities present in the system.

While modeling manipulator links, most of the research efforts in the past have treated the manipulator links as slender beams. However, this assumption may not be quite valid when we consider commercially available industrial manipulators. It is desirable that the model is capable of handling a wider range of aspect ratios, particularly, higher values of aspect ratios that are more common among industrial manipulators. Further, the model is expected to effectively simulate the nonlinear coupling of the flexibility effects with the gross nonlinear motion of the manipulator links. Predicting the end-effector behavior under the influence of such dynamic effects has always been paralleled by a concern for the computational burden for such an analysis. With the above objectives in mind, a simple and efficient finite element will be developed for serial manipulators using Timoshenko beam theory.

A typical manipulator system may accommodate a variety of flexibilities in the form of distributed elasticity in the links, compliant joints, control system flexibilities, etc. This study will comprehensively model the interactions of the gross motions with the system deformations due to the distributed elasticity in the links of the manipulator. Procedures will also be identified to take into account simplistic representations of the effects of servo-compliances that may typically exist in the servo-drives of commercial actuators.

Statement of the Problem

The main objective of this study is to develop an analytical tool to critically examine the elasto-dynamic effects on the dynamic positioning characteristics of the manipulators. In particular, the study will highlight the nonlinear coupling between flexibilities in the links due to distributed elasticity and their gross nonlinear motions. Also, a simplistic representation of the control system effects will be used to augment the model. A dedicated finite element based scheme will be developed to study general serial manipulator configurations with revolute and prismatic pairs. The method will further eliminate any assumption of slenderness for the manipulator links. The manipulator configuration may consist of short (stunt) as well as long (slender) links. This is rendered possible using Timoshenko Beam Theory along with a reduced order integration, in the development of the finite element. Further, the developed methodology is applicable to systems with both revolute as well as prismatic pairs. The above problem will be solved in two phases:

(1) Development of a finite element model for planar, open-loop, revolute jointed configurations.

(2) Extension of the above model to spatial, open-loop manipulator configurations that include both revolute and prismatic pairs.

With the current emphasis in actuator designs directed at direct-drives, the inherent damping and friction in the drive mechanism is greatly diminished. Hence, the sources of link and control system flexibilities in the system are likely to influence the performance of the physical system at a more significant level. Studies such as the one presented in this work would be of great value in recognizing and evaluating those influences.

CHAPTER II

PLANAR MANIPULATORS

Introduction

In this chapter, the basic guidelines for the analysis of a general case of the revolute jointed planar manipulators will be formulated. Such a manipulator is shown in Figure 2. The model will allow for the complete interaction of elastic deformations and the commanded gross motions at the manipulator joints. The governing equations of motion will be derived including the effects of rotatory inertia, transverse shear, and the effects of the gross non-linear motion of each of the links. Further, the effects of joint servo-compliances will be taken into account, while predicting the tip errors for the end-effectors of the planar manipulators.

Problem Formulation

The methodology will consist of the following seven steps:

(1) Description of the configuration of the manipulator

(2) Derivation of the kinematic and kinetic relations for a typical differential segment on a manipulator link

(3) Use of Galerkin's technique to render the equations in

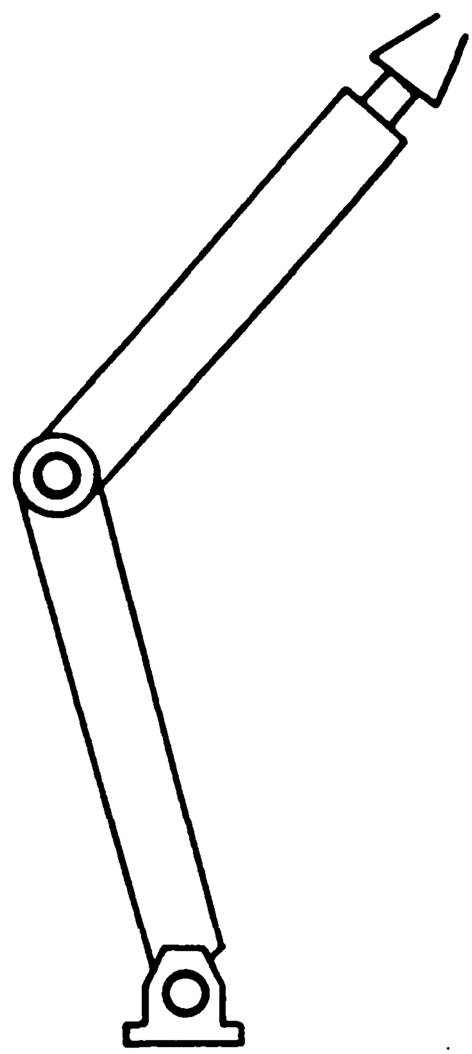

Figure 2. Planar Manipulator

an integral form suitable for a finite element scheme

(4) Development of a special finite element

(5) Derivation of system equations

(6) Augmentation of the system terms for joint servo-compliances, and

(7) Solution of the system equations.

Manipulator Description

Let $(X_bY_bZ_b)_0$ be a ground reference frame attached to the base of the planar manipulator as shown in Figure 3. The serial configuration may consist of any number of links (1,...,n) connected by revolute pairs. According to the notation used in this study, the $(i-1)^{th}$ link will be connected to the i^{th} link, by a revolute pair at joint 'i'. Two orthogonal frames of reference will be attached to each of the manipulator links as shown in Figure 3. For the i^{th} link, the frame $(X_bY_bZ_b)_i$ will be located at the proximal end of the link at joint 'i'. This will be referred to as the 'base reference' of the i^{th} link. Another frame of reference $(X_dY_dZ_d)_i$ will be located at the distal end of link 'i' at joint 'i+1'. This is the 'distal frame' of the i^{th} link. When the manipulator is in its undeformed state, the distal frame can be located by a pure translation of the base reference $(X_bY_bZ_b)_i$ along the length 'L_i' of the link. Also, the Z-axes of these frames will be chosen along a reference line on the link. The commanded motion at joint 'i' will be given by the angle 'ϕ_i'. This will be measured

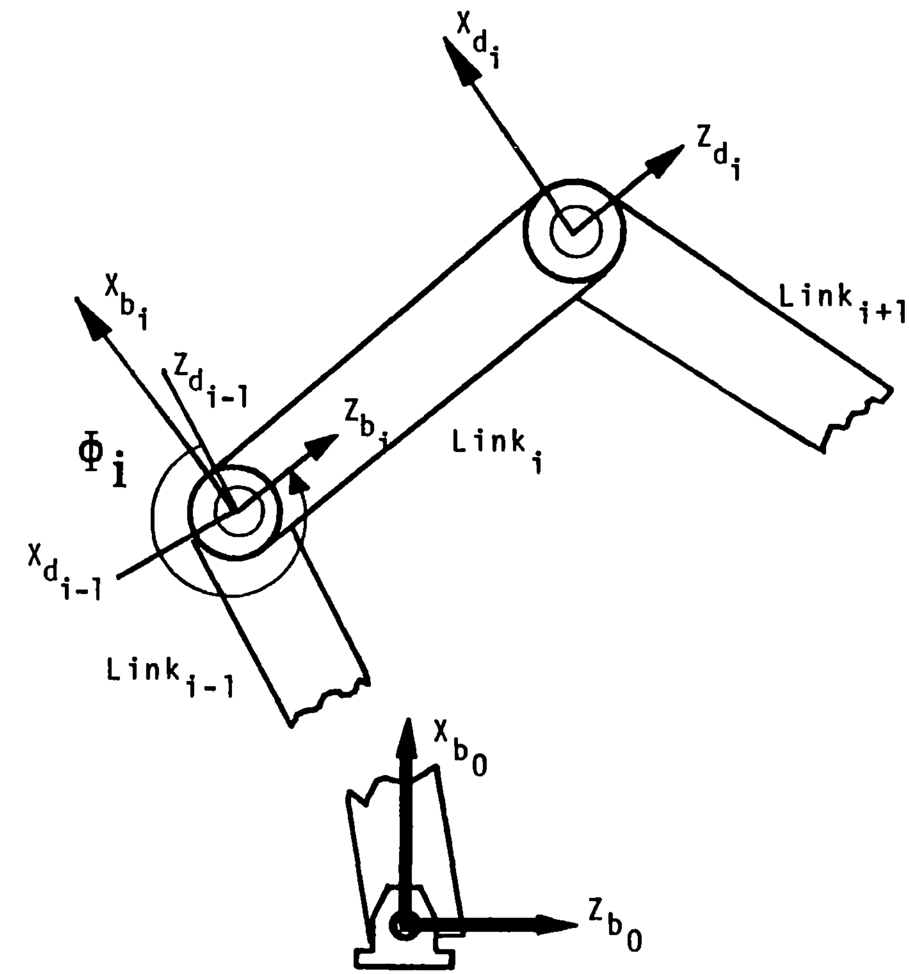

Figure 3. Planar Manipulator Description

in a counter-clockwise direction from $Z_{d_{i-1}}$ to Z_{b_i} about Y_b. The subscript 'i' will be omitted from now on, while referring to the i^{th} link parameters.

Kinematic and Kinetic Relations

The i^{th} link is shown in Figure 4, both in its undeformed state as well as in an exaggerated deformed state. The kinematic and kinetic relations will be derived by considering a differential segment on the i^{th} link, at a distance 's' from the origin of the base reference frame along the Z_b axis. The kinematic parameters of the differential segment will be identified by considering the relative motion of the differential segment with respect to the base reference frame of the link. Let 'xyz' be another frame of reference attached to the center of mass 'G' of a differential segment on the i^{th} link. The following variables will be used in deriving the required expressions.

ρ	Density of the material of the link
γ	Shear Modulus of the material
E	Young's Modulus of the material
A	Area of cross-section of the link
I_y	Area moment of inertia of the link cross-section
L	Length of the link
$\vec{k}_{x_b}, \vec{k}_{y_b}, \vec{k}_{z_b}$	Unit vectors of the base reference frame '$X_b Y_b Z_b$'
$\vec{k}_x, \vec{k}_y, \vec{k}_z$	Unit vectors of the differential segment

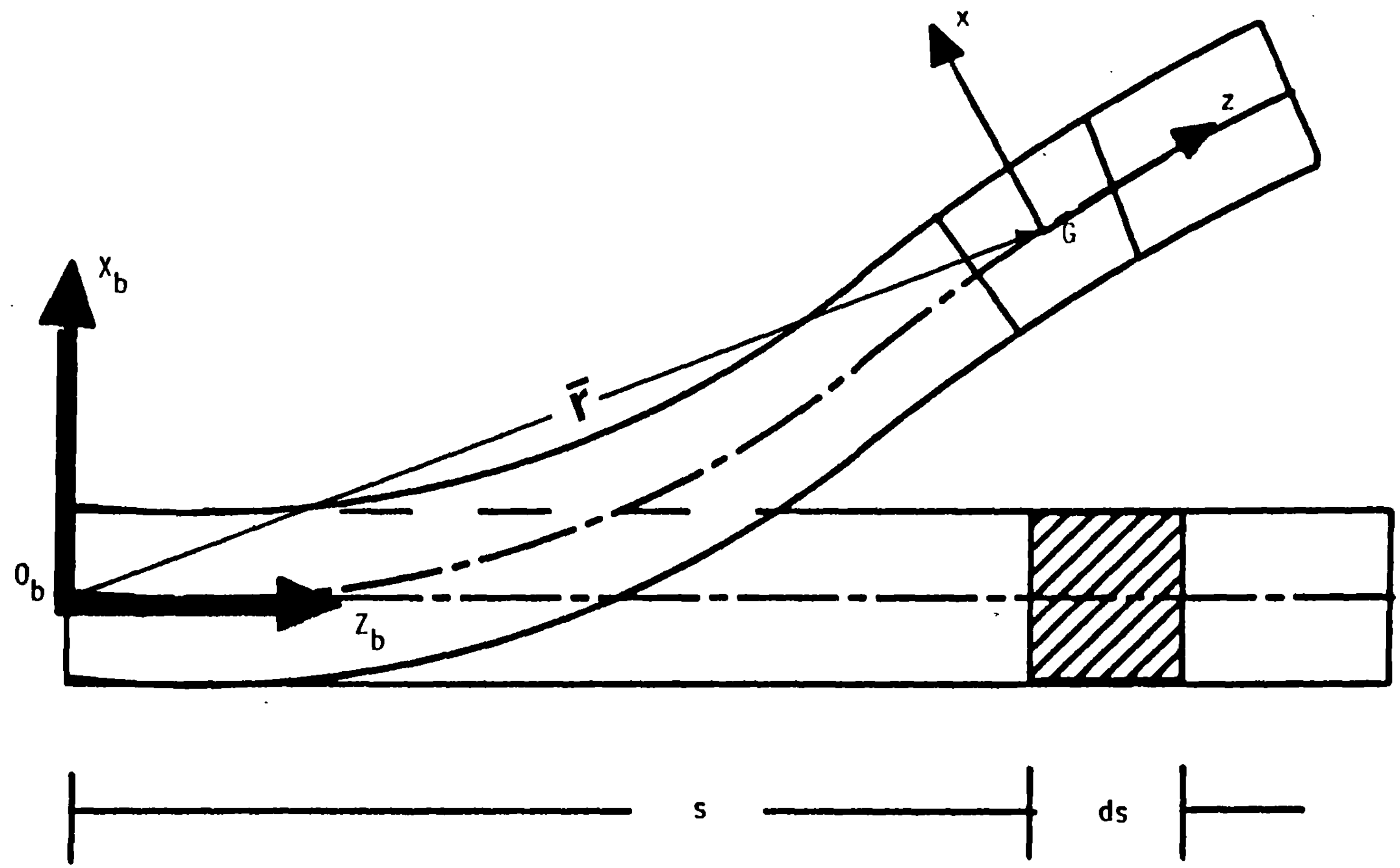

Figure 4. Typical Link of a Planar Manipulator

reference frame 'xyz'

u_x, u_z Deformational displacements of the differential segment along X_b and Z_b axes

θ_y Deformational rotation of the differential segment about 'y' axis with respect to the Z_b axis.

$\dot{\theta}_y$ Deformational angular velocity of the differential segment with respect to the base reference frame

$\ddot{\theta}_y$ Deformational angular acceleration of the differential segment with respect to the base reference frame.

ω_b Absolute angular velocity of the base reference frame.

α_b Absolute angular acceleration of the base reference frame.

ω_s Absolute angular velocity of the differential segment

α_s Absolute angular acceleration of the differential segment.

The Newton-Euler equations can be written for the differential segment as:

$$\vec{F} = dm\, \vec{a}_G \qquad \ldots \quad (2.1)$$

$$\vec{M}_G = \dot{\vec{H}}_G \qquad \ldots \quad (2.2)$$

where, $\vec{F}$ is the resultant force acting on the differential segment, $\vec{a}_G$ is the absolute acceleration of 'G', and $\vec{H}_G$ is the angular momentum of the differential segment about its center of mass. For the planar case, the latter has the simple form as:

$$\dot{\vec{H}}_G = \rho I_y \alpha_s \, ds \, \vec{k}_y \qquad \ldots \quad (2.3)$$

For the planar case, the segment absolute angular velocity and absolute angular acceleration are given by,

$$\begin{aligned} \omega_s &= \omega_b + \dot{\theta}_y \\ \alpha_s &= \alpha_b + \ddot{\theta}_y \end{aligned} \qquad \ldots \quad (2.4)$$

If the distal frame of the i^{th} link has a relative angular velocity of ω_{d_i} with respect to the base reference frame on the i^{th} link, then for the planar case, the absolute angular velocity of the base reference frame (ω_b) is given by,

$$\omega_b = \sum_{j=1}^{i} (\dot{\phi}_j + \omega_{d_{j-1}}) \qquad \ldots \quad (2.5)$$

A similar expression exists for the absolute angular acceleration of the link base reference frame. The absolute acceleration of the center of mass 'G' ($\vec{a}_G$) will be obtained by considering the acceleration of the origin of the base frame 'O_b' ($\vec{a}_b$) and the relative motion of 'G' with respect to the $(X_b Y_b Z_b)$ frame. $\vec{a}_G$ is given by the classical acceleration expression,

$$\vec{a}_G = \vec{a}_b + \vec{\omega}_b \times (\vec{\omega}_b \times \vec{r}) + \vec{\alpha}_b \times \vec{r} + 2\,\vec{\omega}_b \times \vec{v}_{rel} + \vec{a}_{rel} \qquad \ldots \quad (2.6)$$

where,

$$\begin{aligned} r &= u_x \vec{k}_{x_b} + (s + u_z)\,\vec{k}_{z_b} \\ v_{rel} &= \dot{u}_x \vec{k}_{x_b} + \dot{u}_z \vec{k}_{z_b} \\ a_{rel} &= \ddot{u}_x \vec{k}_{x_b} + \ddot{u}_z \vec{k}_{z_b} \\ a_b &= a_{b_x} \vec{k}_{x_b} + a_{b_z} \vec{k}_{z_b} \end{aligned} \qquad \ldots \quad (2.7)$$

'$\vec{r}$' is the vector that locates the center of mass 'G' with respect to the origin of the base reference frame as shown in Figure 4. '$\vec{v}_{rel}$' is the relative linear velocity of the differential segment, and '$\vec{a}_{rel}$' is the relative linear acceleration of the differential segment with respect to the base reference frame. If $\vec{a}_G$ is given by,

$$\vec{a}_G = a_x \vec{k}_{x_b} + a_z \vec{k}_{z_b} \qquad \ldots \quad (2.8)$$

from equation (2.6) we have,

$$\begin{Bmatrix} a_z \\ a_x \end{Bmatrix} = \begin{Bmatrix} a_{b_z} \\ a_{b_x} \end{Bmatrix} + \begin{bmatrix} -\omega_b^2 & -\alpha_b \\ \alpha_b & -\omega_b^2 \end{bmatrix} \begin{Bmatrix} u_z \\ u_x \end{Bmatrix} + \begin{Bmatrix} -\omega_b^2 . s \\ \alpha_b . s \end{Bmatrix}$$

$$+ \begin{bmatrix} 0 & -2\omega_b \\ 2\omega_b & 0 \end{bmatrix} \begin{Bmatrix} \dot{u}_z \\ \dot{u}_x \end{Bmatrix} + \begin{Bmatrix} \ddot{u}_z \\ \ddot{u}_x \end{Bmatrix} \qquad \ldots \quad (2.9)$$

The free-body diagram for the differential segment on the X_bZ_b plane is shown in Figure 5. From Timoshenko beam theory, the transverse shear can be included in the model as

$$Q_x = k_t A \ \gamma(\partial u_x/\partial s - \theta_y) \qquad \ldots (2.10)$$

where, 'k_t' is the Timoshenko Shear Coefficient for the link cross-section. Also, the moment-curvature relations yield,

$$M_y = EI_y \partial\theta_y/\partial s \qquad \ldots (2.11)$$

Referring to Figure 5, let f_x and f_z be the distributed forces acting on the element. In the absence of any other external loading, these will simply represent the gravity loading on the differential segment. We can write the governing equations for the differential segment as:

$$\begin{aligned} \partial Q_x/\partial s + f_x &= \rho A \ a_x \\ \partial M_y/\partial s + Q_x &= \rho I_y \ \alpha_s \\ AE\,\partial^2 u_z/\partial s^2 + f_z &= \rho A \ a_z \end{aligned} \qquad \ldots (2.12)$$

The above partial differential equations will be solved using finite elements in the spatial domain and finite differences in the time domain. In order to be able to use the finite element method, we have to render the equations in an integral form. This will be accomplished by using the Galerkin's method.

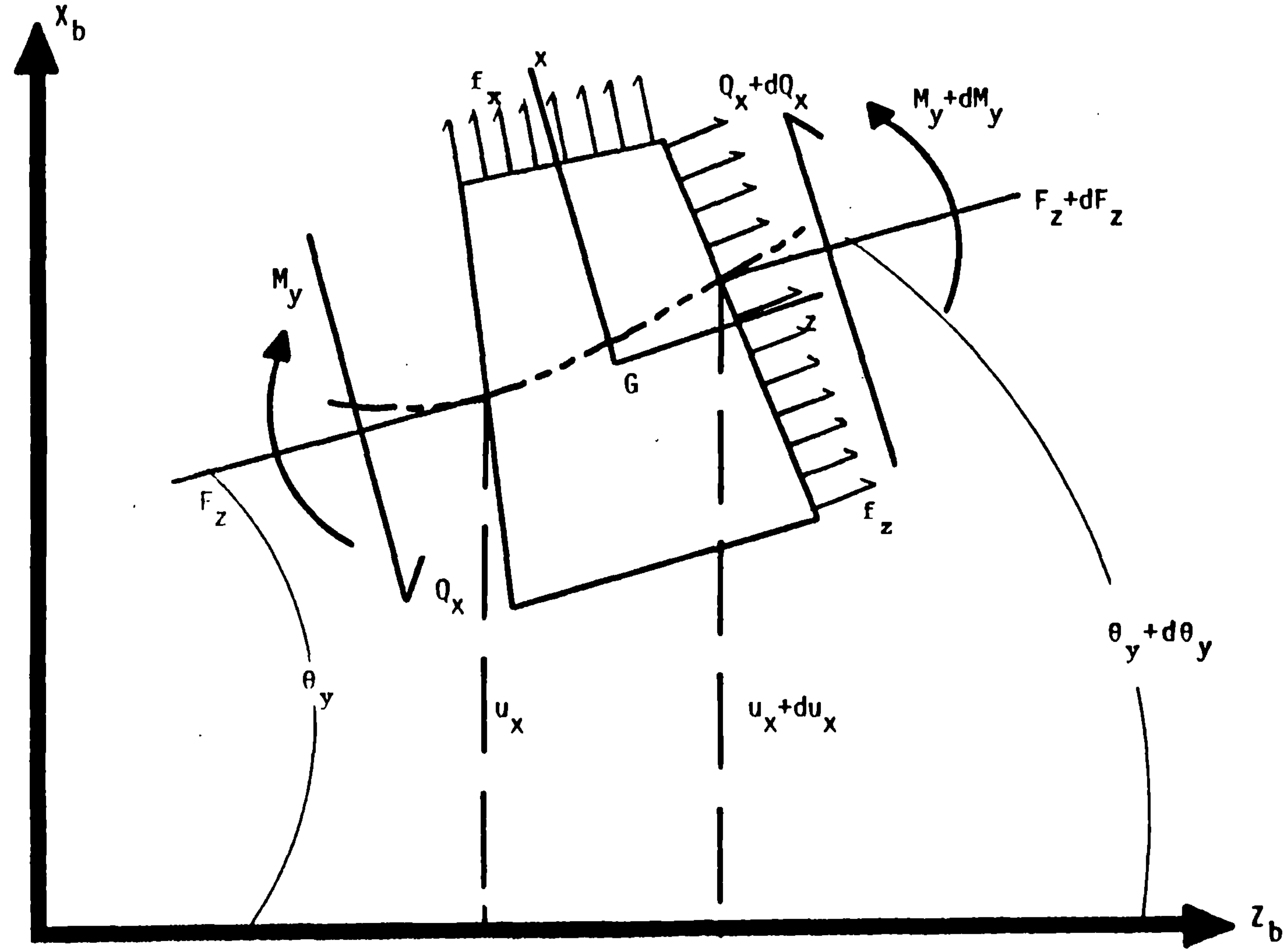

Figure 5. Free-Body Diagram of a Differential Segment

Galerkin's Method

The Galerkin's method offers a generalized mathematical approach to render the governing equations in an integral form. In this method, we shall treat the displacements u_z, u_x and the rotation θ_y as the primary unknowns of the problem. Letting δu_z, δu_x, and $\delta\theta_y$ be the arbitrary variations of these unknowns, by Galerkin's method, we have the following integral:

$$\int_{s_1}^{s_2}\Big[[\rho Aa_x - \partial Q_x/\partial s - f_x]\delta u_x + [\rho Aa_z - AE\partial^2 u_z/\partial s^2 - f_z]\delta u_z$$

$$+ [\rho I_y \alpha_s - \partial M_y/\partial s - Q_x]\delta\theta_y\Big] ds = 0 \qquad \text{... (2.13)}$$

where, s_1 and s_2 locate the finite element on the i^{th} link as shown in Figure 6. Substituting for Q_x and M_y from equations (2.10) and (2.11) into equation (2.13), and partially integrating some of the terms, we have

$$\int_{s_1}^{s_2}\Big[\rho Aa_x\, \delta u_x + \rho Aa_z\, \delta u_z - f_x\, \delta u_x - f_z\, \delta u_z +$$

$$\rho I_y \alpha_s \delta\theta_y + Q_x\, \delta(\partial u_x/\partial s - \theta_y) + M_y\, \delta(\partial\theta_y/\partial s) +$$

$$AE\, \partial u_z/\partial s\, \delta(\partial u_z/\partial s)\Big].ds =$$

$$[\delta u_x Q_x + \delta\theta_y M_y + AE\, \partial u_z/\partial s . \delta u_z]_{s_1}^{s_2} \qquad \text{... (2.14)}$$

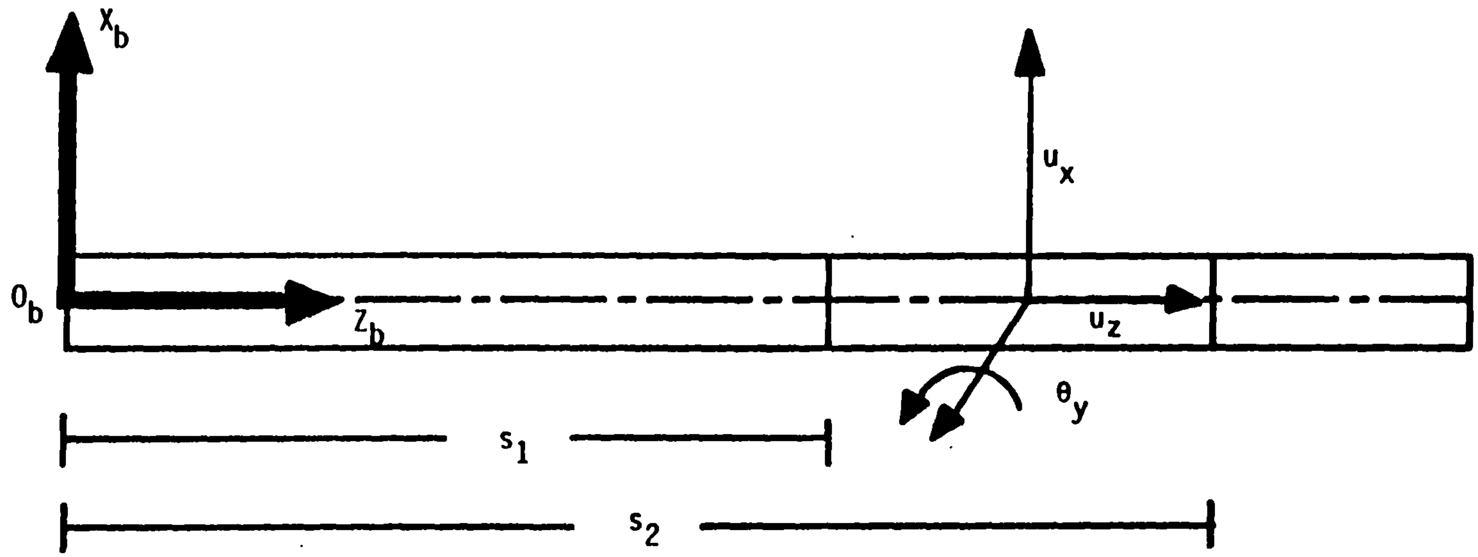

Figure 6. Typical Finite Element for Planar Case

At this stage, the highest order of partial derivative in the integrand is of order '1'. Also, the right hand side of the above equation will equal zero at the limits, as the variations vanish at the boundaries of the finite element at $s=s_1$ and $s=s_2$.

Development of a Special Finite Element

For the development of the finite element, we will assume that the manipulator links are beams of uniform cross-sections. However, this requirement is easily relaxed for a varying cross-section. In that case, the cross-sectional area '$A(s)$' and the area moment of inertia '$I_y(s)$' should be appropriately defined, while evaluating the integral in equation (2.14).

The primary unknowns of the problem are u_z, u_x, and θ_y. These may be expressed as a function of the nodal displacements of the finite element using shape functions $N_1(s)$ and $N_2(s)$. The complexity of these shape functions may be determined by observing the highest order of the partial derivatives in the integrand in equation (2.14). If the highest order is observed to be 'n', then the shape functions are required to have a continuity of at least order 'n-1'.[115] The value of 'n' is equal to '1' in equation (2.14). Therefore, a 0^{th} order continuity is required for the interpolation function. That is, a simple linear interpolation is adequate to model the manipulator links. Therefore, the shape functions $N_1(s)$ and $N_2(s)$ will be given by:

$$N_1(s) = (s_2-s)/(s_2-s_1)$$
$$N_2(s) = (s-s_1)/(s_2-s_1) \qquad \ldots (2.15)$$

If $\{u\}_e$ is the vector of the primary unknowns of the problem,

$$\{u\}_e = [\ u_z \quad u_x \quad \theta_y\ ]^T \qquad \ldots (2.16)$$

and $\{q\}_e$ is the vector of elemental nodal displacements of the finite element given by,

$$\{q\}_e = [(U_z)_1\ (U_x)_1\ (\theta_y)_1\ (U_z)_2\ (U_x)_2\ (\theta_y)_2]^T \qquad \ldots (2.17)$$

then, the vectors $\{u\}_e$ and $\{q\}_e$ will be related by a shape matrix $[N_e]$ as:

$$\{u\}_e = [N_e]\ \{q\}_e \qquad \ldots (2.18)$$

The shape matrix $[N_e]$ will be given by,

$$[N_e] = \begin{bmatrix} N_1(s) & 0 & 0 & N_2(s) & 0 & 0 \\ 0 & N_1(s) & 0 & 0 & N_2(s) & 0 \\ 0 & 0 & N_1(s) & 0 & 0 & N_2(s) \end{bmatrix} \qquad \ldots (2.19)$$

Taking the variations on both sides of equation (2.18), we have,

$$\delta\{u\}_e = [N_e]\ \delta\{q\}_e \qquad \text{... (2.20)}$$

Also,

$$\delta u^T = \delta q^T\ [N_e]^T \qquad \text{... (2.21)}$$

Substituting the above into equation (2.14) and performing the required differentiations and integrations, we have the governing equations of motion for an element on the i^{th} link as:

$$[J]_e\ \{\ddot{q}\}_e + [C]_e\ \{\dot{q}\}_e + [K]_e\ \{q\}_e = \{F\}_e \qquad \text{... (2.22)}$$

where,

$[J]_e$ is the Element Inertia Matrix

$[C]_e$ is the Coriolis Matrix due to the motion of the reference frame $(X_bY_bZ_b)$ of the i^{th} link.

$[K]_e$ is the Element Stiffness Matrix $= [K_c]_e + [K_b]_e$

$[K_c]_e$ is the Conventional Stiffness Matrix

$[K_b]_e$ is the stiffness matrix due to the motion of the frame $(X_bY_bZ_b)$ of the i^{th} link.

$\{F\}_e$ is the element force vector due to external forces, accelerations, gravity, etc.

The element matrices have been included in Appendix A.

Note that there is a pseuo-damping term '$[C]_e$' which is due to coriolis effects and this will be referred to as the Coriolis Matrix. Also, the elemental stiffness matrix is comprised of two parts, namely the conventional or structural stiffness $[K_c]_e$ and a pseudo-stiffness due to the gross motion characteristics of the i^{th} link of the manipulator $[K_b]_e$. If one were to formulate the problem by applying the conventional structural dynamics principles, then the coriolis term and the stiffness term due to base motion would be ignored. Further, the governing equations for the element have been derived taking into consideration the coupling phenomenon between the link gross motions and the link deformations (equations 2.4 - 2.9). The matrix elements of the coriolis matrix $[C_e]$, the stiffness matrix due to base motion $[K_e]$, and the element force vector $\{F_e\}$ are functions of the angular velocities and angular accelerations of the base reference frame of the manipulator link the finite element is associated with. Since these kinematic quantities (ω_b and α_b) are also dependent on the nodal deformations, the elemental equations are coupled, non-linear ordinary equations.

In this section, the elemental equations have been derived using Timoshenko Beam Theory along with a choice of linear interpolation within the finite element. However, it has been well documented in the literature [76,105] that this combination results in parasitic shear effects leading to a stiff system of equations. These parasitic effects are referred to as the 'shear lock effects' and are particularly dominant at lower aspect ratios. In order to avoid the shear lock, reduced order integration has been adopted for the conventional stiffness matrix $[K_c]_e$.[115] The developed model can then be applied to a wider range of aspect ratios. That is, both short links (stunt beams) as well as fairly long links (slender beams) can be modeled using the finite element developed in this section.

Derivation of System Equations

The system equations are to be obtained by identifying the relation between the elemental equations in terms of their local coordinates and their forms in terms of the system coordinates. Then, these equations must be properly assembled along with the appropriate boundary conditions to obtain the final system equations, corresponding to a set of user-defined system coordinates.

Derivation of Global Elemental Equations

The conversion of the elemental equations in terms of the elemental nodal coordinates to equations in terms of the global coordinates (global elemental equations) can be achieved in two ways. One of the methods is to request the user to provide the compatibility conditions between the elemental and global coordinates in terms of matrices for each of the elements. [94,95] A second method is, to automate this process by providing an assembly procedure by choosing an appropriate global coordinate description. The latter approach has been preferred in this study. The global coordinates at the nodes of the element are chosen parallel to the axes of the ground reference frame $(X_b Y_b Z_b)_0$. A typical finite element with its local and global coordinates are shown in Figure 7. By calculating the link orientations as the manipulator changes its configuration, the computer code automatically generates the compatibility conditions for each of the finite elements.

In structural dynamics methodologies, the compatibility matrices for the finite elements have normally been treated to be non-time-dependent. However, for a system such as the manipulator, the configuration undergoes gross changes during the task cycle. Particularly when the motion is executed at high speeds, the rates of these changes may also be significant. Therefore, the time varying nature of these compatibility matrices must be recognized while assembling the system equations.

Let $[\Phi_i(t)]$ be a time-varying compatibility matrix between the elemental and global coordinates at the nodes of the finite element. If $\{q_g\}_e$ is the vector of element global displacements for an element on the ith link, the equations of motion can be written in global coordinates as:

$$[J_g]_e \{\ddot{q}_g\}_e + [C_g]_e \{\dot{q}_g\}_e + [K_g]_e \{q_g\}_e = \{F_g\}_e \quad \ldots \quad (2.23)$$

where,

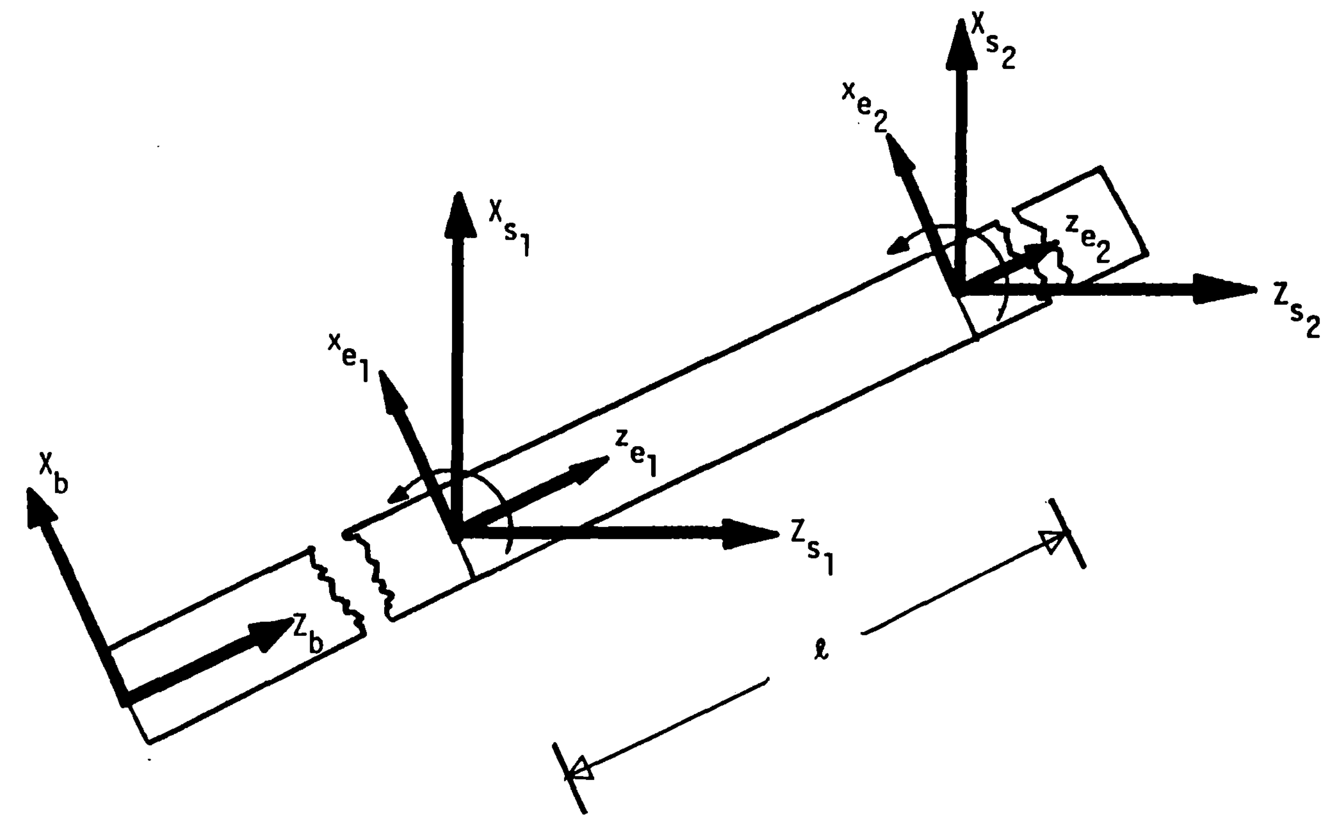

Figure 7. Planar Finite Element with Local and Global Coordinates

$$[J_g]_e = [\Phi_i(t)]^T \, [J]_e \, [\Phi_i(t)]$$

$$[C_g]_e = [\Phi_i(t)]^T \, [\, 2[J]_e \, [\dot{\Phi}_i(t)] + [C]_e \, [\Phi_i(t)] \,]$$

$$[K_g]_e = [\Phi_i(t)]^T \, [\, [J]_e \, [\ddot{\Phi}_i(t)] + [C]_e \, [\dot{\Phi}_i(t)] + [K]_e \, [\Phi_i(t)] \,] \qquad \ldots (2.24)$$

$[\dot{\Phi}_i(t)]$ and $[\ddot{\Phi}_i(t)]$ are the first and second time derivatives of the compatibility matrices. We can observe from the form of equations (2.24) that there is a cross-contribution effect, because of the time varying nature of the compatibility conditions used in this study. The compatibility matrices for the case of revolute jointed planar manipulators may be easily obtained from figure 7, by inspection. These global elemental equations must be appropriately assembled to obtain the final system equations by imposing the boundary conditions of the problem. This assembly procedure is accomplished using a variable correlation table. The details of this method is described in the following section.

Variable Correlation Table

The global element matrices derived in the previous section must be assembled to form the system matrices imposing the appropriate boundary conditions. The element matrices will be assembled to obtain system inertia matrix $[J]_s$, system damping term $[C]_s$, system stiffness matrix

$[K]_s$, and the system force vector $\{F\}_s$.

Variable correlation table is a two-dimensional array, each row of which corresponds to a particular element in the assemblage and each column of which represents one of the element nodal displacements. A typical row of this table is shown in Figure 8. For the case of revolute jointed planar manipulators, the number of columns in the variable correlation table has been set equal to 6, the size of the largest element nodal displacement vector.

Letting $V_c(i,j)$ represent the elements of the variable correlation table , the subscript 'i' will range from 1 to the number of finite elements, and 'j' from 1 to 6. The subscript 'j' refers to the j^{th} nodal displacement of the element 'i'. If the j^{th} nodal displacement of the i^{th} element is 'v', the array $V_c(i,j)$ can be defined as:

$$V_c(i,j) = \begin{cases} 0, \text{ if } v = 0 \\ \text{location of 'v' within the} \\ \text{system deformation numbering} \\ \text{scheme, if } v \neq 0 \end{cases}$$

Let us refer to a typical row of the variable correlation table corresponding to the r^{th} element. If N_1 to N_m are the entries in the 'm' columns of the r^{th} row, then the s^{th} column of the r^{th} element should lie along the $N_s{}^{th}$ column of the system matrix. Similarly the s^{th} row of the r^{th} element should lie along the $N_s{}^{th}$ row of the system matrix. In this manner all element matrices will be assembled to form the system matrices.

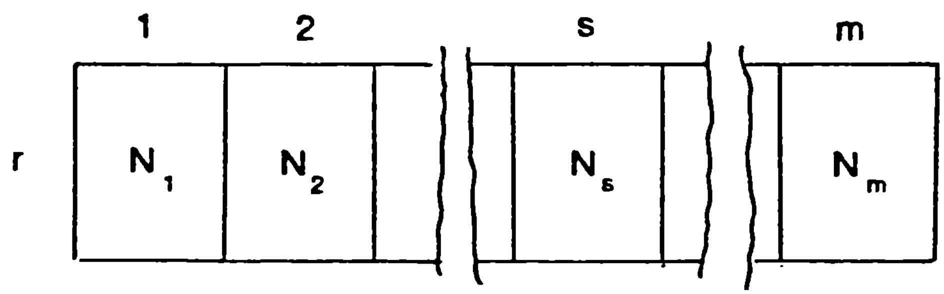

m : Size of the Element Deformation Vector

N_s: N_s^{th} Global (System) Coordinate

Figure 8. Typical Row of the Variable Correlation Table

System Equations

Using the procedures described in the previous sections, we can assemble the system equations. The system equations will be of the form given below:

$$[J(q_s)]_s \{\ddot{q}_s\} + [C(q_s,\dot{q}_s)]_s \{\dot{q}_s\} + [K(q_s,\dot{q}_s,\ddot{q}_s)]_s \{q_s\} = \{F(q_s,\dot{q}_s,\ddot{q}_s)\}_s \quad \ldots (2.25)$$

These equations are non-linear, coupled, ordinary differential equations. The next step is to identify a solution procedure to solve this system of equations.

Augmentation of System Equations for Joint Servo-Compliances

Typically, the actuators of manipulators are driven by electric or hydraulic servo drives. For a simple servo-drive involving position and velocity feedbacks, the transfer function at a particular joint may be written as [73]:

$$\frac{\theta(s)}{\theta_d(s)} = \frac{k_e k_m}{s^2 J + s(F+k_r k_m) + k_e k_m} \quad \ldots (2.26)$$

where,

k_m is the actuator gain

F is the viscous damping term

k_e is the position feedback gain

k_r is the rate feedback gain

J is the reflected inertia at the joint

In order to prevent structural oscillations and to ensure system stability, the characteristic frequency of the control system is usually limited to 50% of the structural frequency. [73] Hence, the maximum value of the servo-stiffness (k_p) is given by,

$$k_p = k_e k_{m_{max}} = \pi^2 f_0^2 J_0 \qquad \text{... (2.27)}$$

where, f_0 is the structural frequency for an inertia value of J_0. Similarly for a critical damping of the above system, the maximum value of the servo-damping (k_v) is given by,

$$k_v = F + k_r k_m = 2\sqrt{J\ k_e k_m} \qquad \text{... (2.28)}$$

If one were to assume that these gains to be constant over the operating range, this might result in overdamping when the reflected inertia values are below the maximum value assumed in the above expression. However, for such an approximation, the perturbative torque (T_p) is given by,

$$T_p = - k_p * (\theta_d - \theta_a) - k_v * (\dot{\theta}_d - \dot{\theta}_a) \qquad \text{... (2.29)}$$

where, θ_d and θ_a are the desired and actual values of the joint positions and ($\theta_d - \theta_a$) is a measure of the compliance at the joint. Thus equation (2.29) may be used to augment the system forcing functions in equation (2.25) to include the effects of the joint servo-compliances.

In describing the above compliant model, the system coordinates representing the rotational deformations in the finite element mesh, will no longer be compatible at the actuators of the manipulator. The difference in their values will represent the compliance at the joint. An analogy will be the modeling of torsional springs and rotational dashpots in structural configurations.

Solution of System Equations

The set of system equations given by equation (2.25) is a set of nonlinear, coupled ordinary differential equations. An iterative numerical procedure will be used to solve the above set of equations. The procedure followed here is one of an incremental linearization and equilibrium iteration.[9] For iteration 'k' of the time step (t+Δt), equation (2.25) may be rewritten as:

$$
\begin{aligned}
&{}^{t+\Delta t}[M]^{(k-1)}\ {}^{t+\Delta t}\{\ddot{U}\}^{(k)} + {}^{t+\Delta t}[C]^{(k-1)}\ {}^{t+\Delta t}\{\dot{U}\}^{(k)} \\
&\qquad + {}^{t+\Delta t}[K]^{(k-1)}\ {}^{t+\Delta t}\{U\}^{(k)} = {}^{t+\Delta t}\{F\}^{(k-1)} \qquad \ldots (2.30)
\end{aligned}
$$

where, the coefficient matrices have been evaluated based on the results of iteration '(k-1)'. Also, the following conditions will apply during the first iteration.

$$
\begin{aligned}
{}^{t+\Delta t}U^{(0)} &= {}^{t}U \\
{}^{t+\Delta t}\dot{U}^{(0)} &= {}^{t}\dot{U} \\
{}^{t+\Delta t}\ddot{U}^{(0)} &= {}^{t}\ddot{U} \\
{}^{t+\Delta t}F^{(0)} &= {}^{t}F \qquad \ldots (2.31)
\end{aligned}
$$

An implicit time integration scheme (Newmark's method) will be used in calculating the dynamic response from the above equations. The method (also referred to as constant average acceleration method or trapezoidal rule) has been proven to be unconditionally stable for a linear parametric system of equations. The stability of the method does not depend on the time step of the analysis. However, the time step is regulated by the accuracy requirements of the problem. Usually, a time step equal to 1% of the fundamental period is recommended to meet the accuracy requirements.[9] From the trapezoidal rule the following expressions may be written:

$$ {}^{t+\Delta t}U = {}^{t}U + \frac{\Delta t}{2}\left({}^{t}\dot{U} + {}^{t+\Delta t}\dot{U}\right) \qquad \ldots (2.32) $$

$$ {}^{t+\Delta t}\dot{U} = {}^{t}U + \frac{\Delta t}{2}\left({}^{t}\ddot{U} + {}^{t+\Delta t}\ddot{U}\right) \qquad \ldots (2.33) $$

From the above, we obtain the expressions for the deformational displacement derivatives, as:

$$ {}^{t+\Delta t}\dot{U} = \frac{2}{\Delta t}\left({}^{t+\Delta t}U - {}^{t}U\right) - {}^{t}\dot{U} \qquad \ldots (2.34) $$

$$ {}^{t+\Delta t}\ddot{U} = \frac{4}{\Delta t^{2}}\left({}^{t+\Delta t}U - {}^{t}U\right) - \frac{4}{\Delta t}\,{}^{t}\dot{U} - {}^{t}\ddot{U} \ldots (2.35) $$

Substituting equations (2.34) and (2.35) in equation (2.30), we obtain the equation:

$$ {}^{t+\Delta t}[K^*]^{(k-1)}\ {}^{t+\Delta t}U^{(k)} = {}^{t+\Delta t}\{F^*\}^{(k-1)} \quad \ldots (2.36) $$

where,

$$ {}^{t+\Delta t}[K^*]^{(k-1)} = \frac{4}{\Delta t^2}\ {}^{t+\Delta t}[M]^{(k-1)} + \frac{2}{\Delta t}\ {}^{t+\Delta t}[C]^{(k-1)} + {}^{t+\Delta t}[K]^{(k-1)} \quad \ldots (2.37) $$

$$ {}^{t+\Delta t}\{F^*\}^{(k-1)} = {}^{t+\Delta t}\{F\}^{(k-1)} - $$

$$ - {}^{t+\Delta t}[M]^{(k-1)} \{ - \frac{4}{\Delta t^2}\ {}^{t}U - \frac{2}{\Delta t}\ {}^{t}\dot{U} - {}^{t}\ddot{U} \} $$

$$ - {}^{t+\Delta t}[C]^{(k-1)} \{ - \frac{2}{\Delta t}\ {}^{t}U - {}^{t}\dot{U} \} \quad \ldots (2.38) $$

${}^{t+\Delta t}[K^*]^{(k-1)}$ is referred to as the tangent stiffness matrix. Using Newton-Raphson iteration, a new approximation to the displacement solution is obtained as below:

$$ {}^{t+\Delta t}U^{(k)} = {}^{t+\Delta t}U^{(k-1)} + \Delta U^{(k)} \quad \ldots (2.39) $$

$$ {}^{t+\Delta t}[K^*]^{(k-1)}\ \Delta U^{(k)} = {}^{t+\Delta t}\{F^*\}^{(k-1)} - {}^{t+\Delta t}[K^*]^{(k-1)}\ {}^{t+\Delta t}U^{(k-1)} = \{F_u\}^{(k)} \quad \ldots (2.40) $$

where, $\{F_u\}^{(k)}$ is the vector of unbalanced forces during the k^{th} iteration and $\Delta U^{(k)}$ is the corresponding incremental correction to the displacement solution.

In order to provide some indication of when both the displacements and the forces are near their equilibrium values, an energy tolerance criterion will be employed.[9]

This criterion will be in terms of the increment in internal energy which is given by the amount of work done by the unbalanced forces on the displacement increments. The ratio of the increment in internal energy during the current iteration to that of the initial internal energy increment (during the first iteration of the current time step) will be compared to a preset energy tolerance value ε_E (usually of the order of 10^{-10}). Therefore, the criterion is given by,

$$\frac{\{\Delta U^{(k)}\}^T \ \{F_u\}^{(k)}}{\{\Delta U^{(I)}\}^T \ \{F_u\}^{(I)}} \leq \varepsilon_E \qquad \ldots (2.41)$$

The flow chart corresponding to this solution procedure is shown in Figure 9.

In this chapter, a finite element based method has been developed to analyze planar manipulator configurations with revolute joints. A special finite element was developed taking into account the complete nonlinear coupling between the link deformations due to distributed elasticity and nonlinear link gross motions due to the commanded motions at the joints. An assembly procedure based on a variable correlation table was used to assemble the elemental matrices into the system equations. These equations were nonlinear, ordinary differential equations. The system equations may also be augmented for any servo-compliant effects that exist at the actuators. An iterative procedure involving an incremental linearization and equilibrium

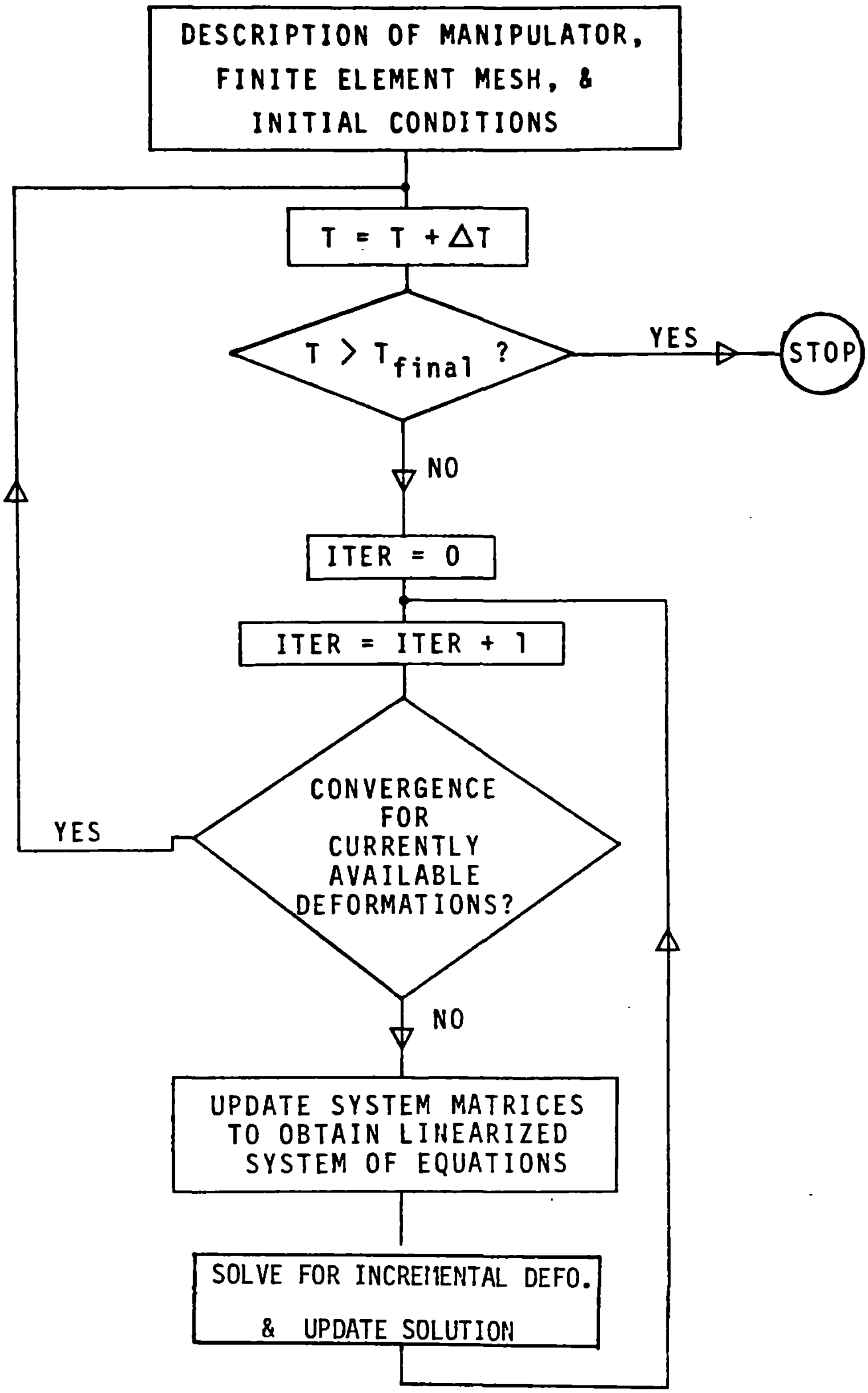

Figure 9. Flow-Chart of the Solution Procedure

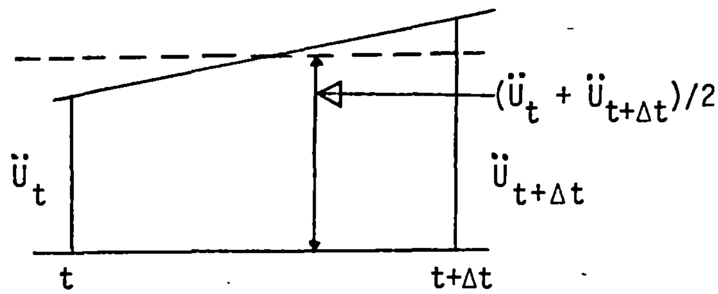

Constant Average Acceleration Method

1. Initialize $\{X\}_0$, $\{\dot{X}\}_0$, and $\{\ddot{X}\}_0$ to zero.

2. Set $\delta = 0.5$ and $\alpha = 0.25$

3. Calculate:

$$a_0 = 1/(\alpha\ \Delta t^2) \qquad a_4 = \delta/\alpha - 1$$
$$a_1 = \delta/(\alpha\ \Delta t) \qquad a_5 = (\delta/\alpha - 2)\ \Delta t/2$$
$$a_2 = 1/(\alpha\ \Delta t) \qquad a_6 = (1 - \delta)\ \Delta t$$
$$a_3 = 1/(2\alpha) - 1 \qquad a_7 = \delta.\Delta t$$

4. Calculate $\{F^{\star}\}_t = \{F\}_t + [M]_t\,(a_0\,\{X\}_{t-\Delta t} + a_2\,\{\dot{X}\}_{t-\Delta t} + a_3\,\{\ddot{X}\}_{t-\Delta t}) + [C]_t\,(a_1\{X\}_{t-\Delta t} + a_4\{\dot{X}\}_{t-\Delta t} + a_5\{\ddot{X}\}_{t-\Delta t})$

5. Solve $[K]_t + a_0\,[M]_t + a_1\,[C]_t\ \{X\}_t = \{F^{\star}\}_t$

6. Compute $\{\ddot{X}\}_t = a_0\,(\{X\}_t - \{X\}_{t-\Delta t}) - a_2\,\{\dot{X}\}_{t-\Delta t} - a_3\,\{\ddot{X}\}_{t-\Delta t}$

$$\{\dot{X}\}_t = \{\dot{X}\}_{t-\Delta t} + a_6\,\{\ddot{X}\}_{t-\Delta t} + a_7\,\{\ddot{X}\}_t$$

7. Repeat from Step 4 for all intervals.

Figure 10. Newmark Algorithm

iteration was identified to solve these differential equations.

Before obtaining the vibrational response of the manipulator, it is necessary to verify the various components of the developed model. Procedures required for such a validation will be developed in the next chapter.

CHAPTER III

PLANAR MODEL VERIFICATION

Introduction

Before solving the planar model to obtain the vibrational response, the performance and correctness of the finite element formulation must be studied. Both analytical and experimental procedures will be employed to accomplish the above objective. The following procedures have been used in this study to check the various components of the planar model developed in the previous chapter.

(i) Eigenvalue analysis

(ii) Static frame analysis

(iii) Quasi-static analysis of a rotating link

(iv) Experimental Investigation of a flexible manipulator, and

(v) Quasi-static analysis of general planar configurations.

Eigenvalue Analysis

The first step in the verification process is an eigenvalue analysis of beams. The finite element developed in Chapter II is a special Timoshenko beam element. Closed form solutions are available in the classical literature for

Timoshenko beams with different boundary conditions. We can compare the eigenvalues obtained with the finite element developed in this study to these analytical solutions.

Consider a beam of uniform cross section, simply supported at both ends. When both shear deformation and rotatory inertia are taken into account, the frequencies of free vibration ω_n of such a beam are given by the roots of the equation:

$$\frac{\rho^2}{k_t E \gamma}\,\omega_n^4 - \left[\frac{\rho}{E}\left(1+\frac{E}{k_t \gamma}\right)(n\pi/L)^2 + \frac{\rho A}{E I_y}\right]\omega_n^2 + (n\pi/L)^4 = 0 \qquad \ldots \quad (3.1)$$

Using the finite elements developed in the last chapter, the eigenproblem is posed as:

$$[J]_s\ \{q\}_s = \frac{1}{\omega_n^2}\,[K_c]_s\ \{q\}_s \qquad \ldots \quad (3.2)$$

Table I compares the exact natural frequencies for a simply supported Timoshenko beam with the numerical results obtained using finite elements. Various values of aspect ratios have been chosen to demonstrate the performance of the finite elements over a wide range of these ratios. The results have also been shown for the case of the conventional stiffness matrix derived using exact integration. It may be observed from the table that the reduced order integration yields a good comparison both at low and high aspect ratios. It is to be noted here, that the

TABLE I

NON-DIMENSIONAL FREQUENCY PARAMETER $\ell^2\omega_n\sqrt{\rho A/EI_y}$
FOR SIMPLY-SUPPORTED TIMOSHENKO BEAM

FINITE ELEMENTS DERIVED USING EXACT INTEGRATION

No. of	ASPECT RATIO ($r/2\ell$)				
Elements	0.02	0.04	0.06	0.08	0.10
1	51.517	27.055	19.245	15.446	13.164
5	19.830	12.936	10.957	9.919	9.173
10	12.913	10.479	9.692	9.131	8.623
20	10.650	9.810	9.367	8.932	8.486
ANALYTICAL	9.839	9.580	9.258	8.866	8.441

FINITE ELEMENTS DERIVED USING REDUCED ORDER INTEGRATION

No. of	ASPECT RATIO ($r/2\ell$)				
Elements	0.02	0.04	0.06	0.08	0.10
1	13.686	13.218	12.553	11.793	11.017
5	10.291	10.052	9.694	9.262	8.795
10	9.915	9.695	9.364	8.963	8.527
20	9.844	9.608	9.284	8.891	8.462
ANALYTICAL	9.839	9.580	9.258	8.866	8.441

agreement of the eigenvalues suggests the correctness of the element inertia matrix and the element conventional stiffness matrix only.

Static Frame Analysis

A simple, planar frame is shown in Figure 11. When the members of this frame are subjected primarily to bending strains (Euler-Bernoulli theory), the deflection at any point on the member is given by,

$$y = \int_0^L \frac{Mm}{EI}\, dx \qquad \ldots \quad (3.3)$$

where, y = Deflection at the point of interest

M = Moment expressed as a function of 'x'

m = Moment due to a unit load placed at the location of the desired deflection and in the direction of the desired deflection expressed as a function of 'x'

L = Length of the structure

The horizontal deflection of the point 'D' in Figure 11 can be analytically calculated to be 3.61 inches using equation (3.3).[10] Table II shows the static solutions obtained using the special finite element developed in this study. Again, the results are observed to be in good agreement.

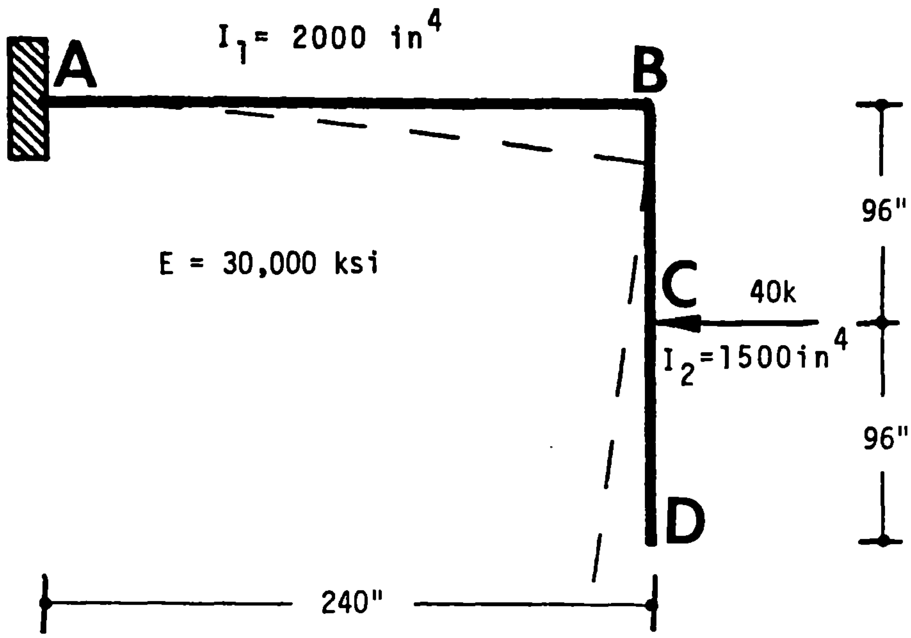

Figure 11. A Planar Frame

TABLE II

HORIZONTAL DEFLECTION AT FRAME TIP

# Elements in AB	BD	Deflection at 'D' (in inches)
2	2	3.55
4	4	3.59
4	6	3.61
Exact Solution		3.61

Quasi-Static Analysis of A Rotating Link

Let us consider the dynamics of a single link rotating at constant angular velocity. Then the inertial loading on the arm will be a triangularly varying, distributed load as shown in Figure 12. For a cantilever beam subjected to such a distributed loading, the equations for the static deflection are given by,

$$y = \frac{W}{120EI} \left[-x^5 - 15L^4x + 5Lx^4 + 11L^5 \right] \quad \ldots \quad (3.4)$$

$$y_{max} = y \Big|_{x=0} = \frac{11}{120EI} WL^3 \quad \ldots \quad (3.5)$$

By imposing the inertial loads as the triangularly varying distributed load, we can provide a close estimate of the dynamic deflections in the link. This static deflection may be referred to as 'quasi-static deflection', since it is the deflection obtained for an equivalent dynamic loading. The vibrational response of the link would then be expected to closely match these results, displaying an oscillatory behavior about the quasi-static solution. The same may be observed from Figure 13.

Experimental Investigation of a Flexible Manipulator

A single link flexible manipulator was designed and fabricated (see Figure 14) to investigate the performance of

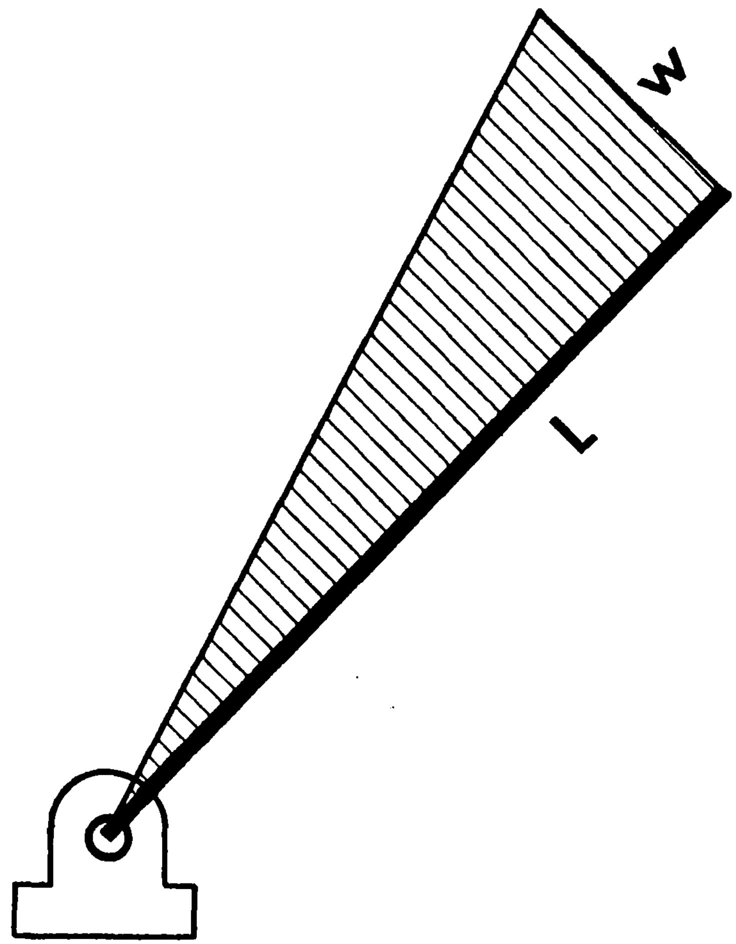

Figure 12. Inertial Loading on a Rotating Link

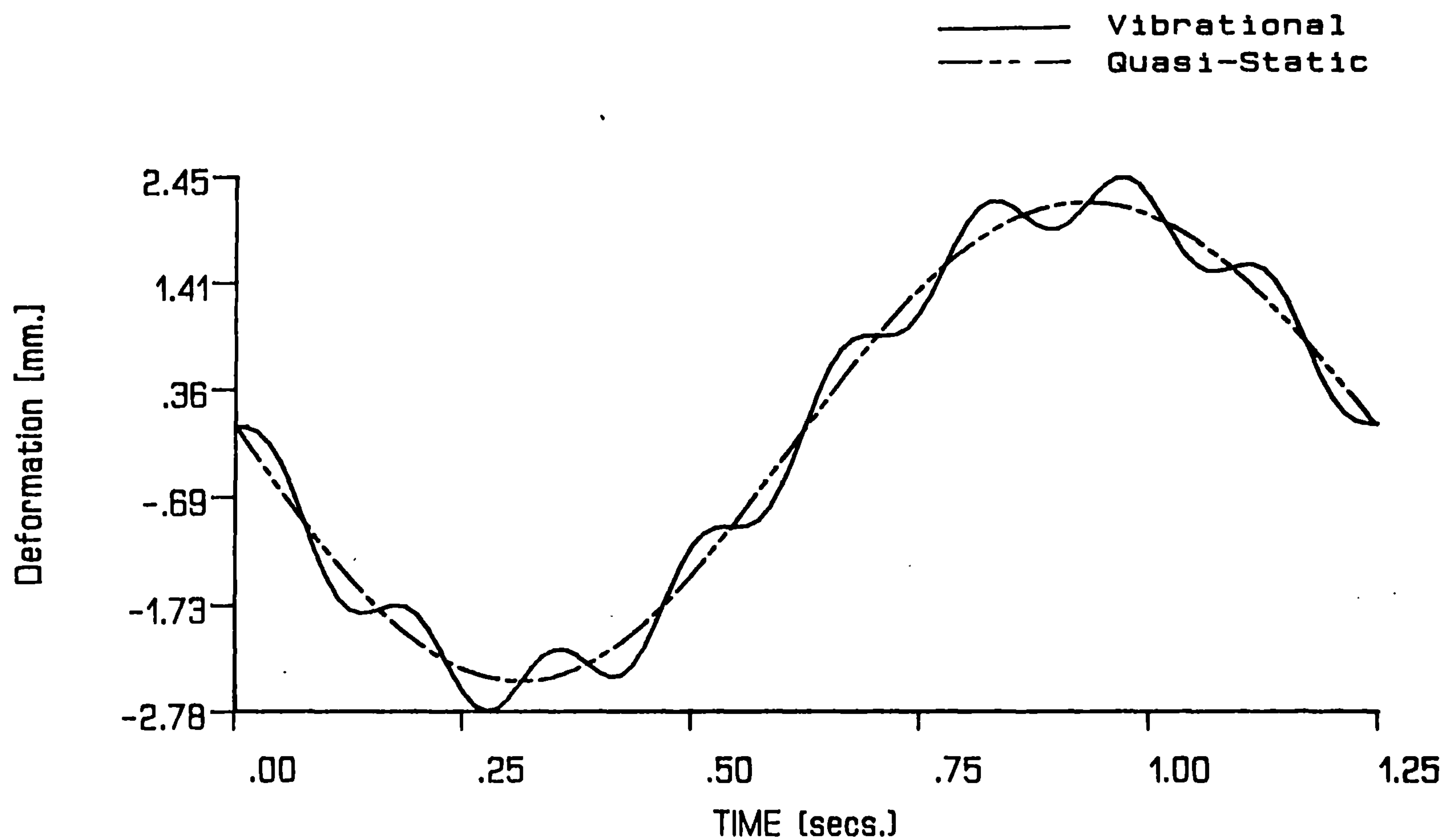

Figure 13. Quasi-Static Deflection

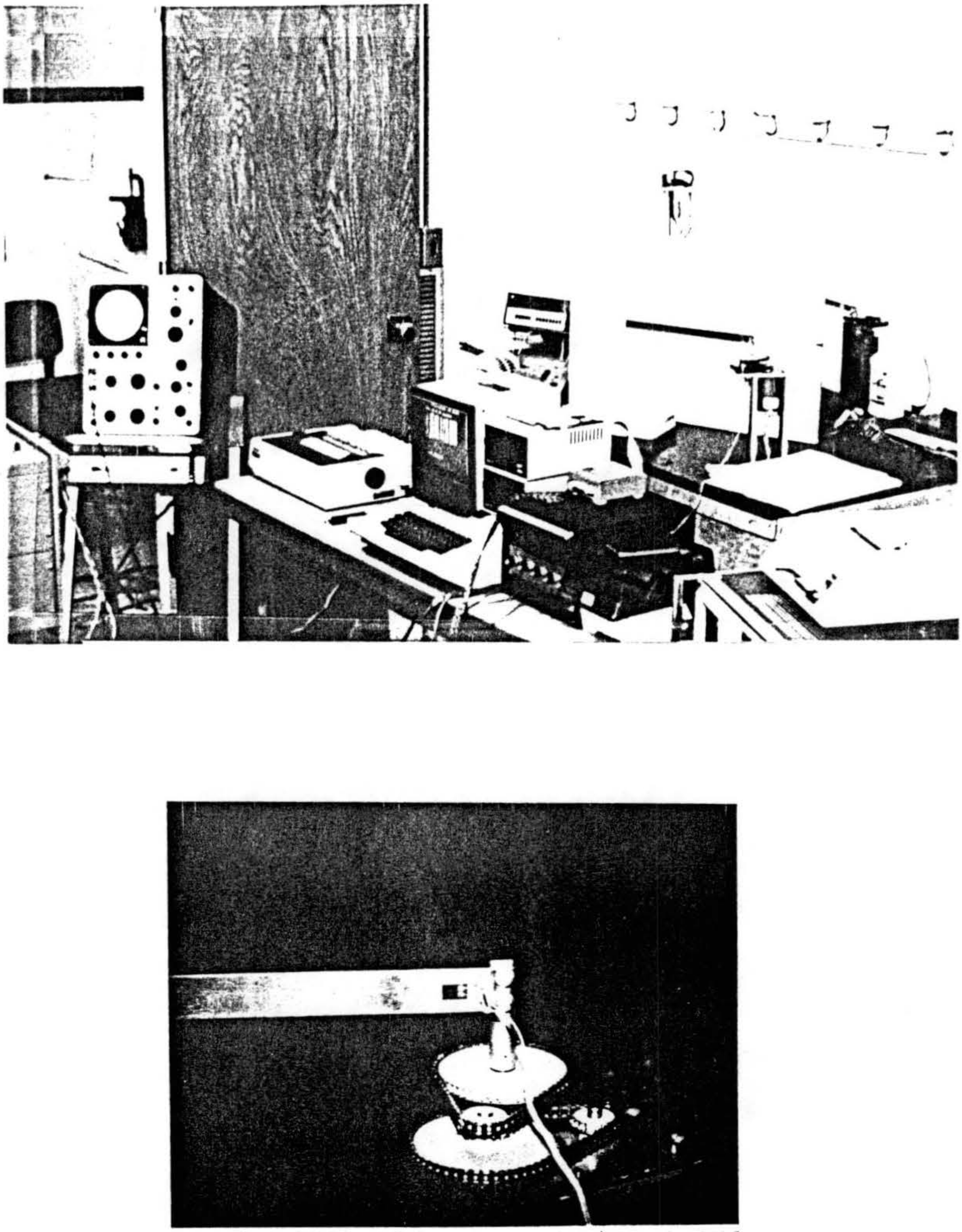

Figure 14. Experimental Set-up for Flexible Manipulator

the special finite element that has been derived in this study. The flexibility effects of the link were emphasized in this experiment. Therefore, the rotational actuator was selected to be the least compliant. A high torque stepper motor was found to be most appropriate for this experimental study due to its good positioning accuracy at lower speeds (1000 rpm or less). The stepper motor employed in this study was rated at 400 steps per revolution (in half stepping mode), or 0.9 degrees per step. In order to reduce the effects of inertial torques at the motor shaft, a zero-backlash chain and sprocket set was used to reduce the speed of the motor by a factor of 9. This also helped to decrease the amplitude of the steps applied to the link, thus achieving a smoother motion for the link.

Links with different values of stiffness and structural damping were tested in this experiment. The fundamental frequencies of these links ranged from 3 Hz to 20 Hz. A trapezoidal acceleration motion program was selected to excite the manipulator, with gross link motions varying from 20 to 180 degrees, for different cycle times. The general form of the excitation function is shown in Figure 15. An APPLE-II Plus microcomputer was used to control the stepper motor. The time delays required to drive the stepper motor were precomputed for a given motion profile and stored in the memory.

Strain gages were mounted on the link to record its dynamic response. A digital strain indicator (Vishay

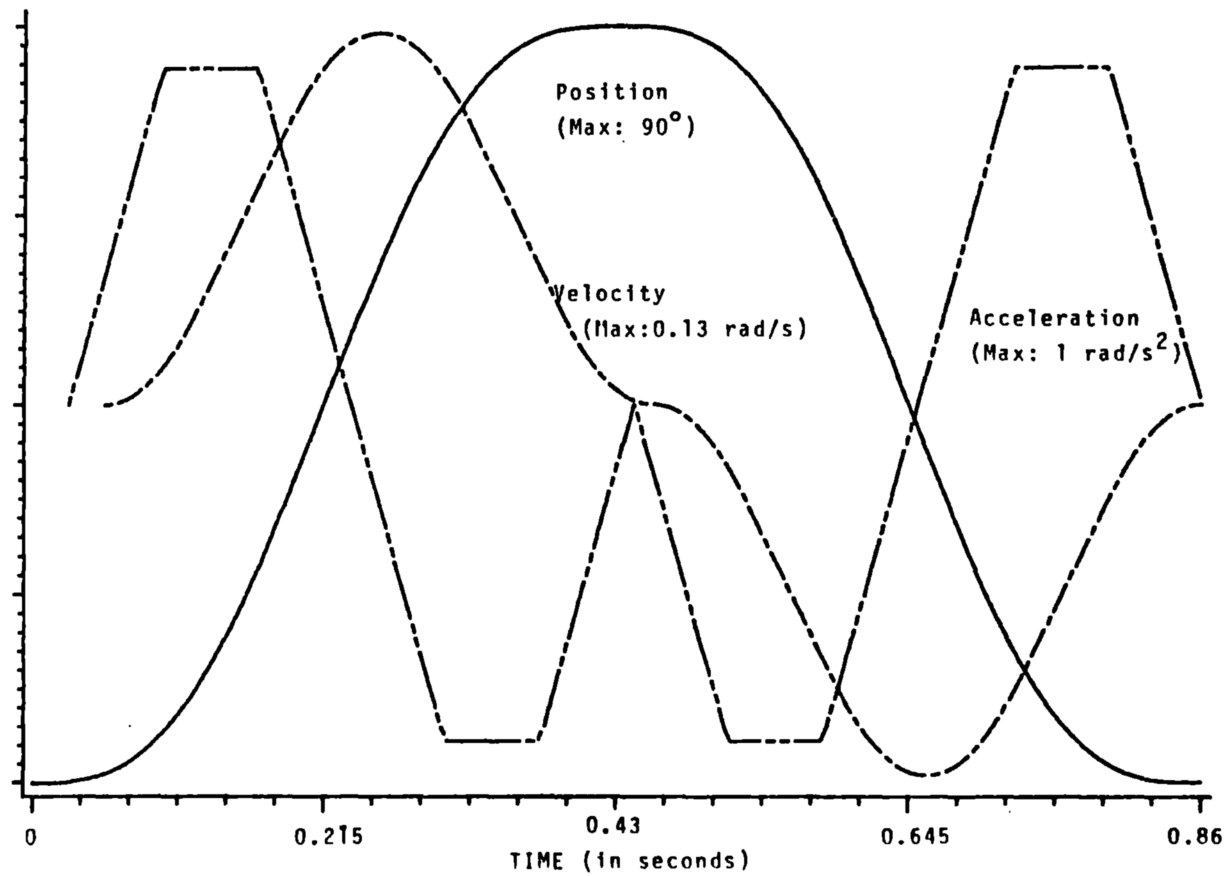

Figure 15. Command Joint Profiles for the Experiment

Ellis-20) was used to measure the strains. This instrument also served as an amplifier (app. 50) for the strain signal. The output signal from the strain indicator was analyzed for its frequency content and amplitude using a Spectral Dynamics SD-345 Spectrascope. This signal was also digitized using a 12-bit A/D converter and stored in the computer memory for post-processing. Hardcopies of the signal were obtained using a strip chart recorder (HP 77026 Sanborn Plotter) and an Axiom EX-850 Video Printer for further examination. The schematic of the experimental set-up is shown in Figure 16.

Typical experimental results are shown in Figure 17 and the corresponding analytically predicted strains are shown in Figure 18. As one would expect, the exciting trapezoidal acceleration motion program can be observed both in the analytical and experimental results. From figures 17 and 18, the experimental and analytical results may be observed to show a highly favorable correlation in the profile of the dynamic response. Also, the analytically predicted peak strains show a good agreement (70 - 85%) with the experimentally recorded strains, thus indicating a good level of performance for the analytical model.

The dynamic response of the link was observed to be extremely sensitive to the value of the cycle time. Due to the absence of a hardware timer on board, the stepper motor time delays were generated by software using 6502 Assembly language. However, this was found to be a major handicap in

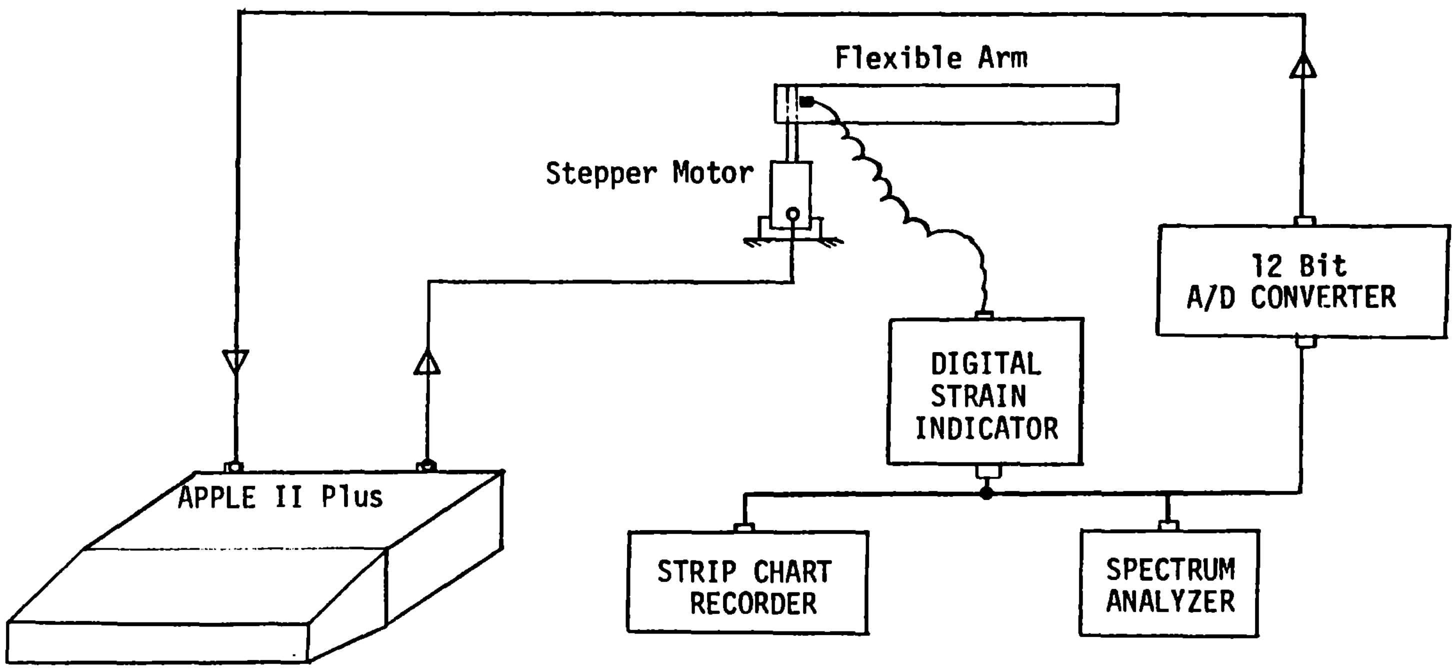

Figure 16. Schematic of the Experimental Set-up

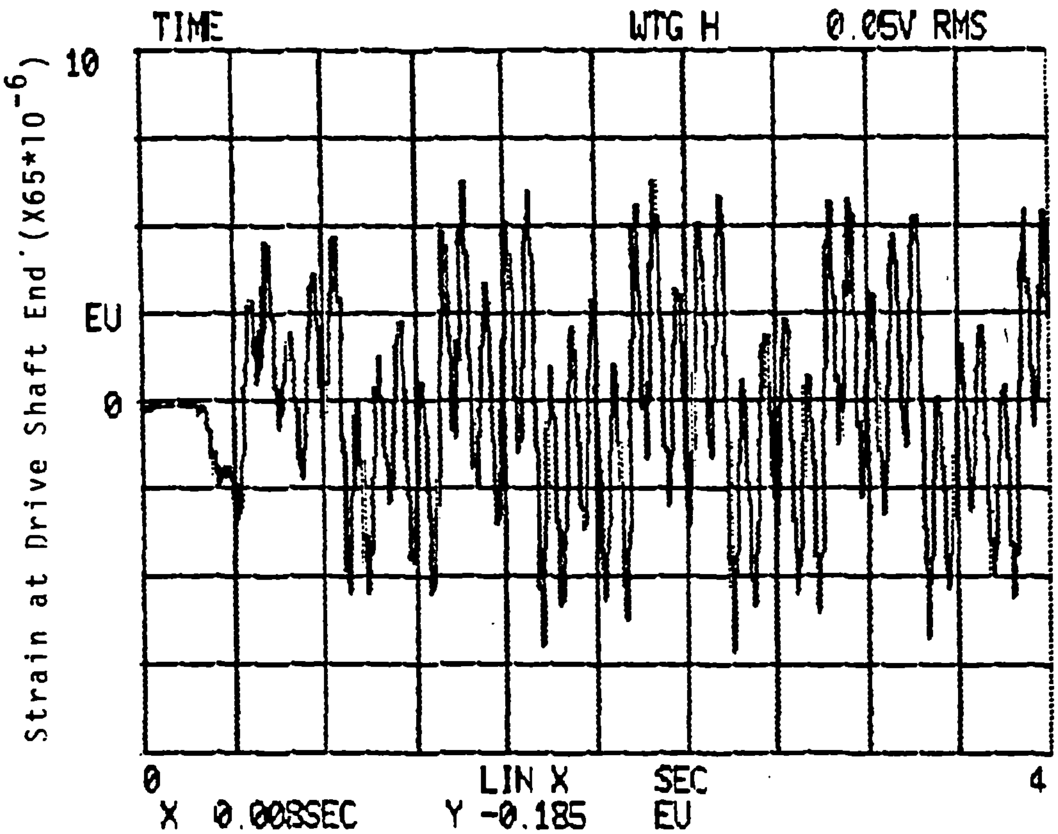

Figure 17. Experimentally Recorded Strains at Shaft End

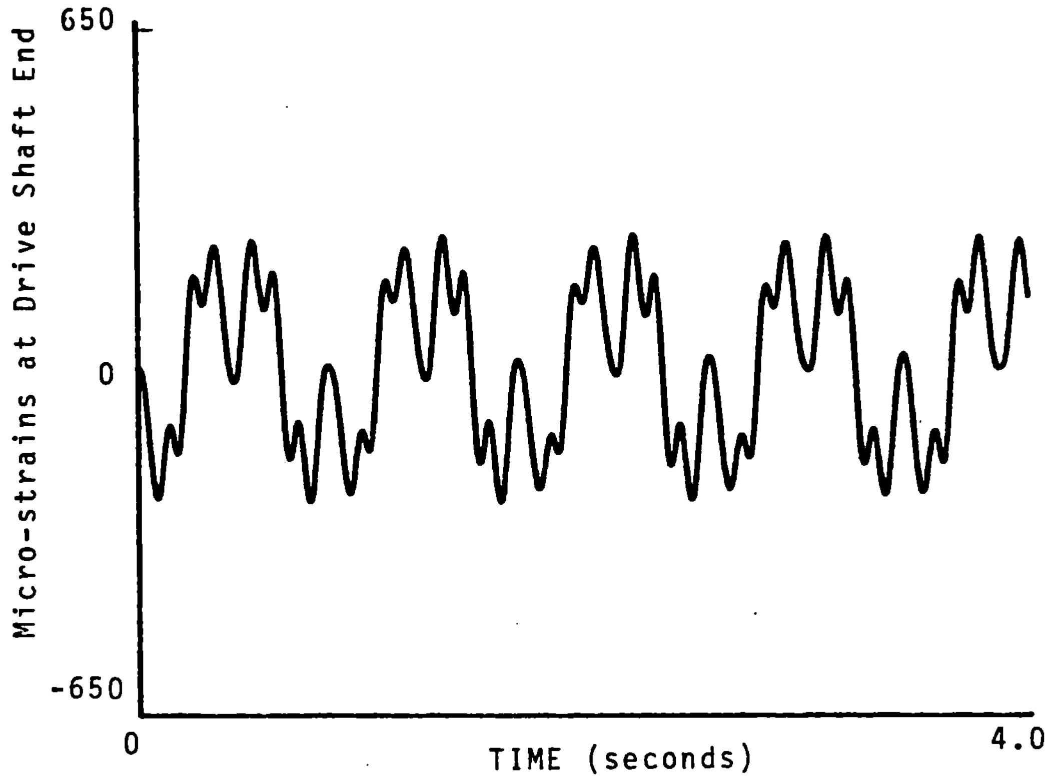

Figure 18. Analytically Predicted Strains at Shaft End

maintaining precise motor control. The lack of an interrupt timer required stalling the microprocessor that prevented proper execution of the other aspects of the experiment, such as strain data collection using an A/D converter. Although the use of a stepper motor was preferrable for the purpose of providing a least compliant actuator, the flexible arm was subjected to additional sources of vibrations. The agreement between the experimental and analytical results would be expected to improve if dedicated hardware could be developed for maintaining precise motor control and real-time data collection.

Quasi-Static Analysis of General Planar Configurations

In the previous section, we were able to obtain a quasi-static solution using an analytical expression, since the physical system consisted of a single link. However, the configuration of a manipulator normally undergoes gross changes while performing a task. In such cases, we can generate a quasi-static solution numerically, by ignoring the mass and damping terms in the system equations (2.25) as:

$$\{q_s\} = [K]_s^{-1} \{F\}_s \qquad \ldots \quad (3.6)$$

Should the numerical solution procedure be stable, the vibrational response should display an oscillatory behavior about this quasi-static solution (figure 13). This will then provide an additional source of reliability for the results obtained using the finite element developed in this study.

In this chapter, procedures such as eigenvalue analysis, static frame analysis, and quasi-static analysis were identified to verify the various components of the planar model developed in Chapter II. In the next chapter, this model will be used to determine the vibrational response of flexible, planar manipulator configurations.

CHAPTER IV

PLANAR MODEL RESULTS

Introduction

In this chapter, planar manipulators with revolute joints will be analyzed using the nonlinear model developed in chapter II. The objective here is to study the relative merits of the nonlinear model against linear and quasi-static models.

Linear Vibrational Model

In chapter II, the system equations were observed to be a set of nonlinear, coupled ordinary equations. This is due to the fact that the model has taken into account the coupling between the gross motion kinematics of the manipulator links and the deformations in the links (equations 2.4 - 2.9). On the other hand, if the system matrices are evaluated by ignoring such interactions, then the final set of equations will be linear, coupled ordinary equations.

$$[J]_s \{\ddot{q}\}_s + [C]_s \{\dot{q}\}_s + [K]_s \{q\}_s = \{F\}_s \qquad \ldots (4.1)$$

This model will be referred to as the 'linear model' in this study. The end-effector positioning errors predicted by the complete nonlinear model formulated in chapter II could then be compared to this linear model. From such an analysis, one may be able to critically examine the merits and limitations of these two models, for a given manipulator configuration.

Quasi-Static Model

A quasi-static solution can be obtained for the problem, by ignoring the inertia and damping terms in equation (4.1) as:

$$\{q\}_s = [K]_s^{-1} \{F\} \qquad \ldots \quad (4.2)$$

The value of the quasi-static solution is in that it provides a quick and reasonable approximation of the deformation time histories.[67,95] Further, the time history of the vibratory response would be expected to display an oscillatory behavior about this quasi-static solution. An approximate bound on the amplitude of the dynamic response can also be obtained from these solutions. However, these observations have been made for fairly rigid mechanisms and manipulators. It will be of interest to compare these solutions to the vibrational response of flexible manipulators operating at higher speeds.

Example Problems

Three example problems will be solved here. One of the studies will be for the case of a fairly flexible manipulator operating at high speeds in a gravity-free environment, similar to the Canadian Arm on the Space Shuttle. The second example will be a fairly rigid design under the influence of gravity, typical of currently available industrial configurations. The third example will be the case of a flexible manipulator with servo-compliant effects.

Flexible Planar Manipulator

A 2-R, planar, revolute-jointed manipulator (Figure 2) has been chosen with the following data for each of its links.

Link Length	=	1000 mm.
Area of Cross-section	=	350 mm^2
Area Moment of Inertia	=	10000 mm^4
Cross-section	:	Circular
Shear Coefficient (k_t)	=	0.8864
Material	:	Aluminium

Figure 19 shows a finite element discretization for the case of 2 elements per link. The number of elements were increased to monitor the convergence of the finite element. Cycloidal motion profiles (Figure 20) were used to command the motion at the two revolute joints. The maximum angular velocity and angular acceleration were respectively

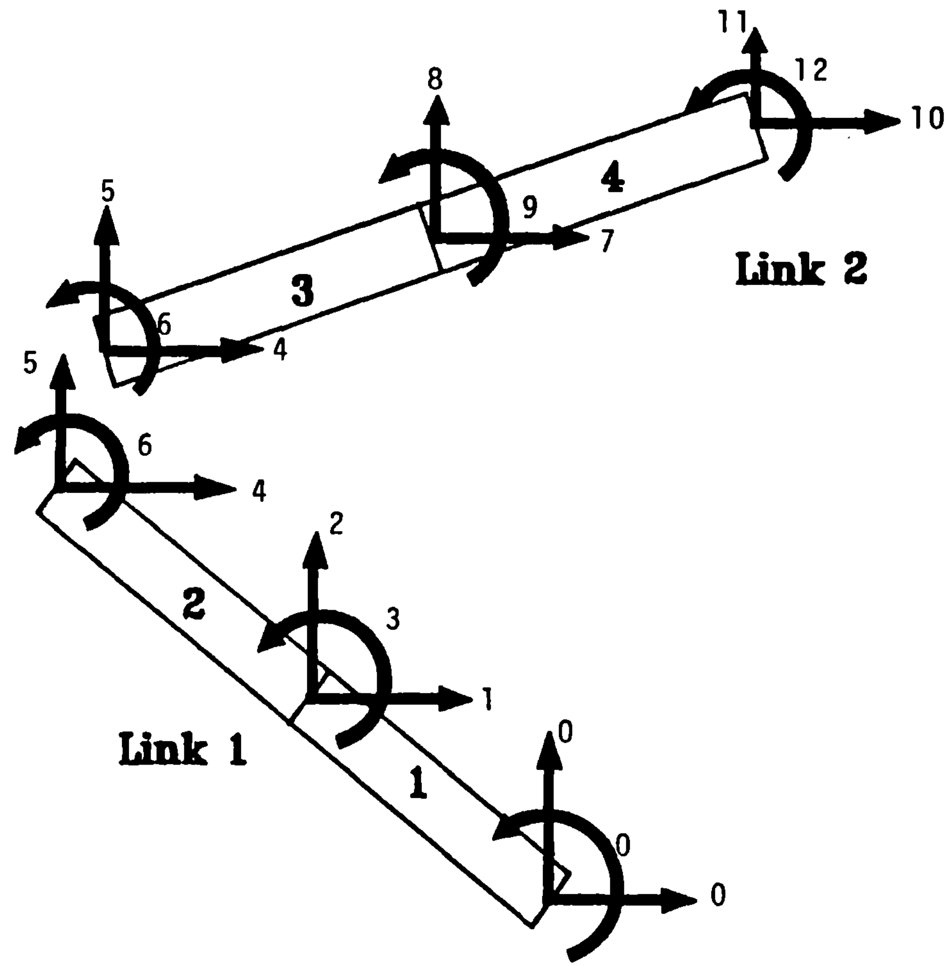

Figure 19. Finite Element Discretization for a Planar Case

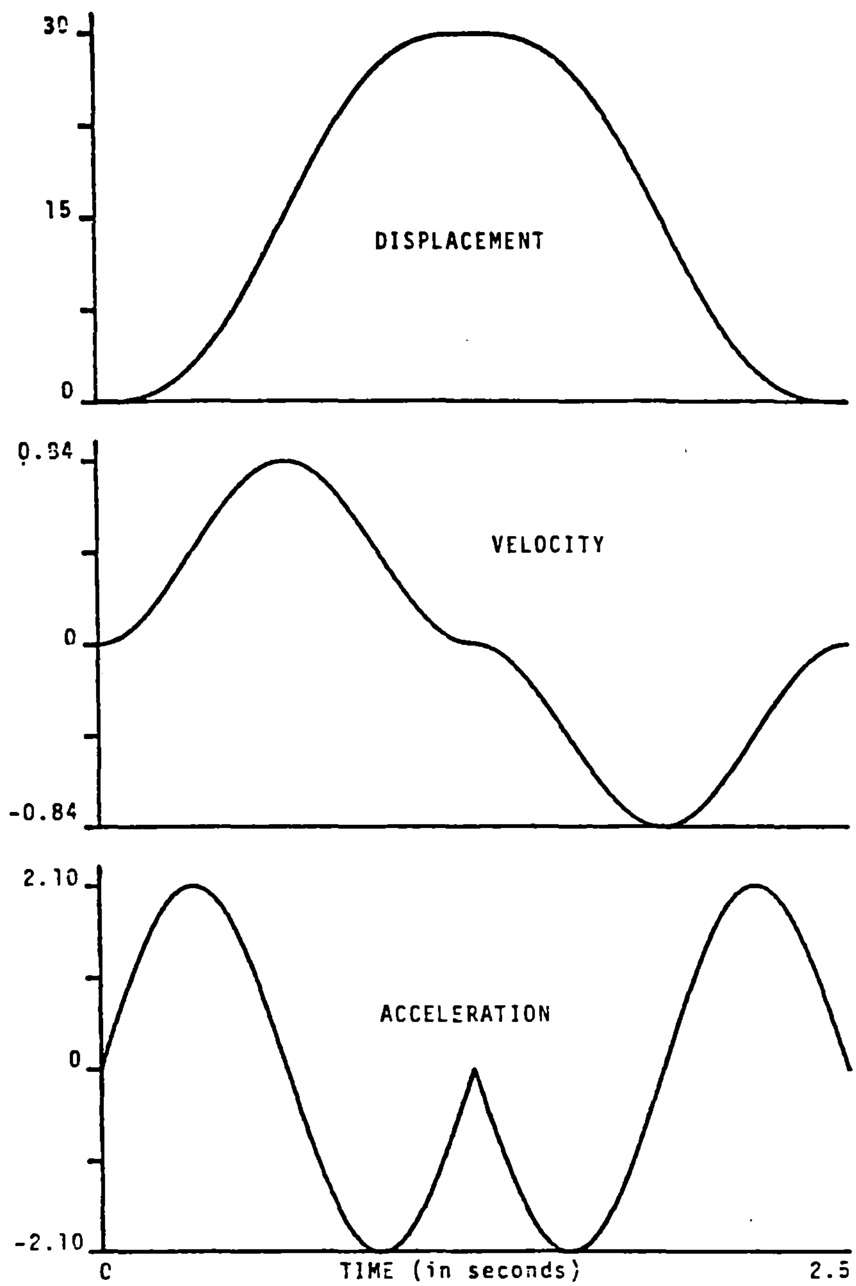

Figure 20. Joint Motion Profiles for Case-Study # 1

0.84 rad/sec and 1.05 rad/sec^2 respectively. As mentioned earlier, results were obtained for the linear, nonlinear, and quasi-static models. The horizontal and vertical end-effector deflections for the linear and nonlinear models have been compared in Figures 21 and 22. Referring to Figure 21 we could see that significantly higher peak amplitudes are registered by the nonlinear model. The amplitudes differ by 15 to 25% at the peaks. Also, the time histories of the results are different. There have been some efforts in the recent past towards the design of controllers taking the flexibility effects into consideration. For the case of flexible arms operating at high speeds, it appears that a linear model may not be adequate to predict the possible dynamic deformations in the system that need correction.

Figure 23 compares a quasi-static estimate of the horizontal displacement error at the end-effector with the vibrational response predicted by the nonlinear model. In this case, the quasi-static solution can be observed to be grossly underpredicting the displacement errors for the manipulator. On the other hand, the vibrational response is shown to display an oscillatory pattern about the quasi-static solution, indicating the stability of the numerical procedure used in obtaining the vibrational response.

Currently available controllers estimate the torque requirements in the system from the assumption that the

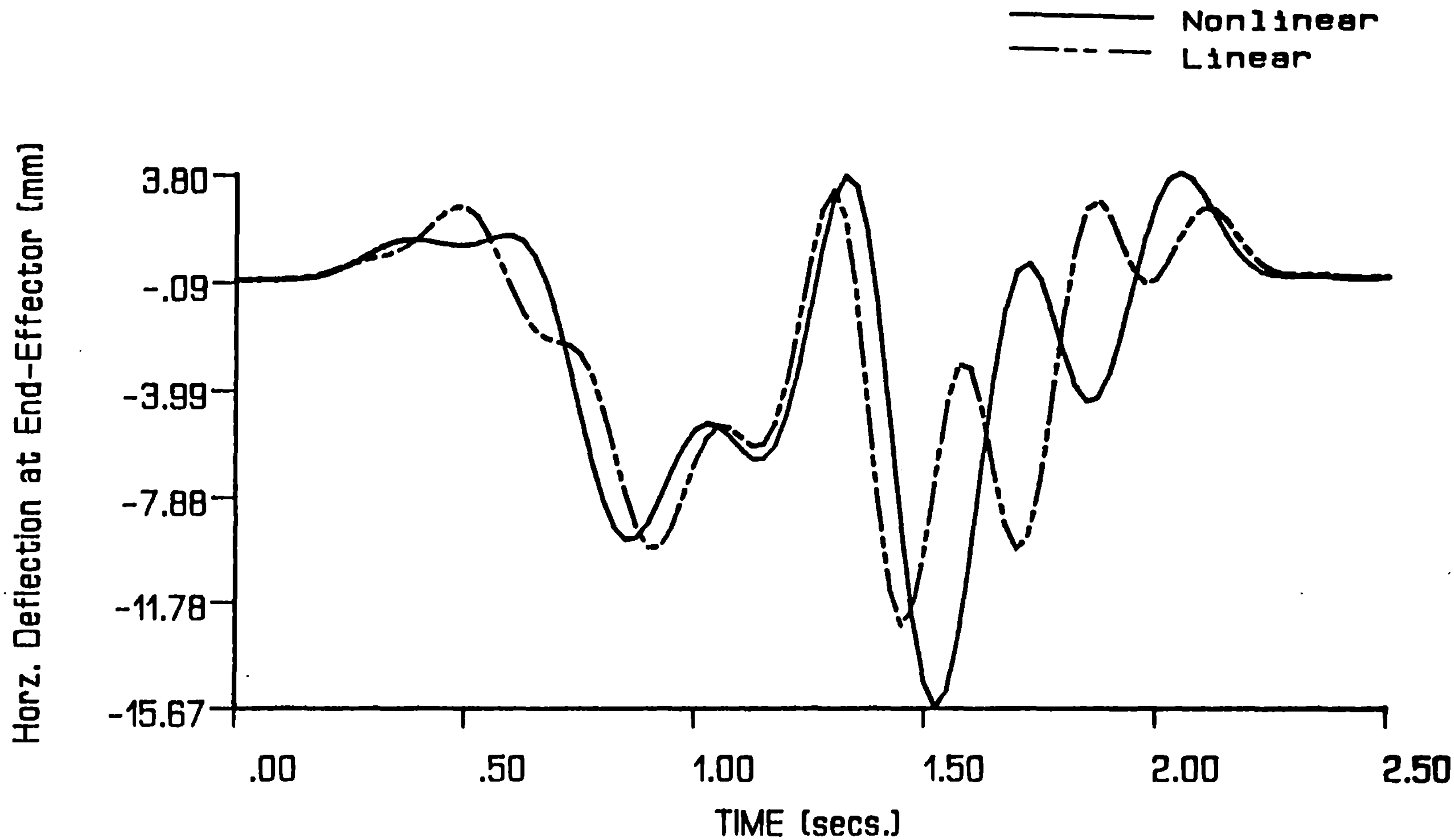

Figure 21. Horizontal End-Effector Deflection for Flexible Manipulator

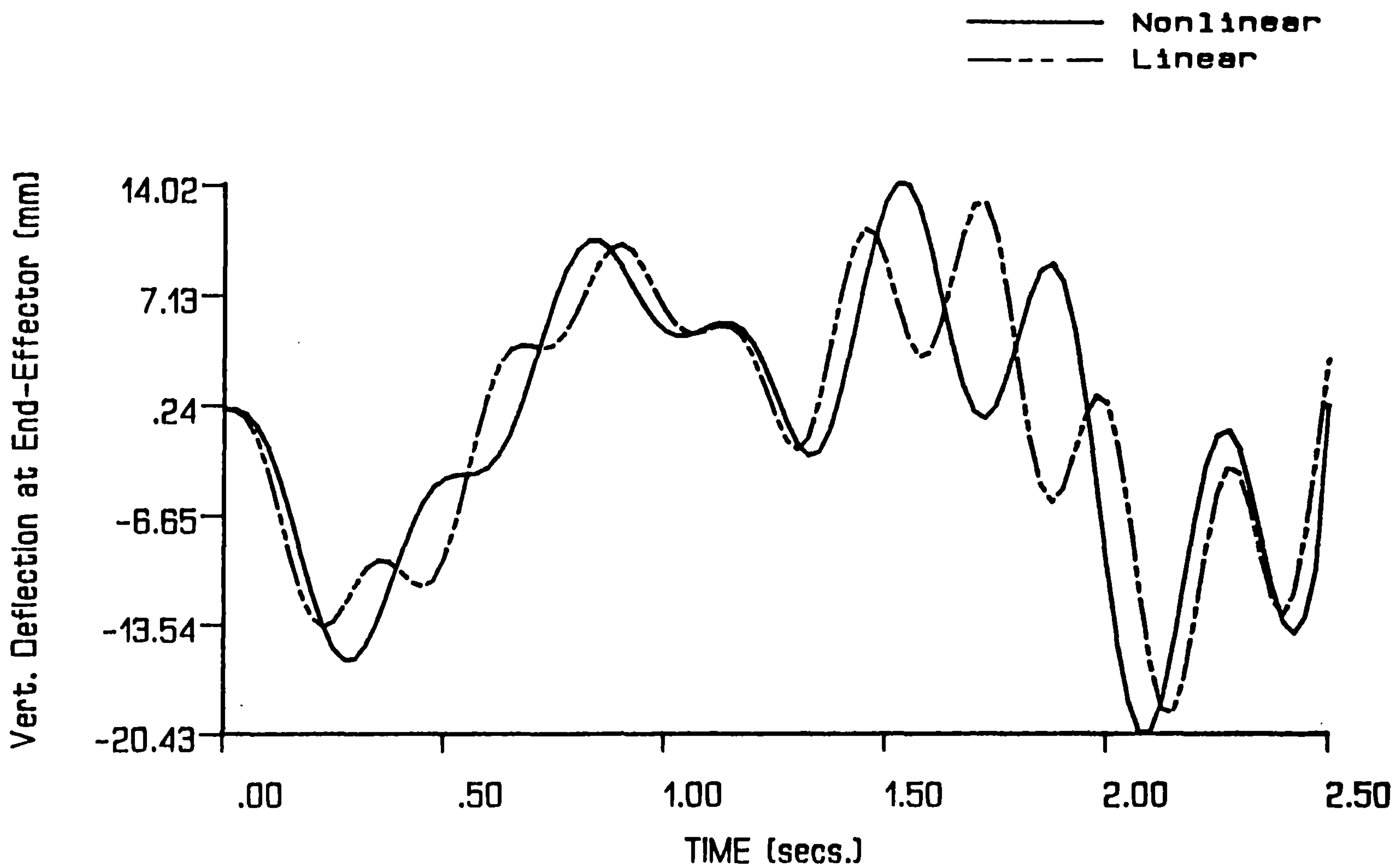

Figure 22. Vertical End-Effector Deflection for Flexible Manipulator

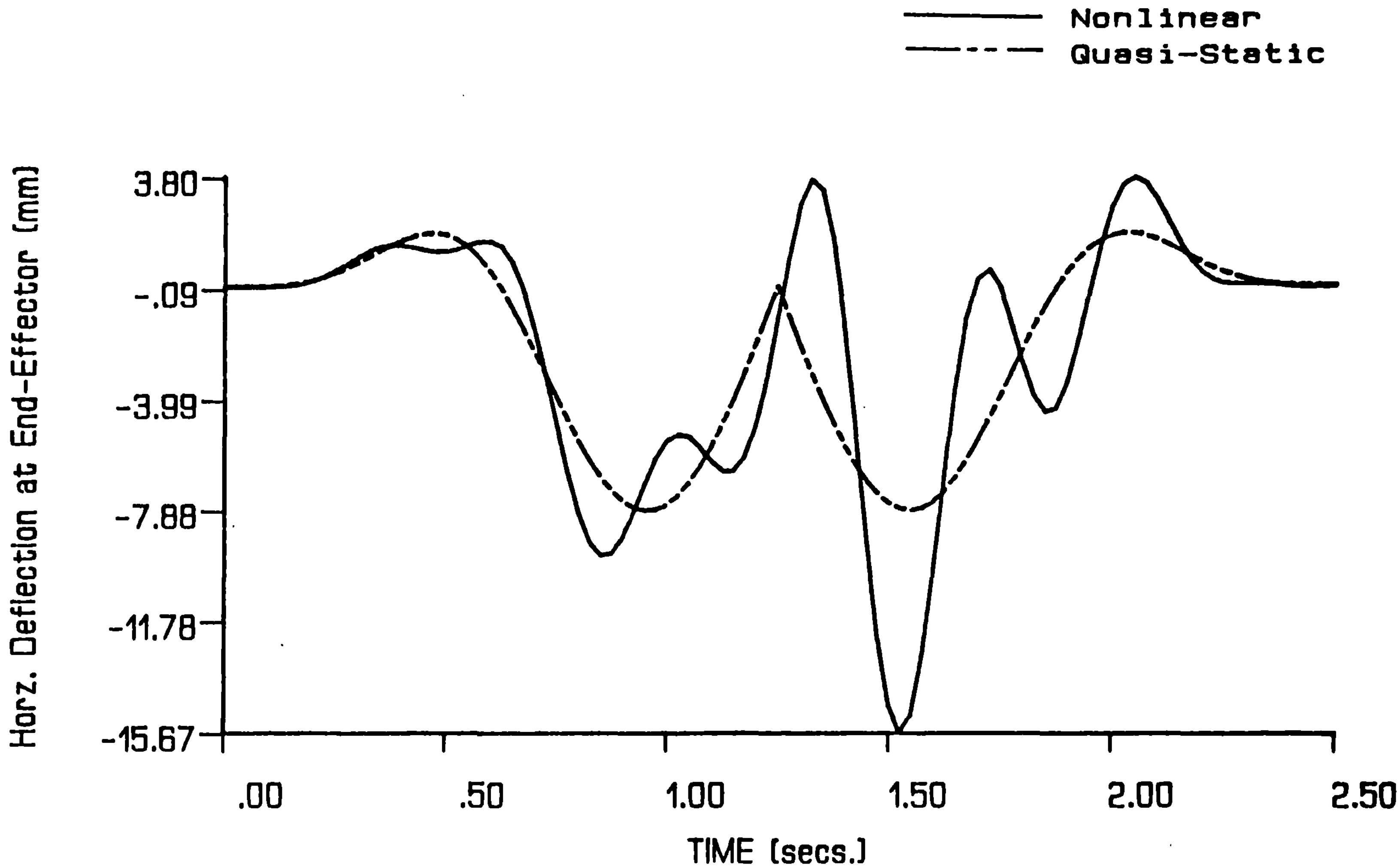

Figure 23. Comparison of Quasi-Static & Nonlinear Vibrational Models

links are rigid. If one were to consider the flexibility effects then the torque requirements at the joints may be significantly altered. Figure 24 compares the base joint torque computed using rigid-body dynamics and the torque requirements computed using the nonlinear model.

From Figure 24, we can observe that the torque requirements at the base joint have been significantly altered by the flexibility effects in the system. We can conclude from the above observations that the coupling between the gross motion kinematics and the deformations in the links are significant for the case of flexible manipulators operating at high speeds. This interaction should therefore be taken into account while designing the controllers for such configurations.

Rigid Planar Manipulators

A second example of planar, 2-R configuration will be considered here. The link dimensions are typical of commercial designs used in the industries. Currently available designs often resort to an arm-weight to payload ratio of 10:1. Hence, the gravity effects should not be ignored while analyzing such configurations. The dimensional data for the manipulator are:

Lengths of links	= 1000 mm, 1500mm
Cross-section	: Tubular
Outside Diameter	= 100 mm
Inside Diameter	= 94 mm

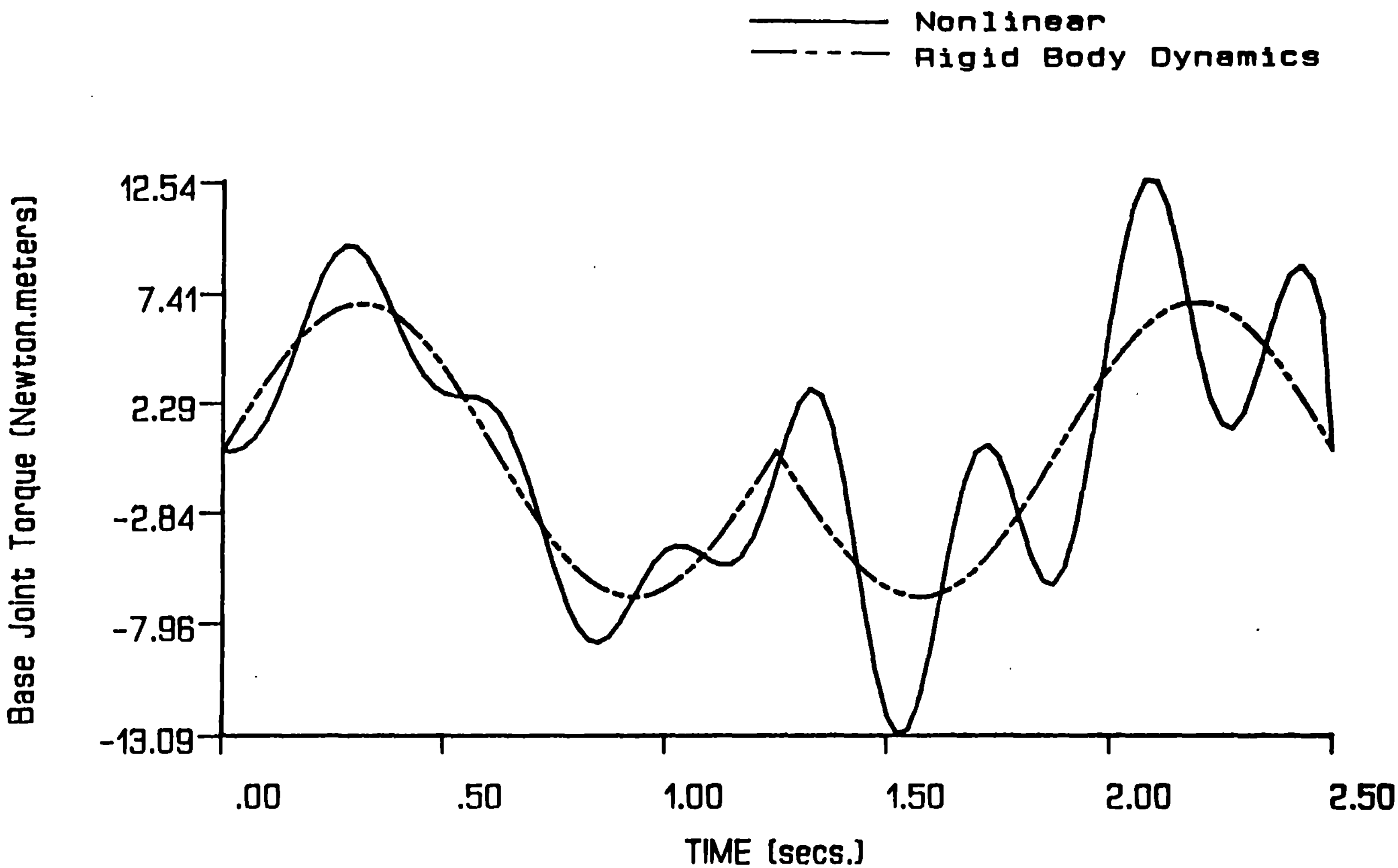

Figure 24. Comparison of Base Joint Torques for Rigid-Body Dynamics and Flexible Body Dynamics

Shear Coefficient = 0.54

Material : Steel

The commanded motion profiles for the joints were chosen from a normally preferred ones in the industry, namely, constant acceleration - constant velocity - constant deceleration - settling phase (dwell).[95] The motion profiles for the joints are shown in Figure 25.

The end-effector dynamic deflections have been plotted in Figures 26-29. Figure 28 compares the linear and nonlinear models. Also a viscous damping factor of 5% was added to the damping terms for the purpose of analysis. We can make the following observations from Figure 28.

(i) The end-effector deformations are of very small magnitude as one would expect in a conservatively (rigidly) designed industrial manipulator.

(ii) As compared to the linear model, the nonlinear model does not appear to register significantly higher peak amplitudes. Hence, for fairly rigid designs, one may not need to model the nonlinearity of the coupling between gross motions and flexibilities.

Figure 29 compares the end-effector vertical deformations for the linear, nonlinear and quasi-static models. We note that the quasi-static model compares very well with the nonlinear and linear models, particularly with a damping factor of 5%. Hence, a quasi-static model appears to be adequate, if one were to be interested in obtaining a quick approximation of the maximum peak amplitudes of the

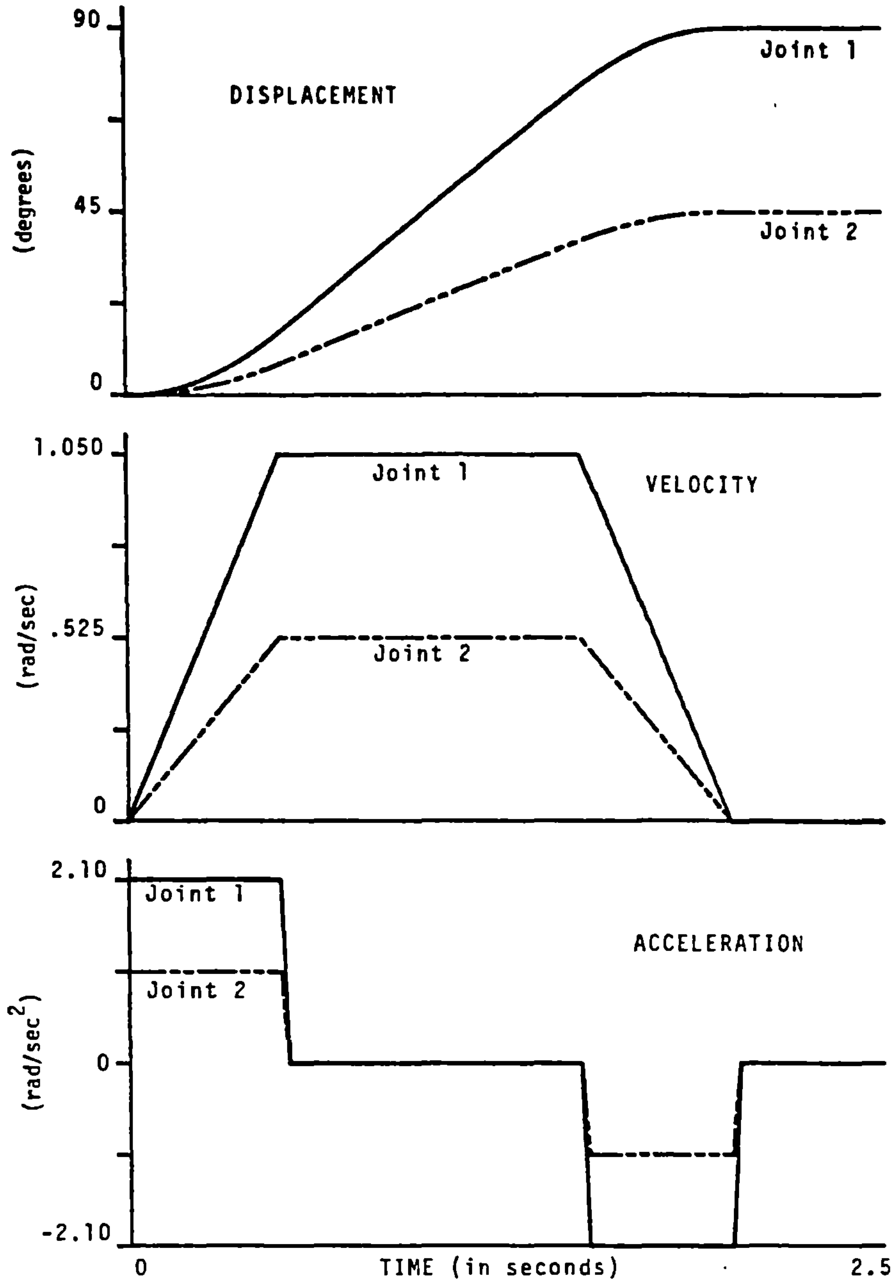

Figure 25. Joint Motion Profiles for Case-Study # 2

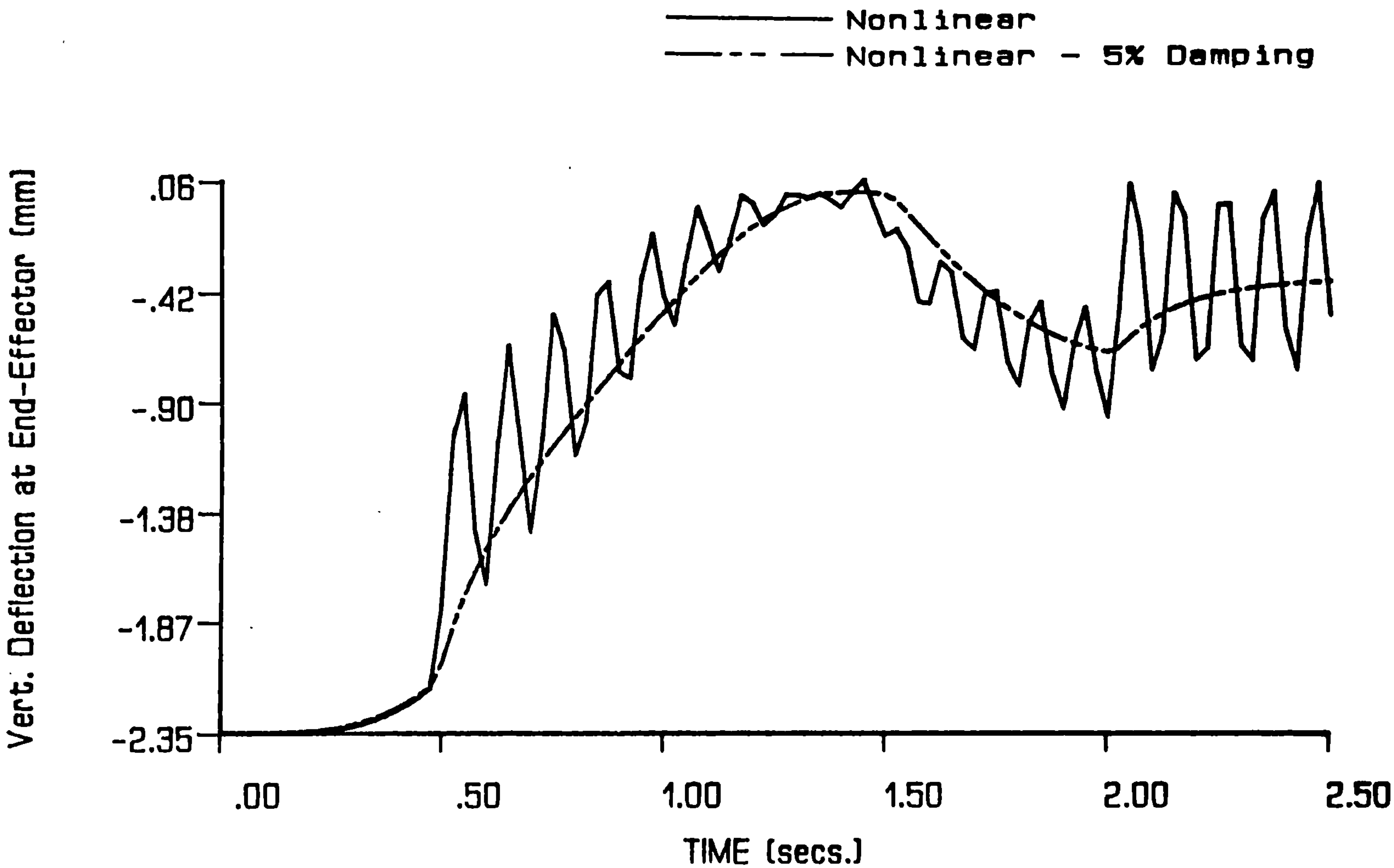

Figure 26. Vertical Deflection at End-Effector

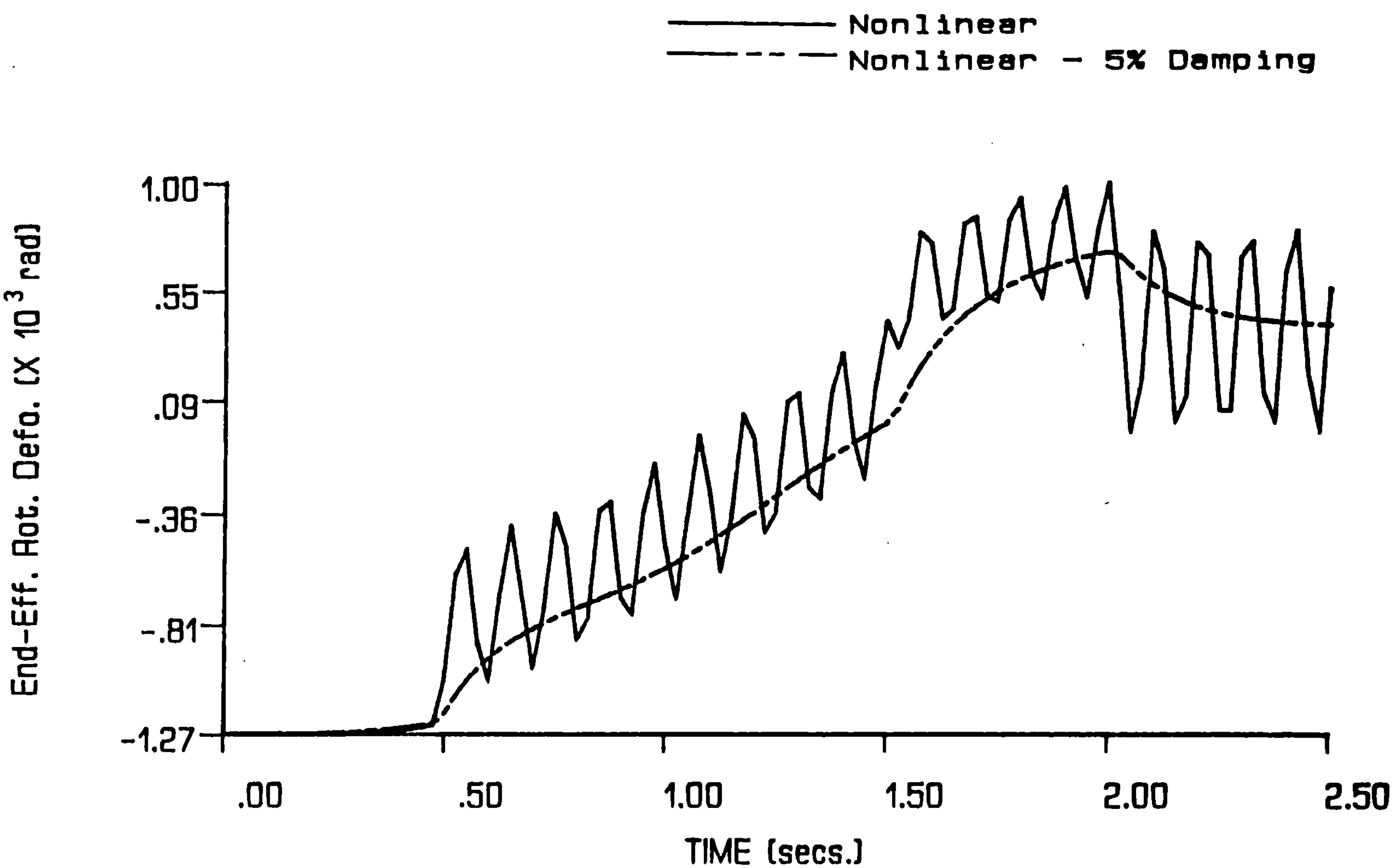

Figure 27. Rotational Deformation at End-Effector

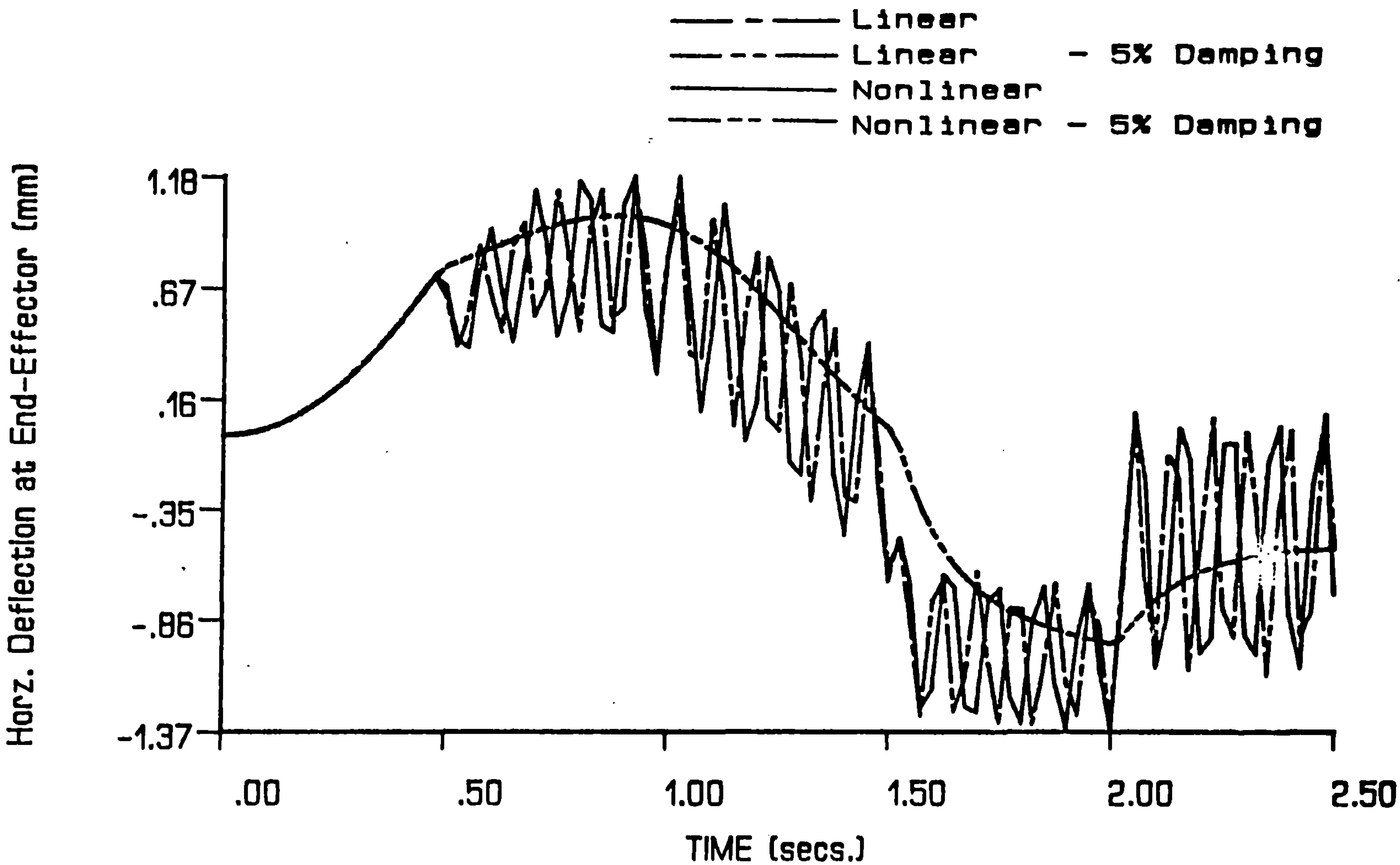

Figure 28. Horizontal Deflection at End-Effector

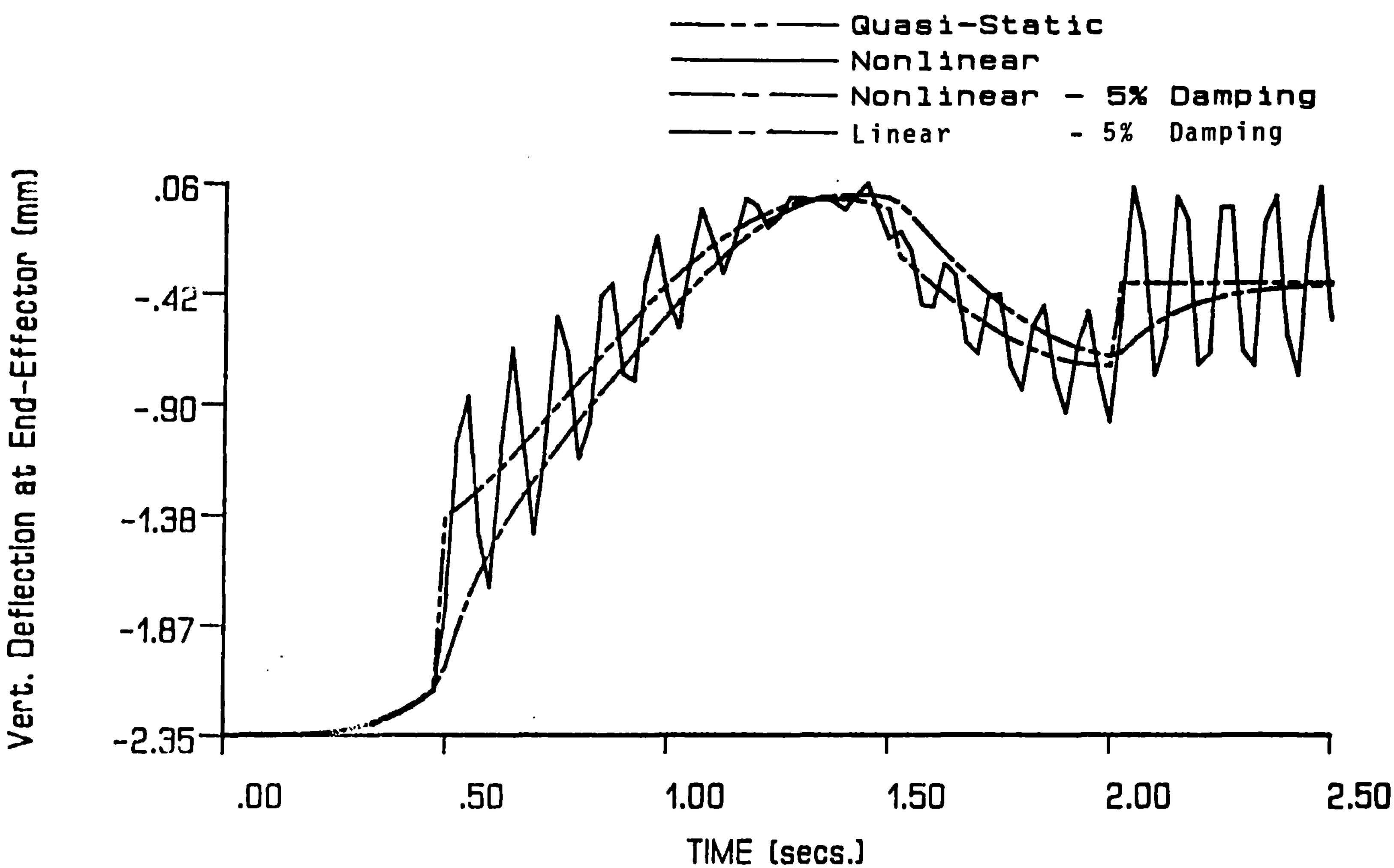

Figure 29. Comparison of Linear, Nonlinear, and Quasi-Static Models

dynamic deformations. This observation is consistent with the author's previous study in the area of mechanisms.[67]

Flexible Planar Manipulators With Effects of Servo-Compliance

A case of a flexible manipulator with joint servo-compliances will be analyzed here. Following the procedures presented in Chapter II, the nonlinear model will be augmented with the effects of joint servo-compliances and the resulting dynamic response of the flexible manipulator will be analyzed. The planar flexible manipulator presented in the first example was chosen. Maximum values of reflected inertia at the joints were computed using a rigid body analysis. These values were then used to compute terms representing servo-compliance. The tip error at the end-effector along the global horizontal axis is presented in Figure 30. The same has been compared to the tip errors predicted by conventional, linearized structural analysis. The tip error predicted by the nonlinear model may be observed to be significantly more than the conventional structural methodology.

In this chapter, three examples of planar, revolute-jointed manipulators were analyzed. The first example was the case of a fairly flexible manipulator operating in a gravity-free environment at high speeds. The link dynamic effects were specifically investigated in this example. For this case, the nonlinear model identified significantly

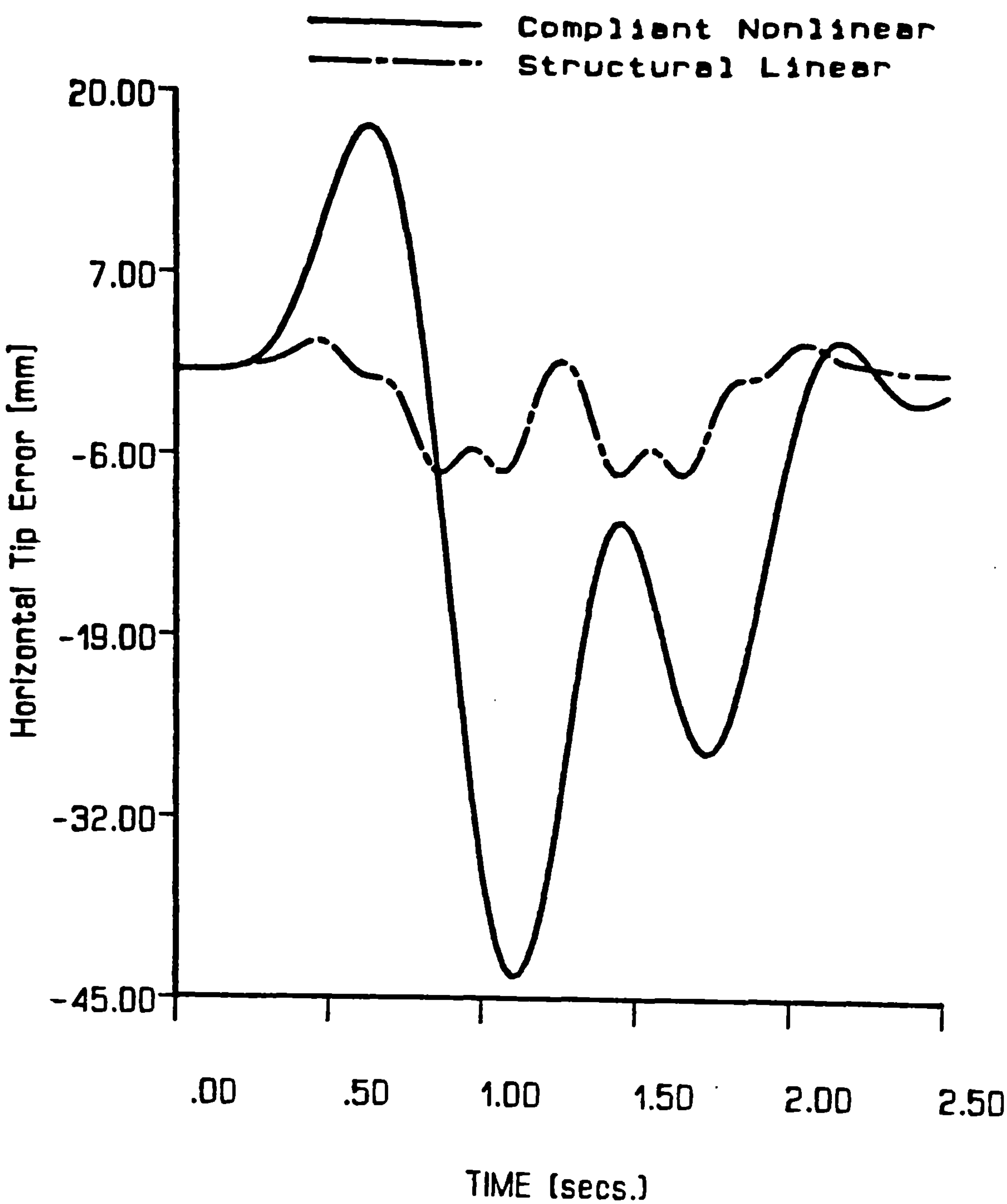

Figure 30. Tip Error Including Effects of Servo-compliance

higher dynamic deflections during the motion cycle. It appears that in such cases either a linear vibrational model or a quasi-static model may not be adequate in predicting the possible deformations in the system. The second example was the case of a conservatively designed rigid manipulator. In this case, all the three models (nonlinear, linear, and quasi- static models) did not differ appreciably from each other. The quasi-static model performed very well in terms of predicting a quick and fairly accurate time history of the deformation. Hence, this model may be preferred for rigid designs from the perspective of computational advantages. The importance of the effects of servo-compliances was investigated in the third example. For conservatively estimated values of these compliances (position and rate feedback gain values), the tip error at the end-effector was found to be significantly affected. Hence, there is a strong need to model these parameters in investigating the dynamic response of flexible manipulators with servo-drives.

The above results emphasize the need for an accurate modeling of the system interactions (between gross motion kinematics and flexibilities) when the manipulators are designed lighter and more flexible. The nonlinearity of these interactions are likely to be more complex, in the case of spatial manipulators executing tasks in a three-dimensional workspace. The modeling procedures for such manipulators will be developed in the next chapter.

CHAPTER V

SPATIAL MANIPULATORS

Introduction

Methodologies will be developed in this chapter for the analysis of spatial manipulators with revolute and prismatic joints. These manipulators normally execute tasks in a three-dimensional workspace. An example of a spatial, revolute manipulator is shown in Figure 31. The model to be analyzed will take into account the complete nonlinear coupling between the three-dimensional nonlinear gross motions of the manipulator links and their elastic deformations. The governing equations of motion will be derived including the effects of rotatory inertia, transverse shear, and the effects of the gross non-linear motion of each of the links. A simple and efficient finite element will be developed for the manipulator links, using Timoshenko Beam Theory.

Problem Formulation

The methodology may be divided into the following five steps:

(1) Description of the manipulator configuration

(2) Formulation of an efficient procedure to derive the

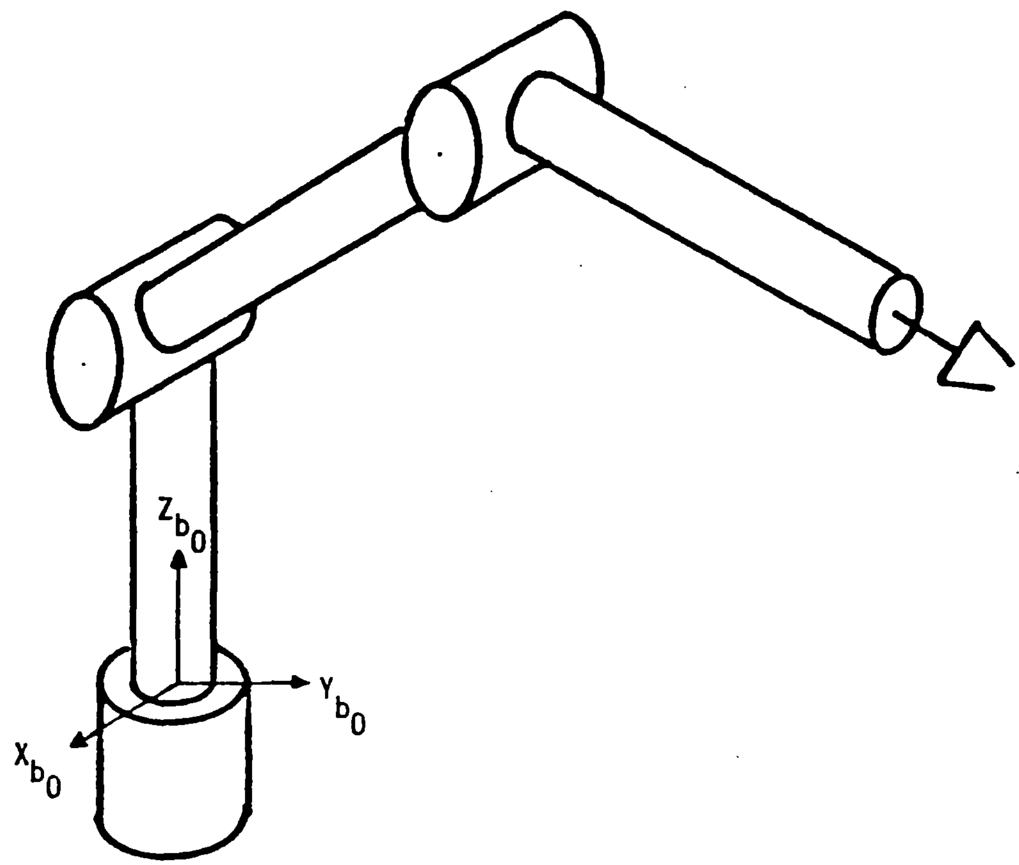

Figure 31. A Spatial Revolute Manipulator

kinematic and kinetic relations for a typical differential segment on a manipulator link

(3) Use of Galerkin's Technique to render the equations in an integral form suitable for a finite element scheme

(4) Development of a special finite element for the spatial manipulator, and

(5) Derivation and solution of system equations.

Description of the Manipulator

The description of the manipulator configuration is an important step in developing the model for the case of spatial manipulators. The choice of reference frames for each of the manipulator links should be made so as to facilitate not only an easy description of the spatial configuration, but also an efficient evaluation of the kinematics and dynamics of the manipulator. Studies in the area of manipulator rigid-body dynamics have commonly preferred to associate the Hartenberg-Denavit frame of reference with each of the manipulator links. The Hartenberg-Denavit parameters a_i, α_i, θ_i, and s_i (refer Figure 32) allow an easy description of the relative location and orientation of two orthogonal frames $X_1Y_1Z_1$ and $X_2Y_2Z_2$. However, when one is aiming at a solution procedure in terms of a generalized scheme such as finite elements, the problem description would be rendered easy, if the choice of reference frame is made relevant to the geometry of the link rather than from a description of the kinematic

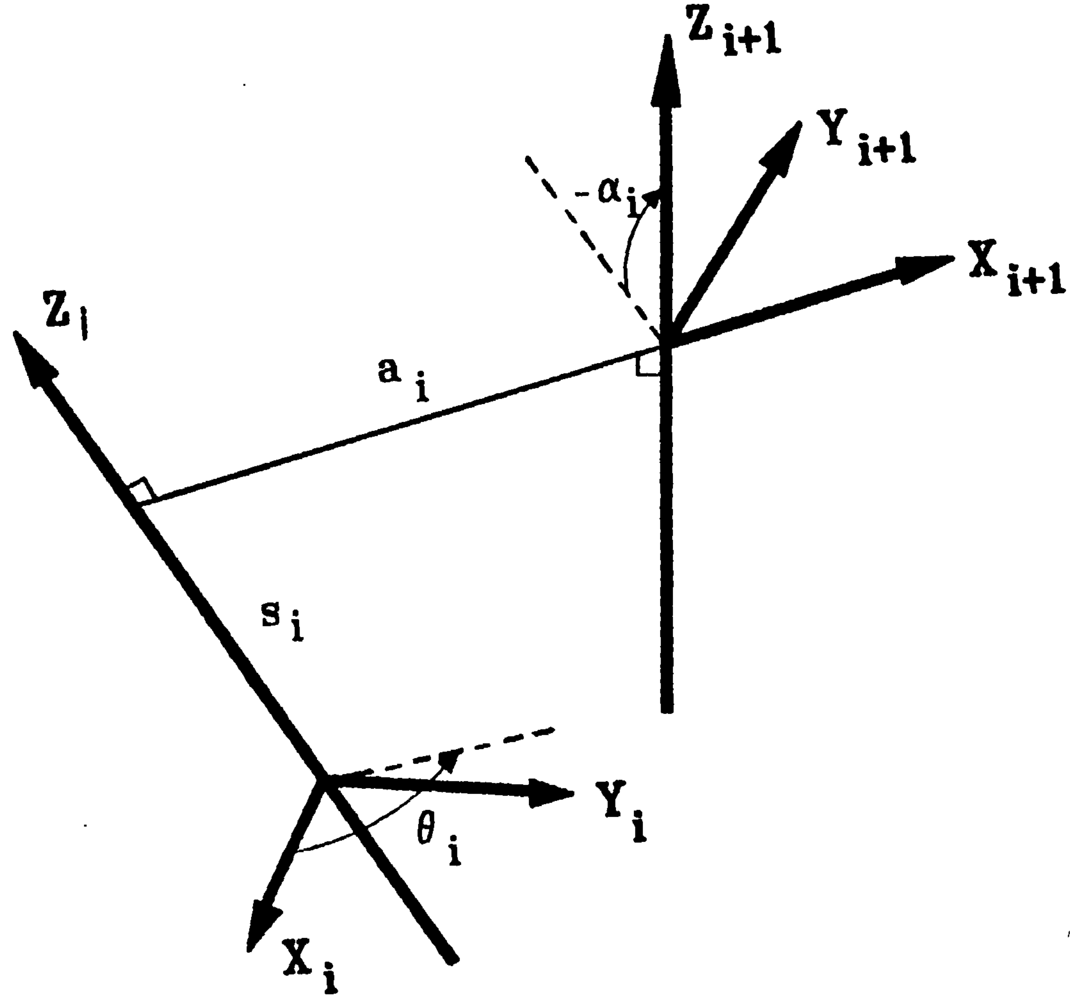

Figure 32. Hartenberg-Denavit Kinematic Parameters

parameters. It would be preferable, however, if we can identify a method by which we could combine the merits of both the methods.

Let $(X_bY_bZ_b)_0$ be a ground reference frame attached to the base of the spatial manipulator as shown in Figure 33. For spatial configuration, the Z_{b_0} axis is chosen along the axis of the first joint. The manipulator configuration may consist of any number of links (1,...,n) connected by revolute and/or prismatic pairs. According to the notation used in this study, the $(i-1)^{th}$ link will be connected to the i^{th} link, by a kinematic pair at joint 'i'. Three orthogonal frames of reference will be attached to each of the manipulator links as shown in Figure 33. For the i^{th} link with a revolute pair at joint 'i', the frame $(X_bY_bZ_b)_i$ will be located at the proximal end of the link (proximal to the base of the manipulator) at joint 'i'. If joint 'i' is a prismatic pair, then the origin of the proximal frame will correspond to the instantaneous location of joint 'i', but rigidly attached to link 'i'. This will be referred to as the 'base reference' of the i^{th} link. Another frame of reference $(X_dY_dZ_d)_i$ will be located at the distal end of link 'i' at joint 'i+1'. This is the 'distal frame' of the i^{th} link. When the manipulator is in its undeformed state, the distal frame can be located by a pure translation of the base reference $(X_bY_bZ_b)_i$ along the effective physical length 'L_i' of the link. Also, the Z-axes of these frames will be chosen along a reference line on the link. Let $(H_xH_yH_z)_i$ be

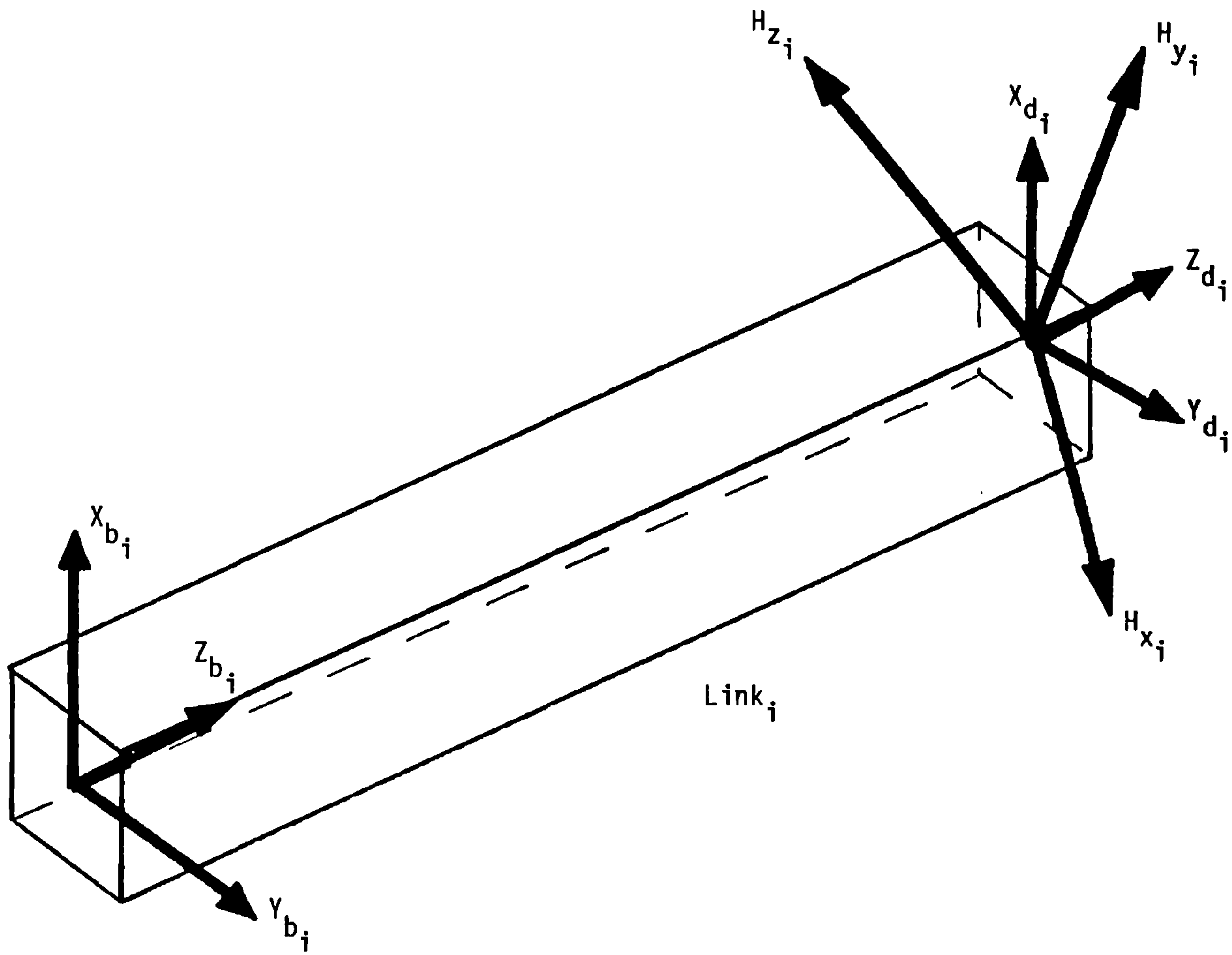

Figure 33. Link Reference Frames

located at the distal end of the link 'i' from a description of the kinematic parameters. This will be the Hartenberg-Denavit frame for link 'i'. The Hartenberg-Denavit frame will maintain a constant orientation with respect to the distal frame of the link $(X_d Y_d Z_d)_i$. This orientation can be easily described in terms of Euler angles, roll-pitch-yaw angles, or direction cosines.

Kinematic and Kinetic Relations

The procedure for deriving the kinematic and kinetic expressions for a differential segment on the i^{th} link may be divided into:

(i) Derivation of link (base reference frame) kinematics

(ii) Derivation of differential segment kinematics and

(iii) Derivation of differential segment kinetics

Link Kinematics

For the purpose of deriving the kinematic expressions, let us consider the i^{th} link of a serial manipulator shown in Figure 34. Let us identify a differential segment on this link, with its frame of reference 'xyz' and its center of mass 'G'. The following notations will be used in deriving the kinematic and kinetic expressions.

ρ	Density of the link material
A	Area of cross section of the link
$\underset{\sim}{I}$	Area Moment of Inertia Dyadic
$\vec{k}_{x_b}, \vec{k}_{y_b}, \vec{k}_{z_b}$	Unit vectors of the frame $(X_b Y_b Z_b)_i$

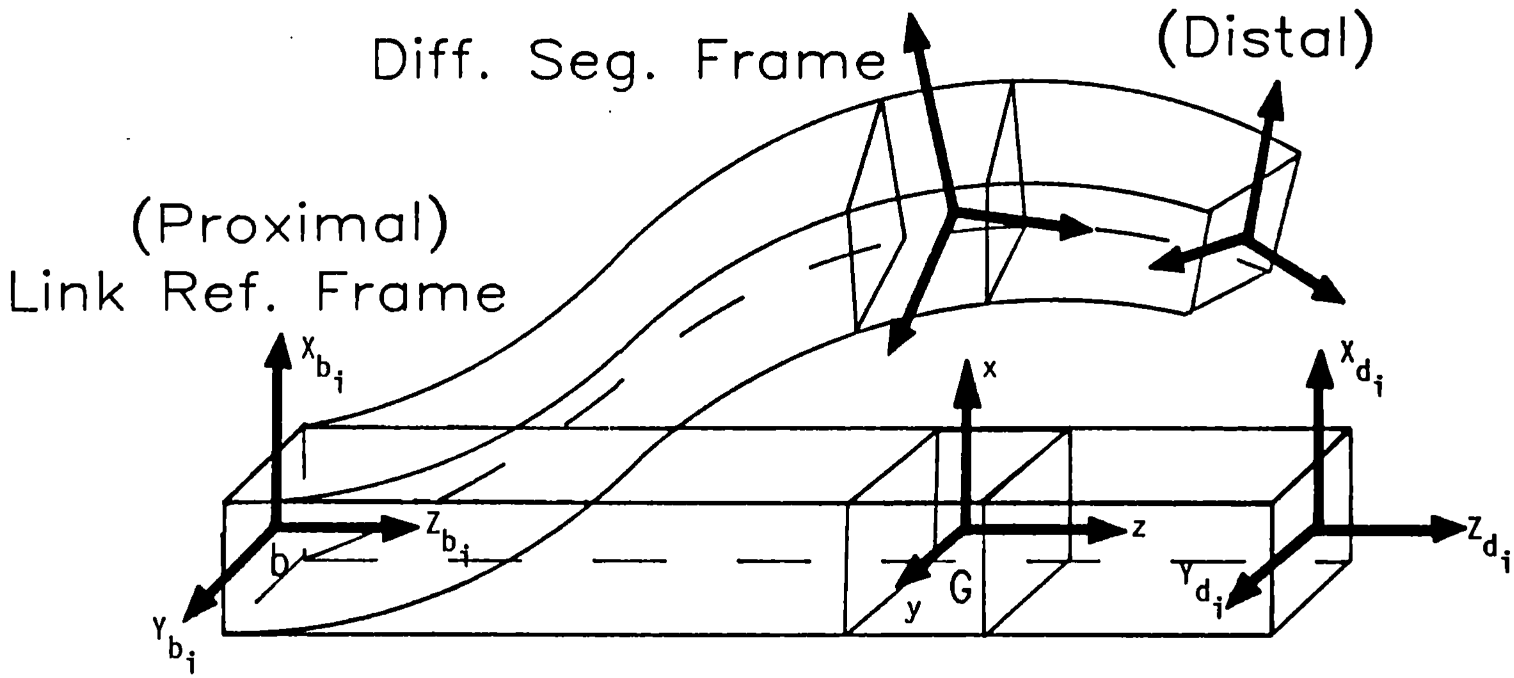

Figure 34 . Typical Link of a Spatial Manipulator

$\vec{k}_x, \vec{k}_y, \vec{k}_z$	Unit vectors of the frame (xyz)
u_x, u_y, u_z	Deformational displacements for the differential segment along the axes of the $(X_b Y_b Z_b)_i$ frame.
$\theta_x, \theta_y, \theta_z$	Angular deformations for the differential segment about the axes of the $(X_b Y_b Z_b)_i$ frame
d_x, d_y, d_z	Deformational displacements of the distal frame along the axes of the $(X_b Y_b Z_b)_i$ frame
ξ_x, ξ_y, ξ_z	Angular deformations of the distal frame about the axes of the $(X_b Y_b Z_b)_i$ frame
$\vec{\omega}_b$	Absolute angular velocity of the $(X_b Y_b Z_b)_i$ frame
$\vec{\alpha}_b$	Absolute angular acceleration of the $(X_b Y_b Z_b)_i$ frame
$\vec{\omega}_d$	Relative angular velocity of the differential segment with respect to the $(X_b Y_b Z_b)_i$ frame
$\vec{\alpha}_d$	Relative angular acceleration of the differential segment with respect to the $(X_b Y_b Z_b)_i$ frame
$\vec{\omega}_s$	Absolute angular velocity of the differential segment
$\vec{\alpha}_s$	Absolute angular acceleration of the differential segment

$\vec{a}_b$ Absolute linear acceleration of the origin 'O_b' of the $(X_b Y_b Z_b)_i$ frame.

Referring to Figure 35, let $[A_i]$ be the orientation matrix at joint 'i' between the distal frame of link 'i-1' and the proximal frame of link 'i'. For a revolute pair, this matrix will be a function of the commanded gross motion, whereas for a prismatic pair this will be a constant transformation. Therefore, we have,

$$\{X_{d_{i-1}}\} = [A_i]\,\{X_{b_i}\} \qquad \ldots (5.1)$$

$$[A_i] = [L_{1_{i-1}}]^{-1}\,[H_i]\,[L_{1_i}]\,[L_{2_i}] \qquad \ldots (5.2)$$

where, $[L_{1_i}]$ is a constant transformation at the distal end of the i^{th} link relating the Hartenberg-Denavit frame $(H_x H_y H_z)_i$, and the distal frame $(X_d Y_d Z_d)_i$. This can be easily described in terms of Euler angles, or direction cosines, or by a Roll-Pitch-Yaw transformation.

$$\begin{Bmatrix} X_{di} \\ Y_{di} \\ Z_{di} \\ 1 \end{Bmatrix} = [L_{1i}]^{-1} \begin{Bmatrix} H_{xi} \\ H_{yi} \\ H_{zi} \\ 1 \end{Bmatrix} \qquad \ldots (5.3)$$

$[L_{2_i}]$ is a transformation relating the proximal and distal frames of the i^{th} link in its undeformed state as:

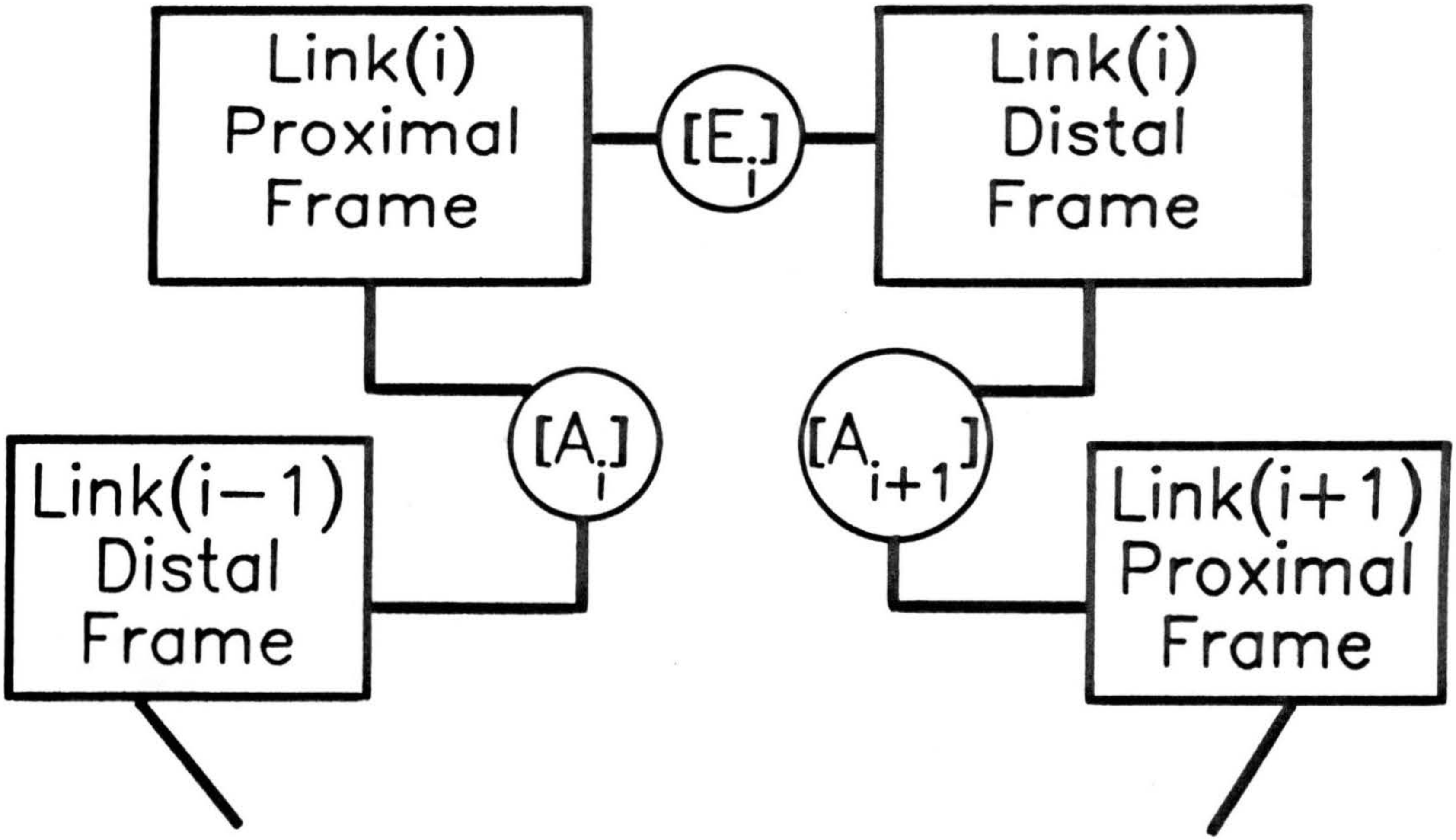

Figure 35. Extended Matrix Method

$$\begin{Bmatrix} X_{d_i} \\ Y_{d_i} \\ Z_{d_i} \\ 1 \end{Bmatrix} = [L_{2_i}] \begin{Bmatrix} X_{b_i} \\ Y_{b_i} \\ Z_{b_i} \\ 1 \end{Bmatrix} \qquad \ldots \quad (5.4)$$

where, $[L_{2_i}]$ is given by,

$$[L_{2_i}] = \begin{bmatrix} 1 & 0 & 0 & 0 \\ 0 & 1 & 0 & 0 \\ 0 & 0 & 1 & -L_i \\ 0 & 0 & 0 & 1 \end{bmatrix} \qquad \ldots \quad (5.5)$$

The effective physical length of the link (L_i) will be time varying in nature in the presence of a prismatic pair at joint 'i'. Let $[H_i]$ be the 4 X 4 transformation matrix between the Hartenberg-Denavit frames attached to the $(i-1)^{th}$ and the i^{th} links. If $\{H_{x_i}\}$ is the Hartenberg-Denavit coordinates associated with the i^{th} link, then

$$\{H_{x_{i-1}}\} = [H_i] \{H_{x_i}\} \qquad \ldots \quad (5.6)$$

$$[H_i] = \begin{bmatrix} \cos\theta_i & -\cos\alpha_i\sin\theta_i & \sin\alpha_i\sin\theta_i & a_i\cos\theta_i \\ \sin\theta_i & \cos\alpha_i\cos\theta_i & -\sin\alpha_i\cos\theta_i & a_i\sin\theta_i \\ 0 & \sin\alpha_i & \cos\alpha_i & s_i \\ 0 & 0 & 0 & 1 \end{bmatrix}$$

$$\ldots \quad (5.7)$$

Apart from the gross motion, referring to Figure 36, let $[E_i]$ represent the transformation due to the deformation

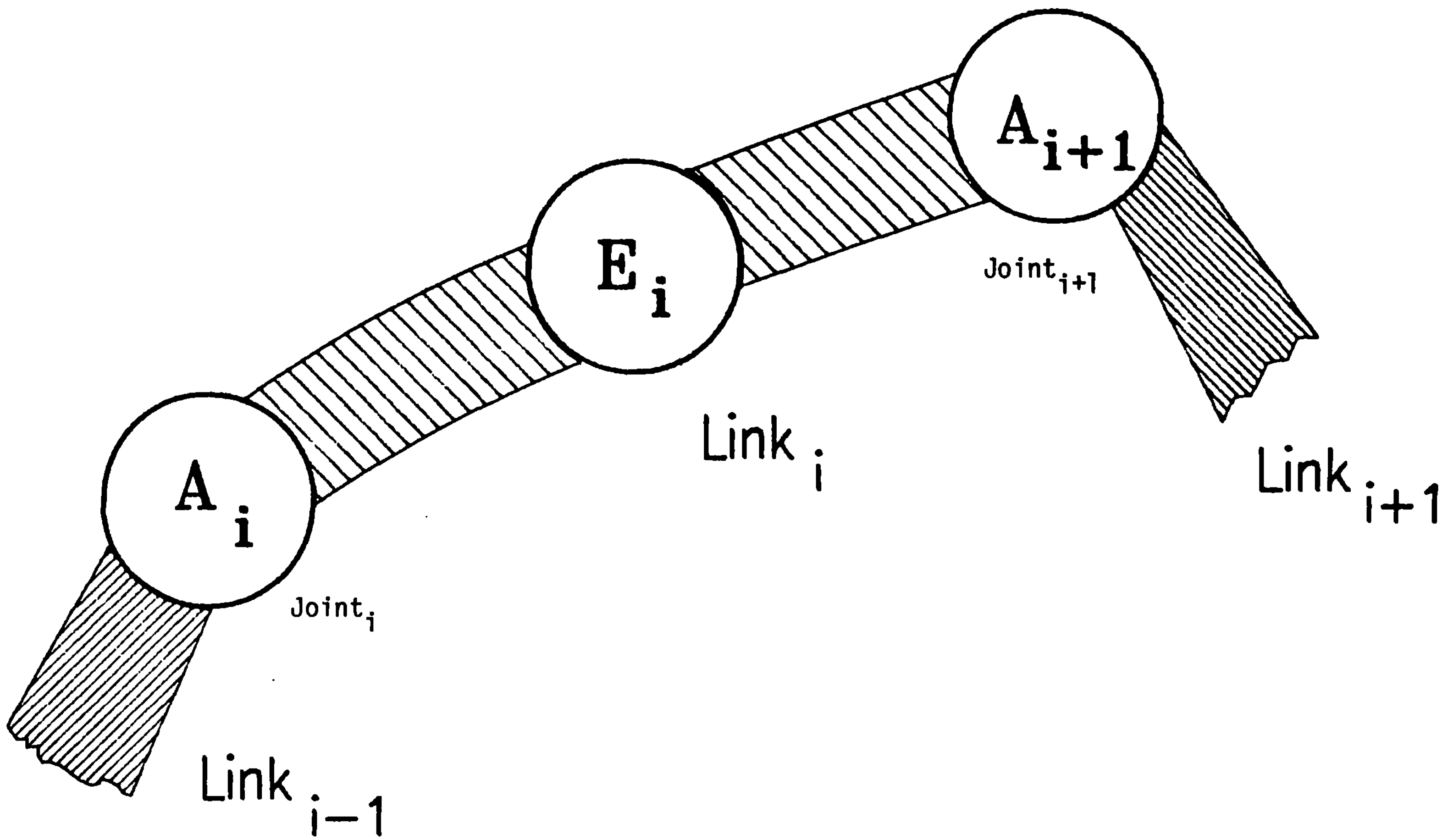

Figure 36. Link Transformations

of the link. This will locate the distal frame with respect to the proximal frame of the link when the link undergoes deformation due to elastic effects. For small perturbations of the distal frame from its rigid-body position, one may model the shape-deformation transformation $[E_i]$ as a differential transformation [73]. However, during the development of the nonlinear model, it was observed that such an approximation results in cumulative computational errors, while calculating the deformational velocities and accelerations. Hence, a Roll-Pitch-Yaw transformation was used using the angles ξ_x, ξ_y, and ξ_z as rotations about the $(X_b Y_b Z_b)_i$ axes, since the order of rotation is immaterial for small angles. Thus, the transformation $[E_i]$ is given by,

$$[E_i] = \begin{bmatrix} C_z C_y & C_z S_y S_x - S_z C_x & C_z S_y C_x + S_z S_x & d_x + L_i \xi_y \\ S_z C_y & S_z S_y S_x + C_z C_x & S_z S_y C_x - C_z S_x & d_y - L_i \xi_x \\ S_y & C_y S_x & C_y C_x & d_z + L_i \\ 0 & 0 & 0 & 1 \end{bmatrix} \quad \ldots \quad (5.8)$$

where, $C_x = \cos \xi_x \quad C_y = \cos \xi_y \quad C_z = \cos \xi_z$

$S_x = \sin \xi_x \quad S_y = \sin \xi_y \quad S_z = \sin \xi_z$

Using the above expressions, the transformation describing the position and orientation of any of the manipulator links $[T_i]$ can be given by,

$$T_i = E_0 . A_1 . E_1 . A_2 . \ldots . E_{i-1} A_i \quad \ldots \quad (5.9)$$

where, $[E_0]$ is an identity matrix.

Also, the derivatives of the above transformation can be obtained as,

$$\dot{T}_i = \sum_{j=1}^{i} [E_0.A_1.E_1.A_2...d(E_{j-1}.A_j)/dt....E_{i-1}A_i] \quad ... (5.10)$$

$$\ddot{T}_i = \sum_{j=1}^{i} [\ \sum_{\substack{k=1 \\ k\neq j}}^{i} [E_0.A_1.E_1.A_2...d(E_{k-1}.A_k)/dt.. \\ ....d(E_{j-1}.A_j)/dt..E_{i-1}A_i] + \\ E_0.A_1.E_1.A_2...d^2(E_{j-1}.A_j)/dt^2....E_{i-1}A_i] \quad ... (5.11)$$

For a revolute pair, the time derivatives of the transformations $[A_j]$ at joint 'j' can be obtained using the operator matrix $[Q_j]$ as below:

$$[\dot{A}_j] = [L_{1_{j-1}}]^{-1}\ \dot{\theta}_j\ [Q_j]\ [H_j]\ [L_{1_j}]\ [L_{2_j}] \quad ... (5.12)$$

$$[\ddot{A}_j] = [L_{1_{j-1}}]^{-1}\ [\ \ddot{\theta}_j\ [Q_j]\ [H_j] + \dot{\theta}_j^{\,2}\ [Q_j]\ [Q_j]\ [H_j]\ ]\ X \\ [L_{1_j}]\ [L_{2_j}] \quad ... (5.13)$$

For a revolute pair, the operator matrix $[Q_j]$ is given by,

$$[Q_j] = \begin{bmatrix} 0 & -1 & 0 & 0 \\ 1 & 0 & 0 & 0 \\ 0 & 0 & 0 & 0 \\ 0 & 0 & 0 & 0 \end{bmatrix} \quad ... (5.14)$$

For a prismatic pair at joint 'i', these derivatives will vanish since the orientation at joint 'i' is not time dependent. The absolute angular velocity and acceleration vectors of the proximal frame $\vec{\omega}_b$ and $\vec{\alpha}_b$ can be obtained in their matrix form from the above transformations as:

$$[\omega_b] = [c_i]^T [\dot{c}_i] [c_i]^T \quad \ldots (5.15)$$

$$[\alpha_b] = [c_i]^T [[\ddot{c}_i] [c_i]^T - [\omega_b] [\omega_b]] \quad \ldots (5.16)$$

The components of these absolute quantities must be resolved along the local reference frame axes.

Differential Segment Kinematics

The absolute velocity and acceleration vectors of the differential segment can be given as,

$$\vec{\omega}_s = \vec{\omega}_b + \vec{\omega}_d \quad \ldots (5.17)$$

$$\vec{\alpha}_s = \vec{\alpha}_b + \vec{\alpha}_d + \vec{\omega}_b \times \vec{\omega}_d \quad \ldots (5.18)$$

Also, the absolute acceleration of the center of mass 'G' of the differential segment may be written using the classical expression,

$$\vec{a}_G = \vec{a}_b + \vec{\omega}_b \times (\vec{\omega}_b \times \vec{r}) + \vec{\alpha}_b \times \vec{r} + 2\,\vec{\omega}_b \times \vec{v}_{rel} + \vec{a}_{rel} \quad \ldots (5.19)$$

where,
$$\vec{r} = u_x \vec{k}_{x_b} + u_y \vec{k}_{y_b} + (u_z+s)\,\vec{k}_{z_b}$$
$$\vec{v}_{rel} = \dot{u}_x \vec{k}_{x_b} + \dot{u}_y \vec{k}_{y_b} + \dot{u}_z \vec{k}_{z_b}$$
$$\vec{a}_{rel} = \ddot{u}_x \vec{k}_{xb} + \ddot{u}_y \vec{k}_{yb} + \ddot{u}_z \vec{k}_{zb} \quad \ldots (5.20)$$

Differential Segment Kinetics

The Newton-Euler equations can be written for the differential segment as:

$$\vec{F} = \rho A \vec{a}_G \, ds \quad \ldots (5.21)$$

$$\vec{M}_G = \dot{\vec{H}}_G = \rho\,[\,\underset{\sim}{I}\cdot\vec{\alpha}_s + \vec{\omega}_s \times (\,\underset{\sim}{I}\cdot\vec{\omega}_s\,)\,ds$$
$$= M_{G_x} \vec{k}_{x_b} + M_{G_y} \vec{k}_{y_b} + M_{G_z} \vec{k}_{z_b} \quad \ldots (5.22)$$

where, $\vec{F}$ is the resultant force acting on the differential segment, $\vec{a}_G$ is the absolute acceleration of 'G', $\vec{M}_G$ is the resultant moment about the center of mass, and $\dot{\vec{H}}_G$ is the rate of change of angular momentum of the differential segment about its center of mass.

The free-body diagram for the differential segment on the two bending planes is shown in Figure 37. From Timoshenko beam theory, the transverse shear can be included in the model as:

$$Q_x = k_t A \gamma (\partial u_x/\partial s - \theta_y)$$
$$Q_y = k_t A \gamma (\partial u_y/\partial s + \theta_x) \quad \ldots (5.23)$$

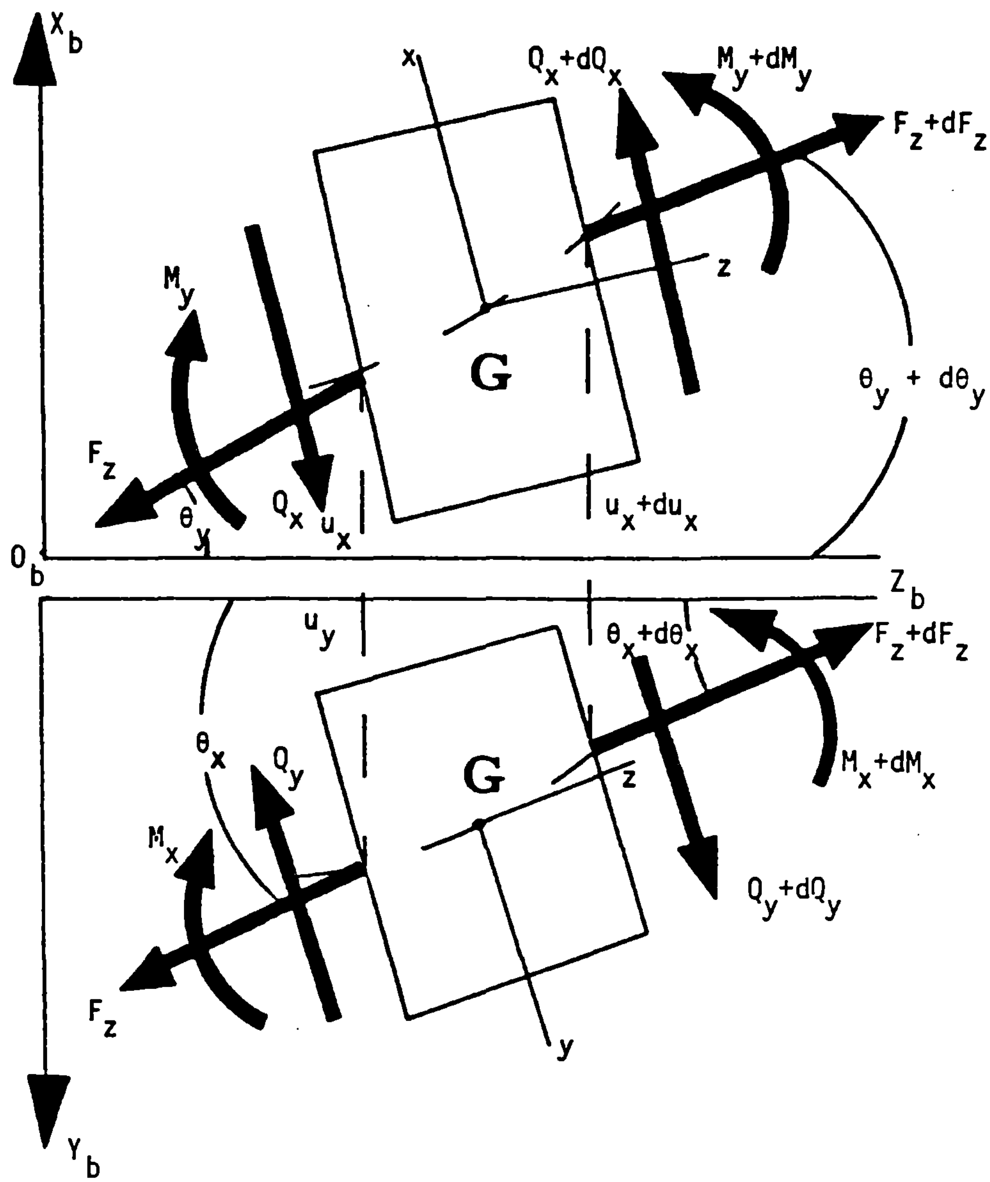

Figure 37. Free-Body Diagram of a Differential Segment

where, 'k_t' is the Timoshenko shear coefficient and 'Υ' is the shear modulus of the link material. Also, the moment-curvature relations yield,

$$
\begin{aligned}
M_x &= EI_x\, \partial\theta_x/\partial s \\
M_y &= EI_y\, \partial\theta_y/\partial s \\
M_z &= \Upsilon I_z\, \partial\theta_z/\partial s
\end{aligned}
\qquad \ldots (5.24)
$$

The governing equations for the differential segment can be written from the free-body diagram shown in Figure 37.

$$
\begin{aligned}
F_x^* &= \rho A a_x - \partial Q_x/\partial s - f_x &= 0 \\
F_y^* &= \rho A a_y - \partial Q_y/\partial s - f_y &= 0 \\
F_z^* &= \rho A a_z - AE\, \partial^2 u_z/\partial s^2 - f_z &= 0 \\
M_x^* &= M_{G_x} - \partial M_x/\partial s + Q_y &= 0 \\
M_y^* &= M_{G_y} - \partial M_y/\partial s - Q_x &= 0 \\
M_z^* &= M_{G_z} - \partial M_z/\partial s &= 0
\end{aligned}
\qquad \ldots (5.25)
$$

where f_x, f_y, and f_z are the distributed external forces (including gravity) per unit length of the link. The above partial differential equations will be solved using finite elements in the spatial domain and finite differences in the time domain. In order to be able to use the finite element method, we have to render the equations in an integral form and this will be accomplished using the Galerkin's method.

Galerkin's Method

Let δu_x, δu_y, δu_z and $\delta\theta_x$, $\delta\theta_y$, $\delta\theta_z$ be the respective arbitrary variations of the primary unknowns. Then, by Galerkin's method, we have the following integral:

$$\int_{s_1}^{s_2} [\, F_x^* \delta u_x + F_y^* \delta u_y + F_z^* \delta u_z + M_x^* \delta\theta_x + M_y^* \delta\theta_y + M_z^* \delta\theta_z \,]\, ds = 0 \qquad \ldots (5.26)$$

where, s_1 and s_2 locate the finite element on the i^{th} link. (Refer Figure 38). Substituting from equation (5.25) and after partially integrating some of the terms, we have:

$$\begin{aligned}\int_{s_1}^{s_2} \Big[& \rho A a_x \; \delta u_x + \rho A a_y \; \delta u_y + \rho A a_z \; \delta u_z \\ & - f_x \; \delta u_x - f_y \; \delta u_y - f_z \; \delta u_z \\ & + M_{G_x} \; \delta\theta_x + M_{G_y} \; \delta\theta_y + M_{G_z} \; \delta\theta_z \\ & + Q_x \; \delta(\partial u_x/\partial s - \theta_y) + Q_y \; \delta(\partial u_y/\partial s + \theta_x) \\ & + M_x \; \delta(\partial\theta_x/\partial s) + M_y \; \delta(\partial\theta_y/\partial s) + M_z \; \delta(\partial\theta_z/\partial s) \\ & + AE \; \partial u_z/\partial s \; \delta(\partial u_z/\partial s) \Big] \; ds = \\ & \Big[\delta u_x \; Q_x + \delta u_y \; Q_y + AE \; \partial u_z/\partial s . \delta u_z \\ & + \delta\theta_x \; M_x + \delta\theta_y \; M_y + \delta\theta_z \; M_z \Big]_{s_1}^{s_2} \qquad \ldots (5.27)\end{aligned}$$

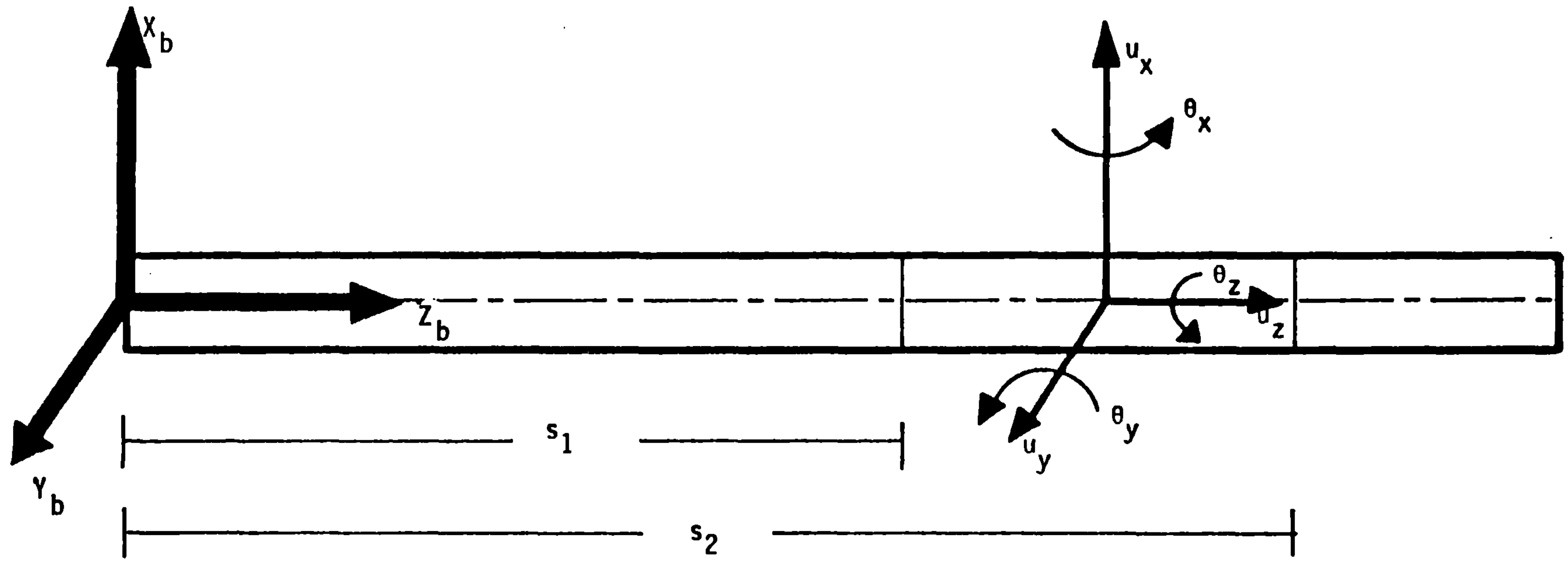

Figure 38. Typical Finite Element for Spatial Manipulator

We can observe that the highest order of partial derivatives in the integrand is of order '1'. Therefore, a simple linear interpolation is adequate for the shape functions in the development of the finite element.

Development of a Special Finite Element

For the development of the finite element, let us assume that the manipulator links are beams of uniform cross-sections. However, this assumption is easily relaxed for varying cross-sections, by treating the cross-sectional area A(s) and the Area Moment of Inertia ($\underset{\sim}{I}$ (s)) as a function of the location parameter 's'. Referring to Figure 38, we can express the displacements and rotations as a function of nodal displacements as:

$$\{u\}_e = [N]_e \{q\}_e \qquad \ldots (5.28)$$

where, $\{u\}_e$ is the vector of elemental deformations,

$$\{u\}_e = [\ u_x \quad u_y \quad u_z \quad \theta_x \quad \theta_y \ \theta_z\ ] \qquad \ldots (5.29)$$

and $\{q\}_e$ is the vector of elemental nodal displacements.

$$\{q\}_e = [(U_x)_1\ (U_y)_1\ (U_z)_1\ (\theta_x)_1\ (\theta_y)_1\ (\theta_z)_1 \\ (U_x)_2\ (U_y)_2\ (U_z)_2\ (\theta_x)_2\ (\theta_y)_2\ (\theta_z)_2\ ] \ldots (5.30)$$

For the spatial link, the shape matrix $[N]_e$ is given by,

$$[N]_e = \begin{bmatrix} N_1 & 0 & 0 & 0 & 0 & 0 & N_2 & 0 & 0 & 0 & 0 & 0 \\ 0 & N_1 & 0 & 0 & 0 & 0 & 0 & N_2 & 0 & 0 & 0 & 0 \\ 0 & 0 & N_1 & 0 & 0 & 0 & 0 & 0 & N_2 & 0 & 0 & 0 \\ 0 & 0 & 0 & N_1 & 0 & 0 & 0 & 0 & 0 & N_2 & 0 & 0 \\ 0 & 0 & 0 & 0 & N_1 & 0 & 0 & 0 & 0 & 0 & N_2 & 0 \\ 0 & 0 & 0 & 0 & 0 & N_1 & 0 & 0 & 0 & 0 & 0 & N_2 \end{bmatrix} \quad \ldots (5.31)$$

where,

$$N_1(s) = (s_2-s)/(s_2-s_1)$$
$$N_2(s) = (s-s_1)/(s_2-s_1) \quad \ldots (5.32)$$

Taking the variation on both sides of equation (5.28), we have,

$$\delta\{u\}_e = [N]_e\,\delta\{q\}_e \quad \ldots (5.33)$$

Substituting the above into equation (5.27) and performing the required differentiations and integrations, we can derive the governing equations of motion for an element on the i^{th} link of the spatial manipulator.

$$[J_e]\{\ddot{q}_e\} + [C_e]\{\dot{q}_e\} + [K_e]\{q_e\} = \{F_e\} \quad \ldots (5.34)$$

$[J_e]$ is the Elemental Inertia Matrix

$[C_e]$ is the Coriolis Matrix due to the motion of the reference frame $(X_b Y_b Z_b)_i$ of the i^{th} link.

$[K_e]$ is the Elemental Stiffness Matrix $= [K_c]_e + [K_b]_e$

$[K_c]_e$ is the Conventional Stiffness Matrix

$[K_b]_e$ is the stiffness matrix due to the motion of the frame $(X_b Y_b Z_b)_i$ of the i^{th} link.

$\{F_e\}$ is the element force vector due to external forces, accelerations, gravity, etc.

Derivation and Solution of System Equations

For the case of general spatial manipulators, the following issues should be considered while defining the finite element mesh and the corresponding system coordinates.

(i) The finite elements adjacent to the prismatic pair must be treated as 'variable-length' finite elements. Therefore, a typical link of the manipulator with a prismatic pair may have both 'constant-length' and 'variable-length' finite elements.

(ii) The finite elements adjacent to the actuators with servo-compliance, will have displacement compatibilities only along the normals to the slider axis. There will be no deformational compatibility along the slider axis.

(iii) In the presence of servo-compliance effects, the orientations of the system deformations (finite element nodal deformations) will also vary as the configuration of the manipulator changes during the task cycle.

(v) The algorithm should take into account possible singularities that may arise due to the nature of the 'variable-length finite elements' in the presence of prismatic pairs in the manipulator configuration.

The elemental equations are to be properly assembled along with the appropriate boundary conditions to obtain the final system equations, corresponding to a set of user-defined system coordinates. To start with, the element matrices in the local coordinates should be transformed to their corresponding form in global (system) coordinates. This will be achieved by using time-varying compatibility matrices $[\Phi_i(t)]$ and their derivatives as discussed for the planar case in Chapter II. However, in the spatial case, the compatibility matrix will be a 12 X 12 matrix, as against the 6 X 6 matrix for the planar case. In this study, these compatibility matrices are most conveniently obtained as combinations of 3 X 3 sub-matrices. These 3 X 3 matrices may be the orientation part of the transformation matrices ($[T_i]$) or the joint transformation matrices ($[A_i]$) or simply identity matrices. The first of the three situations occur when the system coordinates are described along the direction of a base global reference $(X_b Y_b Z_b)_0$, as for the case of non-compliant joints. The joint transformation matrices should be used in the presence of servo-compliance effects, when the system coordinates must be described along the local coordinates of the adjacent link at the kinematic pair. When the local and system coordinates are oriented along the same direction, the compatitibility matrix will simply become an identity matrix. These global element matrices will then be assembled using a variable correlation table (refer Chapter II) to yield the system equations. The final set of system equations will be in the form of:

$$[J(q_s)]_s \{\ddot{q}_s\} + [C(q_s,\dot{q}_s)]_s \{\dot{q}_s\} + [K(q_s,\dot{q}_s,\ddot{q}_s)]_s \{q_s\}$$

$$= \{F(q_s,\dot{q}_s,\ddot{q}_s)\} \qquad \ldots (5.35)$$

While modeling the servo-compliance, the system equations may be suitably augmented with the values of servo-stiffness and servo-damping terms as described for the planar case in Chapter II. These nonlinear ordinary differential equations will then be solved using a procedure of incremental linearization and equilibrium iteration.

Numerical Examples

To demonstrate the feasibility of the methodology and the algorithm that has been developed in this study, two cases of spatial manipulators will be analyzed in this section. The first example will be the case of a revolute spatial manipulator shown in Figure 31. The second case will be a general spatial R-P configuration as shown in Figure 39. In order to study the effect of the nonlinear kinematic coupling, the tip errors will be predicted by the complete nonlinear model taking into account the link flexibilities only.

Example 1

A 3-R spatial manipulator is chosen with the design parameters shown in Table III. Typical industrial motion profiles are used to drive the three revolute pairs, namely the hip, shoulder, and elbow joints as shown in Figure 40. A 5% damping factor is modeled in the system representative of the total damping and friction effects. Gravity effects are included in the analysis. The nonlinear and quasi-static solutions for the tip errors along the global horizontal and vertical directions have been shown in Figures 41 and 42. The stability of the nonlinear solution scheme may be observed from the fact that the nonlinear solution displays a bounded oscillatory pattern about the quasi-static solution.

Example 2

A R-P manipulator configuration will be analyzed here to demonstrate the capability of the developed methodology to analyze general spatial configurations that include both revolute and prismatic pairs. The design parameters for the manipulator are shown in Table IV. The flexible manipulator

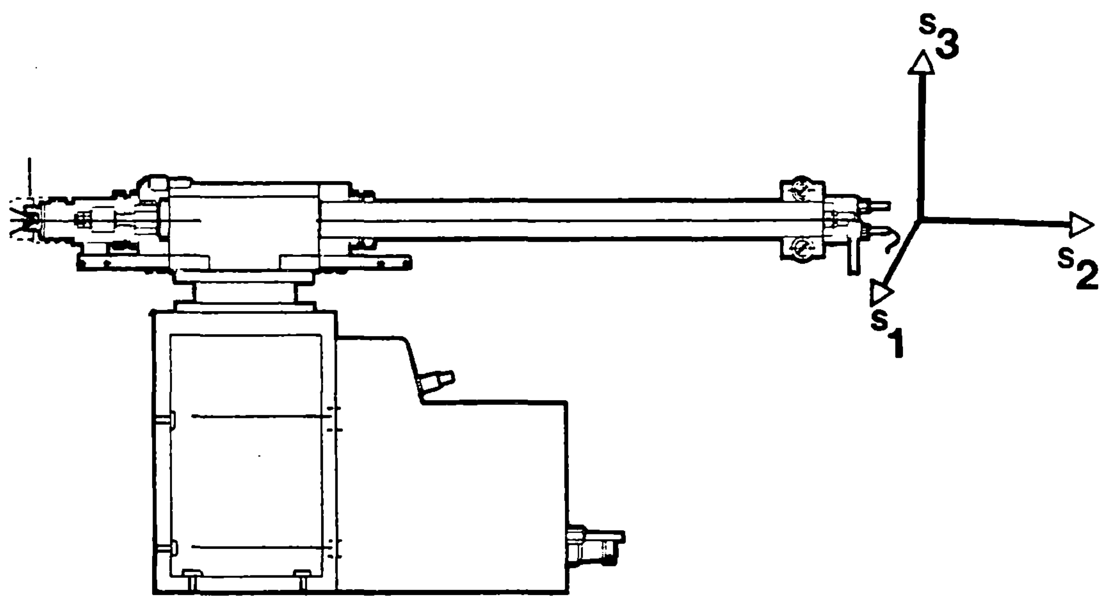

Figure 39. Industrial Manipulator with R- and P- Pairs

TABLE III

DESIGN PARAMETERS FOR 3-R MANIPULATOR

Sl. NO.	Link Length (mm)	Twist Angle (degrees)	Kink-Length (mm)
1	0.0	90.0	500.0
2	1000.0	0.0	0.0
3	1000.0	0.0	0.0

Area of cross section = 915 mm^2
Area Moment of Inertia = 1.08×10^6 mm^4
Material : Steel
Cross-section : Tubular

TABLE IV

DESIGN PARAMETERS FOR FLEXIBLE R-P MANIPULATOR

Sl. NO.	Link Length (mm)	Twist Angle (deg)	Kink Length (mm)	Rotation Angle (deg)
1	0.0	-90.0	500.0	Variable
2	0.0	0.0	Variable	0.0

Area of cross section = 315 mm^2
Area Moment of Inertia = 10000 mm^4
Material : Aluminium
Cross-section : Tubular

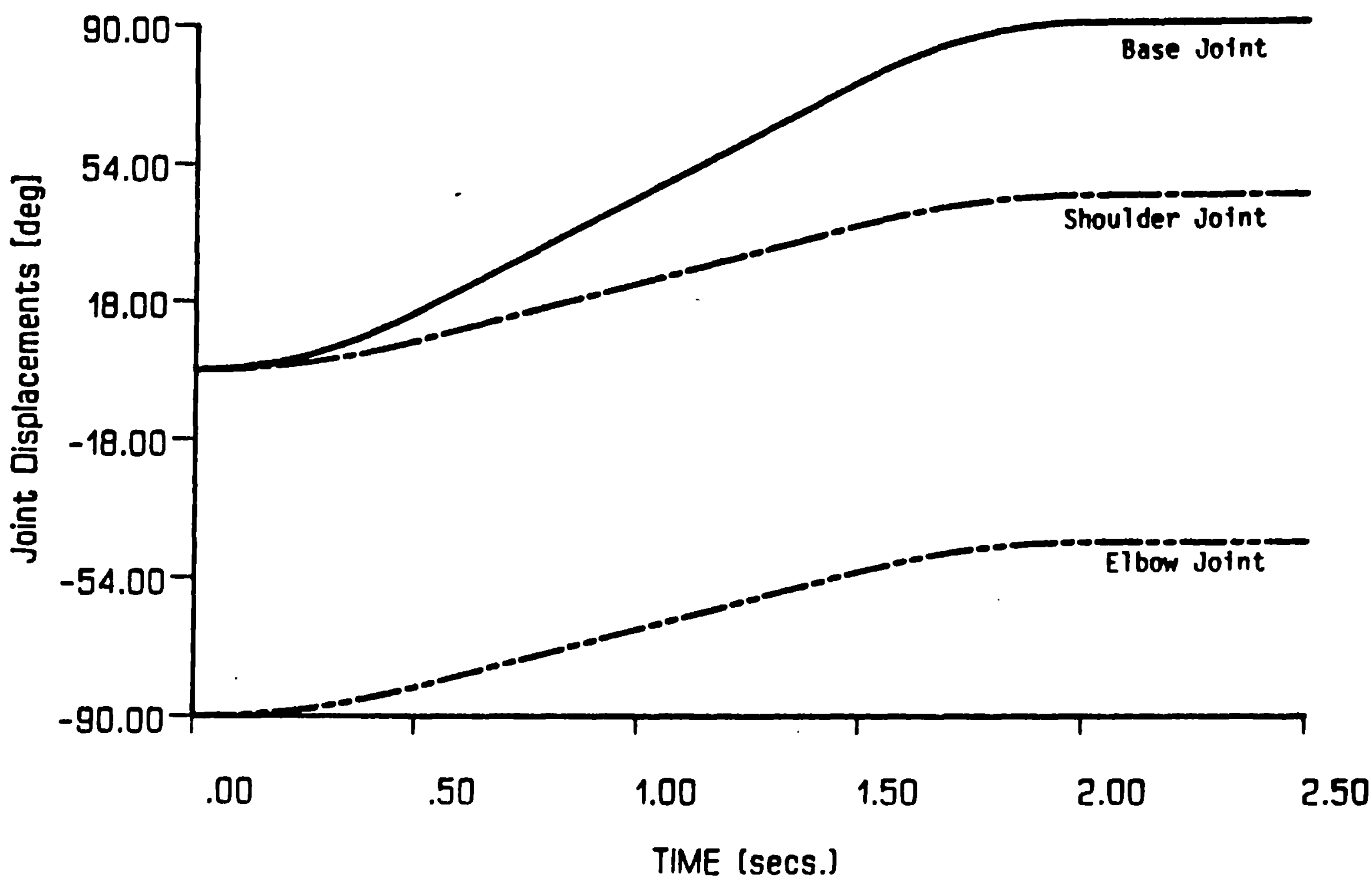

Figure 40. Joint Motion Profile for Example 1

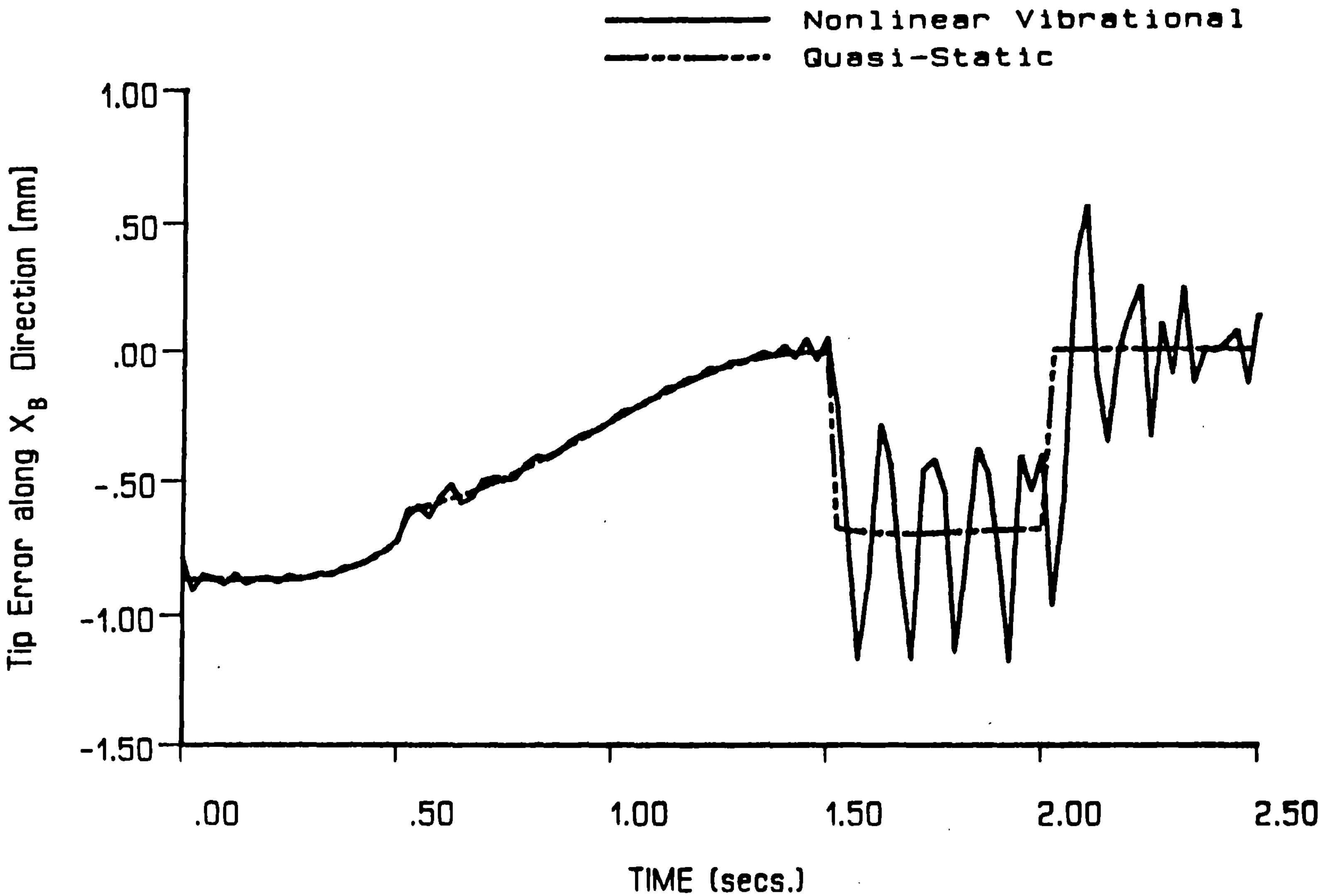

Figure 41. Tip Error Along X_{b_0} Direction for 3-R Manipulator

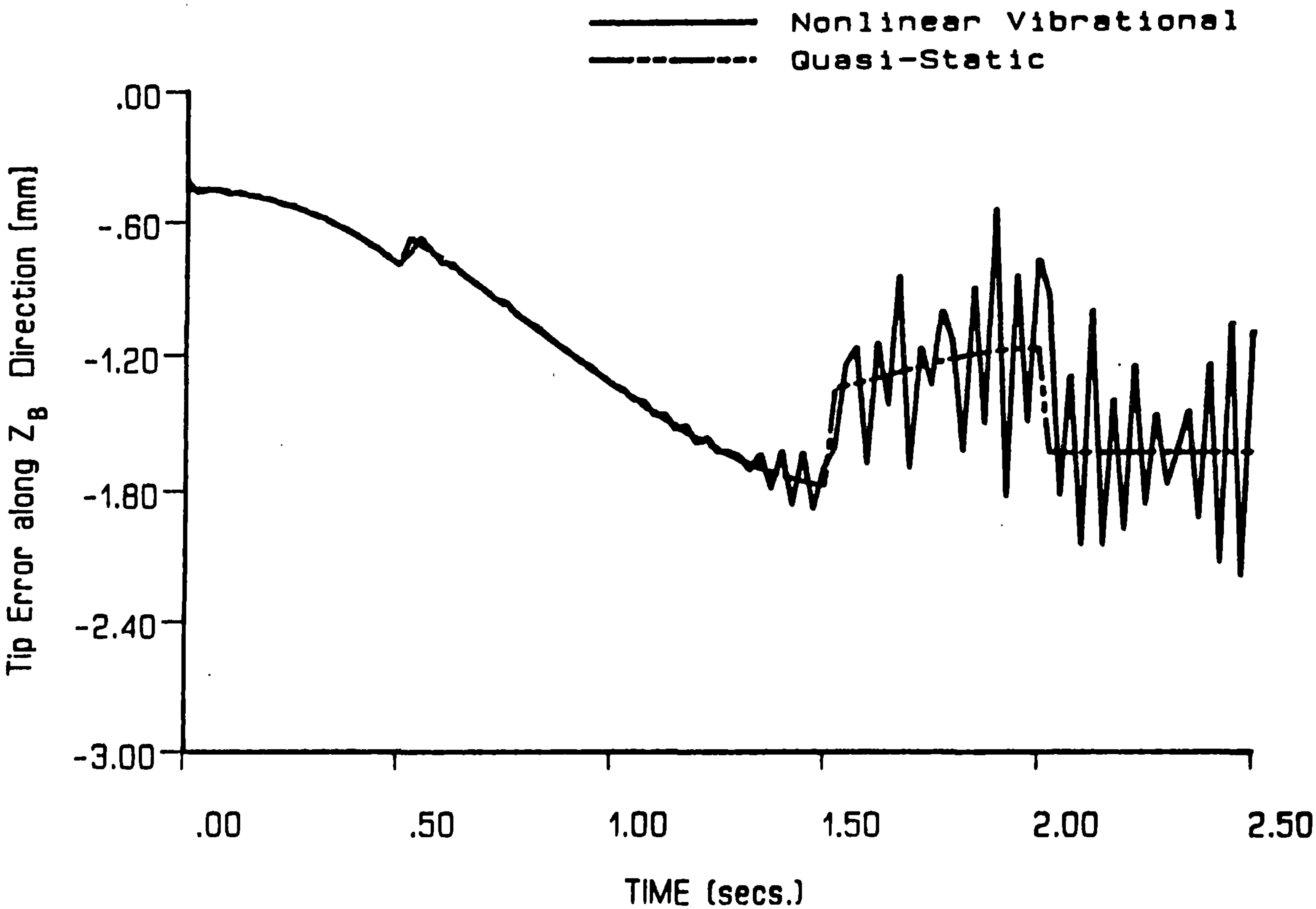

Figure 42. Tip Error Along Z_{b_0} Direction for 3-R Manipulator

was actuated using cycloidal motion profiles at the joints. Figure 43 shows the tip error along the global horizontal $(X_b)_0$ direction. Even for the case of the flexible configuration that has been considered in this example, the tip errors are found to be much smaller in magnitude as compared to the results presented for the all-revolute configurations. This would be expected to be the case, since the dynamic forces arising due to the commanded gross motion influence the bending mode more directly for the case of a revolute pair. However, for the case of the prismatic joint, these dynamic forces are dominantly axial in nature, causing negligible deformations in the system.

In this chapter, a methodology based on a finite element scheme was developed to analyze the nonlinear coupling effects of gross motion kinematics and the distributed flexibilities in general spatial manipulator configurations that include both revolute and prismatic pairs. A special finite element was derived from first principles to model the links of these manipulators. Two numerical examples were presented to demonstrate the capabilities of the computer code developed based on this algorithm.

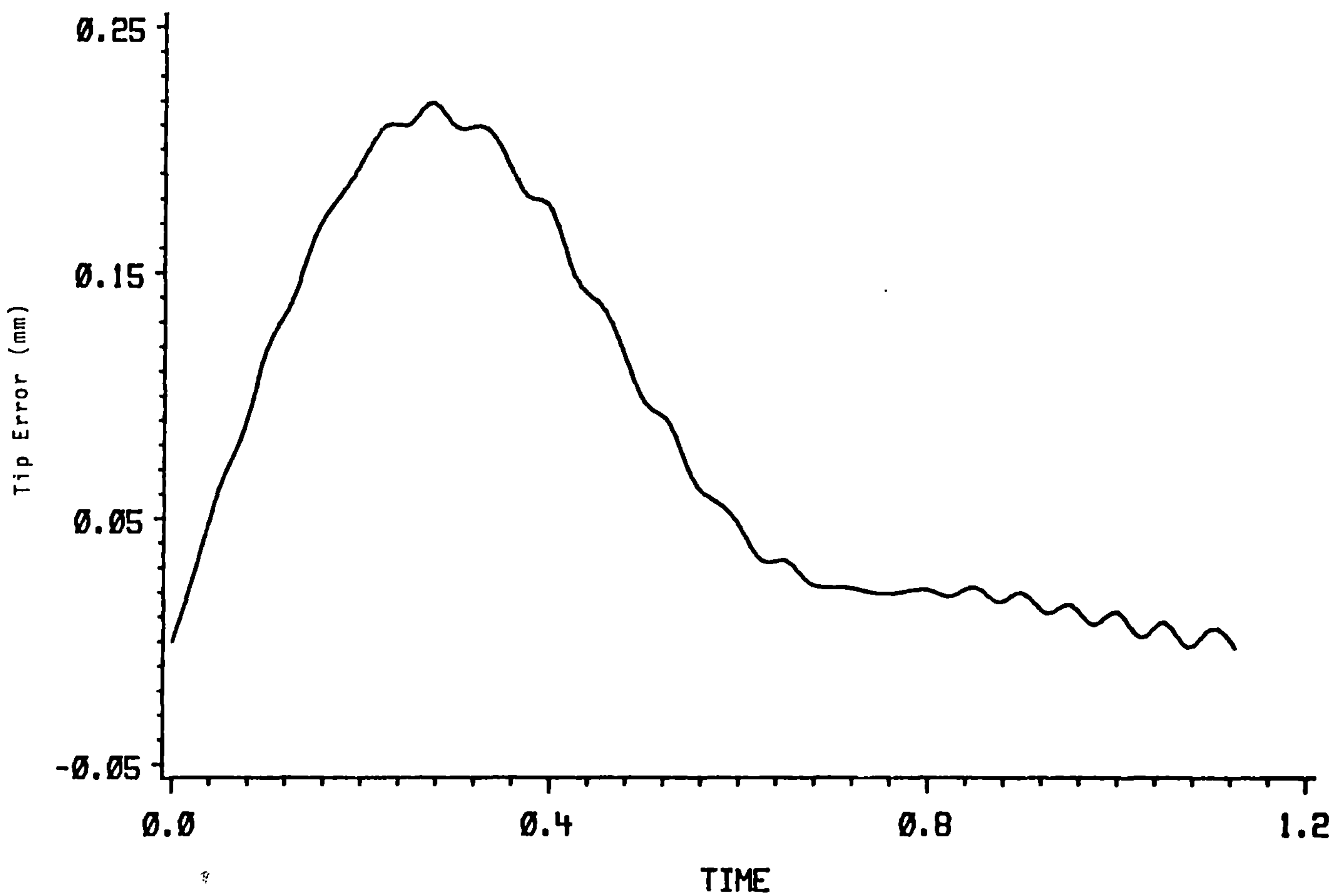

Figure 43. Deformation S_1 for R-P Manipulator

CHAPTER VI

SUMMARY AND RECOMMENDATIONS

Summary

The main objective of this study was to develop a comprehensive and dedicated methodology to analyze the nonlinear kinematic coupling effects in flexible, spatial manipulators. The developed methodology has taken into account the complete nonlinear coupling effects between the commanded gross motions of the links and the compliance in the system due to distributed elasticity in the links. The dynamic response of the end-effector was predicted for a given set of commanded joint motion profiles. The methodology was developed in two stages.

First, a particularized methodology was developed for the case of revolute jointed, planar flexible manipulators. A special finite element was derived from first principles for the links of the planar manipulators based on Timoshenko Beam Theory and a Newton Euler formulation. The development took into account the complete nonlinear kinematic coupling between the nonlinear gross motion kinematics of the manipulator and the deformations in the links due to distributed flexibility. Reduced order integration was adopted in the derivation of the conventional stiffness matrix. This provided a mechanism to avoid the parasitic shear effects (shear lock phenomenon) in the analysis, which appear when a linear interpolation scheme is used together with the Timoshenko Beam Theory. A simple linear interpolation was proved to be adequate for the finite element developed in the study. The study assumed uniform cross sections for the links of the manipulator. However, such an assumption may be easily relaxed for varying cross-sections, if the cross-sectional area and the area moment of inertia are represented as functions of the locations of the cross-sections on the manipulator link. Should numerical evaluation of the matrices be desired for complex cross-sections, the use of the linear interpolation would facilitate a more simple and thus, a computationally efficient evaluation of the element matrices. The commanded gross motion effects were observed to be present as coupled nonlinear terms in the elemental matrices in the form of pseudo-stiffness and pseudo-damping matrices. Time varying compatibility matrices were used to assemble the elemental terms to form the system equations. Since almost all practical manipulators are driven by servo-actuators, the complete nonlinear model was also augmented with simplistic representations of the joint servo-effects in the form of effective servo-stiffness and servo-damping terms. A solution scheme involving incremental linearization and equilibrium iteration was identified to solve the system equations.

Both analytical and experimental procedures were pursued to verify the correctness of the derivation of the special finite element model. Analytical procedures included such methods as eigenvalue analysis of Timoshenko beams, deformational studies on planar frames, and quasi-static analysis of a single rotating link. An experimental investigation of a single link flexible manipulator was also undertaken to evaluate the performance of the special finite element. Favorable correlations were observed between the analytical and experimental results, thus confirming the applicability of the finite element for practical flexible manipulators.

The computer algorithm that was developed based on the above methodology facilitated analysis of flexible manipulators in three modes through a soft switch in the algorithm. The first mode was a complete, nonlinear analysis using the nonlinear model developed in this study. The final set of equations was a set of nonlinear, coupled ordinary differential equations. The second mode is the linearized analysis, wherein the nonlinear coupling effects were ignored while evaluating the link kinematics. This resulted in a linear, parametric system of equations and hence the name, linearized analysis. Studies in the past have preferred to follow this approach and this is analogous to conventional structural dynamics methodology. The last of the modes was a quasi-static analysis wherein the inertia and damping effects were ignored and a quasi-static response was computed.

Numerical case studies identified significant nonlinear, kinematic coupling effects in flexible, manipulator configurations. Higher peak errors were observed for the nonlinear model as compared to the linearized and the quasi-static models. Also, the profiles of the computed reaction torques at the joints (drive torques for the given joint motion) were found to be significantly altered from their forms corresponding to rigid body dynamics computations. Also, for conservatively estimated values of joint servo-compliances, the nonlinear model registered significantly higher tip errors as compared to the linearized model with non-compliant joint assumptions.

Following similar guidelines, a comprehensive nonlinear model was developed to analyze spatial manipulators with both revolute and prismatic pairs, operating in a three-dimensional workspace. The methodology allowed for an easy description of the spatial manipulator in its initial configuration using the Hartenberg-Denavit parameters. An extended matrix method based on 4 X 4 homogeneous transformations was developed for a versatile modeling of the nonlinear kinematic coupling effects in spatial manipulators with both revolute and prismatic pairs. Similar to the case of planar manipulators described earlier, a special finite element was derived from first principles based on Timoshenko Beam Theory and a

Newton-Euler formulation. The choice of a reduced order integration in the development of element conventional stiffness matrices allowed for the simultaneous modeling of stunt and slender beams as manipulator links. This is particularly desirable for spatial manipulator configurations. Also, the matrix scheme allowed for the modeling of spatial manipulator links with offsets (kink links) by simply modeling additional passive or structural joints in the system. The algorithm is fully automated in being capable of generating the required time varying compatibility matrices (between local finite element nodal coordinates and nodal system coordinates), requiring no user effort.

Two numerical examples were presented to demonstrate the feasibility of the algorithm developed in this study. The algorithm was found to be computationally intensive because of the larger size of the elemental matrices that require repeated evaluations during the iterative scheme. The first of the examples analyzed a 3-R spatial manipulator and the second example was the case of a more general spatial R-P configuration. The tip errors for the latter case was observed to be very small as compared to the revolute configurations. This is to be expected, since the dynamic forces due to commanded gross motion at a revolute pair, influences the bending mode of a flexible link more directly. For the case of the prismatic pair, these dynamic forces are dominantly axial in nature, thus resulting in negligible structural deformations.

From the results presented for the planar and spatial manipulators, the nonlinear kinematic coupling effects appear to influence the performance of flexible manipulator configurations both in terms of end-effector positioning errors as well as distortions of drive-torque profiles. Hence, it appears that the nonlinear kinematic coupling effects should be particularly recognized in the development of controllers for flexible configurations. Thus, the methodology developed in this study offers the most comprehensive of the techniques available today for the analysis of flexible manipulators.

Recommendations For Future Research

Excellent perspectives exist to further the scope of the research presented in this work. The need for the utilization of flexible manipulators in outer-space as well as in mobile defense applications have been well identified by the researchers in this area. The advantage of manipulator compliance in such applications as miniature assembly have also been recognized in the past. The foremost of the future challenges is the need for a more thorough modeling of the actuators and their drive trains. The lack of a complete understanding of all the nonlinear effects in these mechanisms have often posed a big hurdle in the control issues of even, rigidly designed manipulators. These problems are only compounded by the distributed link flexibilities in flexible manipulators. Both analytical as well as experimental studies may be needed to fully explore and identify the effects of all compliances that exist in a typical actuator. Beyond the analysis of the effects of flexibilities, exists the issue of control. Sophisticated controllers must be designed to take into account the effects of flexibilities and the means to take advantage of these compliances, in order to efficiently execute the commanded tasks. The control issues are further complicated by the fact that in practice, manipulators are expected to handle varying end-effector load conditions. These load conditions may vary both in terms of the mass of the payload and as well as its moment of inertia. The latter is particularly important in outer space applications which involve manipulation of large space structures. Therefore, improved models for the manipulator dynamics are needed in representing the dynamic plant in the controller design process. It is hoped that the methodology developed in this work is yet another progressive step towards answering the above issues.

A SELECTED BIBLIOGRAPHY

1. Ahmad, S., "Second Order Nonlinear Kinematic Effects and Their Compensation," Proc. of the IEEE Conference on Robotics and Automation, 1985, pp. 307-315.

2. Albus, J.S., "A New Approach to Manipulator Control: The Cerebellar Model Articulation Controller (CMAC)," ASME Journal of Dynamic Systems, Measurement and Control, Vol. 97, 1975, pp. 270-277.

3. Albus, J.S., "Data Storage in the Cerebellar Model Articulation Controller (CMAC)," ASME Journal of Dynamic Systems, Measurement and Control, Vol. 97, 1975, pp. 228-233.

4. Armstrong, W.W., "Recursive Solution to the Equations of Motion of an N-Link Manipulator," Proc. of the 5th IFToMM Conference, Montreal, Canada, Vol. 2, July 1979, pp. 1343-1346.

5. Asada, H., Kanade, T., and Takeyama, I., "Control of a Direct-Drive Arm," Paper presented at the ASME Winter Annual Meeting, Phonenix, Arizona, Nov. 14-19, 1982. Also in Robotics Research and Advanced Applications, ed. Dr. W.J. Book, Published by ASME, pp. 63-72.

6. Bagci, C., "Computer-aided Continuous Correction of End-effector Position and Orientation Errors in Industrial Robots due to Elastic Deformations," ASME Paper No. 84-DET-142.

7. Bagci, C. and Dado, M.H.F., "Observations on Analytical and Experimental Elasto-dynamic Response of Mechanisms involving Flexural Line Elements, Lumped Mass Systems, and Dynamic Damping Factors; and Applications to Kineto-elasto-dynamic Analysis of Industrial Robots," ASME Mechanisms Conference, 1984, ASME Paper 84-DET-141.

8. Bahgat, B.M. and Willmert, K.D., "Finite Element Vibrational Analysis of Planar Mechanisms," Mechanism and Machine Theory, Vol. 11, 1976,

pp. 47-71.

9. Bathe, K.J., Numerical Methods in Finite Element Analysis, Prentice Hall Inc., 1984.

10. Beaufait, F.W., Rowan, W.H. Jr., Hoadley, P.G., and Hackett, R.M., Computer Methods of Structural Analysis, Prentice Hall Inc., 1970.

11. Beazley, W.G., "The small Motion Dynamics of Bilaterally Coupled Kinematic Chains with Flexible links," Ph.D Dissertation, University of Texas, Austin, Texas, August 1978.

12. Bejczy, A.K., "Dynamic Analysis for Robot Arm Control," Proc. of the American Control Conference 1983, Paper TA6-10:00, pp. 503-504.

13. Bejczy, A.K. and Paul, R.P., "Simplified Robot Arm Dynamics for Control," Proc. of the Joint Automatic Control Conference, Paper WP1-4:00, 1981, pp. 261-262.

14. Book, W.J, "Recursive Lagrangian Dynamics of Flexible Manipulator Arms," International Journal of Robotics Research, Vol. 3, No. 3, Fall 1984, pp. 87-101.

15. Book, W.J., "Study of Design and Control of Manipulators (Modeling Manipulator Arms with Distributed Flexibility for Design and Control)," NASA Final Report for Contract NAS8-28055, Massachusetts Institute of Technology, January 31, 1974.

16. Book, W.J., "Analysis of Massless Elastic Chains with Servo-Controlled Joints," ASME Journal of Dynamic Systems, Measurement, and Control, Vol. 101, No. 3, September 1979, pp. 187-192.

17. Book, W.J., "Modelling, Design, and Control of Flexible Manipulator Arms," Ph.D Dissertation, Department of Mechanical Engineering, Massachusetts Institute of Technology, April 1974.

18. Book, W.J., Majette, M., and Ma, K., "The Distributed Systems Analysis Package (DSAP) and its Application to Modeling Flexible Manipulators," Georgia Institute of Technology, School of Mechanical Engineering, Report for Subcontract No. 551 to Charles Stark Draper Laboratory, Inc., NASA Contract No. NAS9-13809, July 1979.

19. Book, W.J., Majette, M., and Ma, K., "Frequency Domain Analysis of the Space Shuttle Manipulator Arm and its Payloads; Vol I: Analysis and Conclusions; Vol II: Computer Program Description and Listings," Georgia Institute of Technology, School of Mechanical Engineering, Subcontract No. 586 to Charles Stark Draper Laboratory, Inc., NASA Contract No. NAS9-13809, Feb. 1981.

20. Book, W.J., Neto, M.O., and Whitney, D.E., "Feedback Control of Two Beam, Two Joint Systems with Distributed Flexibility," ASME Journal of Dynamic Systems, Measurement and Control, December 1975, pp. 424-431.

21. Chace, M.A., "Development and Application of Vector Mathematics for Kinematic Analysis of Three-Dimensional Mechanisms," Ph.D Dissertation, Mechanical Engineering Dept., University of Michigan, Ann Arbor, Michigan, 1964.

22. Clough, R.W. and Penzien, J., Dynamics of Structures, McGraw-Hill Book Company, 1975.

23. Cvetkovic, V. and Vukobratovic, M., "Computer-Oriented Algorithm for Modeling Active Spatial Mechanisms for Robotics Applications," IEEE Transactions on Systems, Man, and Cybernetics, Vol. SMC-12, No. 6, November-December 1982, pp. 838-847.

24. Dado, M. and Soni, A.H., "Complete Analysis of Elastic Linkages," To appear in the ASME Journal of Mechanisms, Transmission, and Automation in Design, 1986.

25. Dawe, D.J., "A Finite Element for the Vibration Analysis of Timoshenko Beams," Journal of Sound and Vibration, Vol. 60, No. 1, 1978, pp. 11-20.

26. Dawe, D.J., Matrix and Finite Element Displacement Analysis of Structures, Oxford University Press, New York, 1984.

27. Denavit, J. and Hartenberg, R.S., "A Kinematic Notation for Lower-Pair Mechanisms Based on Matrices," ASME Journal of Applied Mechanics, June 1955, pp. 215-221.

28. Dubowsky, S. and Gardner, T.N., "Dynamic Interactions of Link Elasticity and Clearance Connections in Planar Mechanical Systems," ASME Journal of Engineering for Industry, Vol. 97, No. 2, May 1975, pp. 652-661.

29. Erdman, A.G., "A General Method for Kineto-Elasto-Dynamic Analysis and Synthesis of Mechanisms," Ph.D Dissertation, Rensselaer Polytechnic Institute, Troy, New York, 1971.

30. Featherstone, R., "Calculation of Robot Joint Rates and Actuator Torques from End-Effector Velocities and Applied Forces," Mechanism and Machine Theory, Vol. 18, No. 3, 1983, pp. 193-198.

31. Featherstone, R., "The Calculation of Robot Dynamics using Articulated Body Inertias," International Journal of Robotics Research, Vol. 2, No. 1, Spring 1983, pp. 13-30.

32. Good, M.C., Sweet, L.M., and Strobel, K.L., "Dynamic Models for Control System Design of Integrated Robot and Drive Systems," Journal of Dynamic Systems, Measurement, and Control, Vol. 107, March 1985, pp. 53-59.

33. Hastings, G.G. and Book, W.J., "Verification of a Linear Dynamic Model for Flexible Robotic Manipulators," Proc. of the 1986 IEEE conference on Robotics and Automation, San Francisco, CA, March 27-31, 1986, pp. 1024-1029.

34. Herrick, S., "Model Reference Adaptive Control of an Industrial Manipulator," M.S. Thesis, University of California, Los Angeles, California, 1982.

35. Hill, J. and Park, W.T., "Real Time Control of a Robot with a Mobile Camera," Proc. of the 9th International Symposium on Industrial Robots, March 13-15, 1979, pp. 233-246.

36. Ho, J.Y.L., "Direct Path Method for Flexible Multibody Spacecraft Dynamics," Journal of Spacecraft and Rockets (AIAA), Vol. 14, No. 2, February 1977, pp. 102-110.

37. Hollerbach, J.M., "A Recursive Lagrangian Formulation of Manipulator Dynamics and a Comparative Study of Dynamics Formulation complexity," IEEE Transactions on Systems, Man, and Cybernetics, Vol. SMC-10, No. 11, November-December 1980, pp. 730-736.

38. Hollerbach, J.M., "Wrist-Partitioned Inverse Kinematic Accelerations and Manipulator Dynamics," International Journal of Robotics Research, Vol. 2, No. 4, 1983, pp. 61-76.

39. Hooker, W.W., "A Set of r-Dynamic Equations for an

Arbitrary n-Body Satellite having r Rotational Degrees of Freedom," AIAA Journal, Vol. 8, No. 7, 1970, pp. 1205-1207.

40. Hooker, W.W. and Margulies, G., "The Dynamical Attitude Equations for an n-Body Satellite," Journal of Astronautical Sciences, Vol. 12, No. 4, 1965, pp. 123-128.

41. Hopkins, A.S., "The Motion of Interconnected Flexible Bodies," Ph.D Dissertation, University of California, Los Angeles, California, 1976.

42. Horak, D.T., "A Simplified Modeling and Computational Scheme for Manipulator Dynamics," ASME Journal of Dynamic Systems, Measurement, and Control, Vol. 106, December 1984, pp. 350-352.

43. Horn, B.K.P. and Raibert, M.H., "Configuration Space Control," The Industrial Robot, pp. 69-73, June 1978.

44. Hossne, A.J., Soni, A.H., and Harvey, J.W., "Kineto-elasto-dynamic Analysis of Mechanisms by Finite Element Formulations," ASME Paper 80-DET-103.

45. Huston, R.L., "Multibody Dynamics Including the Effects of Flexibility and Compliance," Computers and Structures, Vol. 14, No. 5-6, 1981, pp. 713-720.

46. Huston, R.L. and Kelly, F.A., "Development of Equations of Motion of Single Arm Robots," IEEE Transactions on Systems, Man, and Cybernetics, Vol. SMC-12, No. 3, May-June 1982, pp. 259-266.

47. Huston, R.L. and Passerello, C.E., "Multibody Structural Dynamics Including Translation Between the Bodies," Computers and Structures, Vol. 12, No. 5, 1980, pp. 713-720.

48. Huston, R.L., Passerello, C.E., and Harlow, M.W., "Dynamics of Multi-Rigid Body Systems," ASME Journal of Applied Mechanics, Vol. 45, No. 4, December 1978, pp. 889-894.

49. Judd, R.D. and Falkenburg, D.R., "Dynamics of Non-rigid Articulated Robot Linkages," Proc. of the American Control Conference 1983, Paper No. FA-9:45, pp. 1045-1049.

50. Kahn, M.E. and Roth, B., "The Near Minimum-Time Control of Open-Loop Articulated Kinematic Chains," ASME Journal of Dynamic Systems,

Measurement, and Control, Vol. 93, Series G, No. 3, September 1971, pp. 164-172.

51. Kane, T.R. and Levinson, D.A., "The Use of Kane's Dynamical Equations in Robotics," International Journal of Robotics Research, Vol. 2, No. 3, Fall 1983, pp. 3-21.

52. Kane, T.R. and Levinson, D.A., "Multibody Dynamics," ASME Journal of Applied Mechanics, Vol. 50, December 1983, pp. 1071-1078.

53. Kane, T.R. and Wang, C.F., "On the Derivation of Equations of Motion," Journal of the Society of Industrial and Applied Mathematics, Vol. 13, 1965, pp. 487-492.

54. Lee, C.S.G., "Robot Arm Kinematics, Dynamics, and Control," IEEE Computer, Vol. 15, No. 12, December 1982, pp. 62-80.

55. Likins, P.W., "Dynamic Analysis of a System of Hinge-Connected Rigid Bodies with Non-rigid Appendages," Technical Report 32-1576, Jet Propulsion Laboratory, Pasadena, California, February 1974.

56. Luh, J.Y.S., Walker, M.W., and Paul, R.P., "On-line Computational Scheme for Mechanical Manipulators," ASME Journal of Dynamic Systems, Measurement and Control, Vol. 102, June 1980, pp. 69-76.

57. Maatuk, J., "A Study of the Dynamics and Control of Flexible Spatial Manipulators," Ph.D Dissertation, Mechanics and Structures Dept., University of California, Los Angeles, California, 1976.

58. Mahil, S.S., "Mathematical Model of an Industrial Manipulator - A Closed Form Solution using Lagrange's Method," Proc. of the 7th International Symposium of Industrial Robots, 1977, pp. 115-122.

59. Mahil, S.S., "On the Application of Lagrange's Method to the Description of Dynamic Systems," IEEE Transactions on Systems, Man, and Cybernetics, Vol. SMC 12, No. 6, November 1982, pp. 877-889.

60. Majette, M.W., "Modal State Variable Control of a Linear Distributed Mechanical System Modled with the Transfer Matrix Method," Master's Thesis, Department of Mechanical Engineering, Gerogia

Institute of Technology, June 1985.

61. Martin, H.C. and Carey, G.F., Introduction to Finite Element Analysis: Theory & Application, McGraw-Hill Book Company, 1973.

62. Naganathan, G. and Soni, A.H., "Dynamic Response of a Manipulator," Proc. of the 9th Applied Mechanisms Conference, St. Louis, Missouri, October 27-30, 1985.

63. Naganathan, G. and Soni, A.H., "Robot Simulation by Rigid-Body Modeling," Proc. of the 9th Applied Mechanisms Conference, St. Louis, Missouri, October 27-30, 1985.

64. Naganathan, G. and Soni, A.H., "Nonlinear Flexibility Studies for Spatial Manipulators," Proc. of the 1986 IEEE conference on Robotics and Automation, San Francisco, CA, March 27-31, 1986.

65. Naganathan, G. and Soni, A.H., "Coupling Effects of Kinematics and Flexibility in Manipulators," to appear in the International Journal of Robotics Research, 1986.

66. Naganathan, G. and Soni, A.H., "Nonlinear Modeling of Kinematics and Flexibility Effects in Manipulator Design," To appear in the ASME Journal of Mechanisms, Transmissions, and Automation in Design, 1986.

67. Naganathan, G. and Willmert, K.D., "Special Finite Elements for Quasi-Static Deformations and Stresses in Planar Mechanisms," ASME Paper WA-80/DSC-35, ASME Winter Annual Meeting, November 1980, Chicago.

68. Nelson, W.L. and Mitra, D., "Load Estimation and Load-Adaptive Optimal Control for a Flexible Arm," Proc. of the 1986 IEEE conference on Robotics and Automation, San Francisco, CA, March 27-31, 1986, pp. 206-211.

69. Orin D.E., McGhee, R.B., Vukobratovic, M., and Hartoch, G, "Kinematic and Kinetic Analysis of Open-chain Linkages Utilizing Newton-Euler Method," Mathematical Biosciences, Vol. 43, 1979, pp. 107-130.

70. Orin, D.E. and Oh, S.Y., "Control of Force Distribution in Robotic Mechanisms Containing Closed Kinematic Chains," ASME Journal of Dynamic Systems, Measurement and Control, Vol. 103,

No. 3, June 1981, pp. 134-141.

71. Orlandea, N. and Berenyi, T., "Dynamic Continuous Path Synthesis of Industrial Robots using ADAMS Computer Program," ASME Journal of Mechanical Design, Vol. 103, July 1981, pp. 602-607.

72. Patwardhan, A.S. and Soni, A.H., "Kineto-elasto-dynamic Synthesis of a Four Bar Mechanism for path guidance,", ASME Paper No. 76-DET-73.

73. Paul, R.P., Robot Manipulators, The MIT Press, Cambridge, Massachusetts, 1981.

74. Paul, R.P., Rong, MA and Zhang, Hong, "The Dynamics of Puma Manipulator," Proc. of the American Control Conference 1983, TA6 8:30, pp. 491-496.

75. Pennock, G.R. and Yang, A.T., "Dynamic Analysis of a Multi-Rigid-Body Open-chain System," ASME Journal of Mechanisms, Transmissions, and Automation in Design, Vol. 105, March 1983, pp. 28-34.

76. Prathap, G. and Bhashyam, G.R., "Reduced Integration and the Shear-Flexible Beam Element," International Journal for Numerical Methods in Engineering, Vol. 18, 1982, pp. 195-210.

77. Przemieniecki, J.S., Theory of Matrix Structural Analysis, McGraw-Hill Book Company, 1980.

78. Raibert, M.H., "A Model for Sensorimotor Control and Learning," Biological Cybernetics, Vol. 29, 1978, pp. 29-36.

79. Rakhsha, F. and Goldenberg, A.A., "Dynamics Modeling of a Single-Link Flexible Robot," Proc. of the IEEE Conference on Robotics and Automation, 1985, pp. 984-989.

80. Roberson, R.E. and Wittenberg, J., "A Dynamical Formalism for an Arbitrary Number of Interconnected Rigid Bodies, with Reference to the Problem of Satellite Attitude Control," Proc. of the 3rd International Congress of Automatic Control, London, 1966, pp. 46D.1-46D.8.

81. Russell, W.J., "On the Formulation of Equations of Rotational Motion for an N-Body Spacecraft," Report TR-0200(4133)-2, Aerospace Corporation, El Segundo, California, 1969.

82. Salisbury, K.J. and Roth, B., "Kinematic and Force Analysis of Articulated Mechanical Hands," ASME

Journal of Mechanisms, Transmissions, and Automation in Design, Vol. 105, 1983, pp. 35-41.

83. Schmitt, D., Soni, A.H., Srinivasan, V., and Naganathan, G., "Optimal Motion Programming of Robot Manipulators," ASME Journal of Mechanisms, Transmissions, and Automation in Design, Vol. 107, June 1985, pp. 239-244.

84. Shabana, A.A., "Transient Analysis of Flexible Multi-Body Systems. Part I: Dynamics of Flexible Bodies," Journal of Computer Methods in Applied Mechanics and Engineering, Vol. 54, 1986, pp. 75-91.

85. Shastry, B.P. and Rao, G.V., "Dynamic Stability of Bars Considering Shear Deformation and Rotatory Inertia," Computers and Structures, Vol. 19, No. 5/6, 1984, pp. 823-827.

86. Sheth, P. and Uicker, J.J. Jr., "IMP (Integrated Mechanisms Program) - A Computer Aided Design Analysis System for Mechanisms and Linkages," ASME Journal of Engineering for Industry, Vol. 94, No. 2, May 1972, pp. 454-464.

87. Silver, W.M., "On the Equivalence of Lagrangian and Newton-Euler Dynamics for Manipulators," International Journal of Robotics Research, Vol. 1, No. 2, Summer 1982, pp. 60-70.

88. Singh, R.P. and Likins, P.W., "Manipulator Interactive Design with Interconnected Flexible Elements," Proc. of the American Control Conference 1983, Paper No. TA6-11:00, pp. 505-512.

89. Soni, A.H., "Application of 3 x 3 Screw Matrix to Kinematic and Dynamic Analysis of Mechanisms." VDI Colloquim on Dynamics of Mechanism, Dusseldorf, West Germany, Published in VDI-Berichete No. 127, 1968.

90. Srinivasan, V. and Soni, A.H., "Seismic Analysis of a Rotor-Bearing System," Earthquake Engineering and Structural Dynamics, Vol. 12, 1984, pp. 287-331.

91. Srinivasan, V. and Soni, A.H., "Seismic Analysis of Rotating Mechanical Systems," A Final Report to National Science Foundation, Grant Nos. CEE 8108119 and CEE 8243133, Oklahoma State University, Stillwater, Oklahoma.

92. Stepanenko, Y. and Vukobratovic, M., "Dynamics of Articulated Open-Chain Active Mechanisms,"

Mathematical Biosciences, Vol. 28, No. 1-2, 1976, pp. 137-170.

93. Sunada, W.H. and Dubowsky, S.,"The Application of Finite Element Methods to the Dynamic Analysis of Flexible Spatial and Co-Planar Linkage Systems," ASME Journal of Mechanical Design, Vol. 103, No. 3, July 1981, pp. 643-651.

94. Sunada, W.H. and Dubowsky, S., "On the Dynamic Analysis and Behavior of Industrial Robotic Manipulators with Elastic Members," ASME Journal of Mechanisms, Transmissions, and Automation in Design, Vol. 105,March 1983, pp. 42-51.

95. Sunada, W.H., "Dynamic Analysis of Flexible Spatial Mechanisms and Robotic Manipulators," Ph.D Dissertation, University of California, Los Angeles, California, 1981.

96. Takano, M., Koji, Y. and Seiji, Y., "Development of Computer Simulation System of Kinematics and Dynamics of Robot," Journal of the Faculty of Engg., University of Tokyo, Japan, Vol. XXXVI, No. 4, 1982, pp. 677-711.

97. Thomas, M. and Tesar, D., "Dynamic Modeling of Serial Manipulator Arms," ASME Journal of Dynamic Systems, Measurement and Control, Vol. 104, No. 3, September 1982, pp. 218-228.

98. Truckenbrodt, A., "Dynamics and Control Methods for Moving Flexible Structures and Their Application to Industrial Robots," Proc. of the 5th IFToMM Conference, Montreal, Canada, 1983, pp. 831-834.

99. Truckenbrodt, A., "Motion Behavior and Control of Elastic Robot Structures," Proc. of the 8th International Symposium of Industrial Robots, Vol. 2, 1978, pp. 152-157.

100. Uicker, J.J. Jr., "On the Dynamic Analysis of Spatial Linkages using 4 X 4 matrices," Ph.D Dissertation, Northwestern University, Illinois, 1965.

101. Velman, J.R., "Simulation Results for a Dual-Spin Spacecraft," Proc. of the Symposium on Attitude Stabilization and Control of Dual-Spin Spacecraft, Air Force Report SAMSO-TR-68-191, Aerospace Corporation, Report TR-0158(3307-01)-16, El Segundo, California, 1967.

102. Vukobratovic, M., "Dynamics of Active Articulated Mechanisms and Synthesis of Artificial Motion," Mech. and Mach. Theory, Vol. 13, 1978, pp. 1-18.

103. Vukobratovic, M., "Computer Method for Dynamic Model Construction of Active Articulated Mechanisms using Kineto-static Approach - Part 2," Mech. and Mach. Theory, Vol. 13, 1978, pp. 19-39.

104. Vukobratovic, M., "Synthesis of Functional Artificial Motion - Part 3,"Mech. and Mach. Theory, Vol. 13, 1978, pp. 41-56.

105. Vukobratovic, M. and Hristic, D., "Design of an Anthropomorphic Manipulator for Industrial Application," Journal of Mechanical Engineering Sciences, Vol. 21, No. 5, 1979, pp. 313-316.

106. Vukobratovic, M., Kojik, M.R., and Nikolic, I.Z., "The Contribution to the Study of Dynamics of Flexible Manipulation of Robots," Proc. of the 6th IFToMM Conference, New Delhi, India, 1983, pp. 1021-1024.

107. Walker, M.W., "A Unified Approach to Manipulator Modeling," Proc. of the IEEE Conference on Robotics and Automation, 1985, pp. 729-736.

108. Walker, M.W. and Orin, D.E., "Efficient Dynamic Computer Simulation of Robotic Mechanisms," ASME Journal of Dynamic Systems, Measurement and Control, Vol. 104, September 1982, pp. 205-211.

109. Wang, T. and Kohli, D., "Closed and Expanded Form of Manipulator Dynamics using Lagrangian Approach," ASME Mechanisms Conference 1984, ASME Paper 84-DET-122.

110. Waters, R.C., "Mechanical Arm Control," M.I.T. Artificial Intelligence Lab. Memo. 549, October 1979.

111. Williams, R.J. and Seireg, A., "Interactive Modeling and Analysis of Open or Closed Loop Dynamic Systems with Redundant Actuators," ASME Journal of Mechanical Design, Vol. 101, July 1979, pp. 407-416.

112. Winfrey, R.C., "Dynamic Analysis of Elastic Mechanisms by Reduction of Coordinates," ASME Journal of Engineering for Industry, Vol. 94, No. 1, May 1972, pp. 557-581.

113. Woo, L.S. and Freudenstein, F., "Dynamic Analysis of

Mechanisms Using Screw Coordinates," ASME Journal of Engineering for Industry, Vol. 93, No. 1, February 1971, pp. 273-276.

114. Yang, A.T., "Inertia Force Analysis of Spatial Mechanisms," ASME Journal of Engineering for Industry, Vol. 93, No. 1, February 1971, pp. 27-33.

115. Zienkiewicz, O.C., The Finite Element Method, 3rd Edition, McGraw-Hill Book Company, London, 1977.

116. Zienkiewicz, O.C., "The Generalized Finite Element Method - State of the Art and Future Directions," ASME Journal of Applied Mechanics, Vol. 50, December 1983, pp. 1210-1217.

APPENDIXES

APPENDIX A

ELEMENT MATRICES FOR PLANAR MANIPULATORS

APPENDIX A

ELEMENT MATRICES FOR PLANAR MANIPULATORS

The governing equations for a finite element on the i^{th} link is given by equation (2.22) as:

$$[J]_e \{\ddot{q}\}_e + [C]_e \{\dot{q}\}_e + [K]_e \{q\}_e = \{F\}_e \qquad \ldots \quad (A.1)$$

where,

$[J]_e$	is the Element Inertia Matrix
$[C]_e$	is the Coriolis Matrix due to the motion of the reference frame $(X_b Y_b Z_b)$ of the i^{th} link.
$[K]_e$	is the Element Stiffness Matrix $= [K_c]_e + [K_b]_e$
$[K_c]_e$	is the Conventional Stiffness Matrix
$[K_b]_e$	is the stiffness matrix due to the motion of the frame $(X_b Y_b Z_b)$ of the i^{th} link.
$\{F\}_e$	is the element force vector due to external forces, accelerations, gravity, etc.

The element matrices have been shown in figures 44-48.

$$\begin{bmatrix} \rho A\ell/3 & 0 & 0 & \rho A\ell/6 & 0 & 0 \\ 0 & \rho A\ell/3 & 0 & 0 & \rho A\ell/6 & 0 \\ 0 & 0 & \rho I_y\ell/3 & 0 & 0 & \rho I_y\ell/6 \\ \rho A\ell/6 & 0 & 0 & \rho A\ell/3 & 0 & 0 \\ 0 & \rho A\ell/6 & 0 & 0 & \rho A\ell/3 & 0 \\ 0 & 0 & \rho I_y\ell/6 & 0 & 0 & \rho I_y\ell/3 \end{bmatrix}$$

Figure 44. Planar Element Inertia Matrix

$$
\begin{bmatrix}
0 & -2\rho A\omega_b \ell/3 & 0 & 0 & -\rho A\omega_b \ell/3 & 0 \\
2\rho A\omega_b \ell/3 & 0 & 0 & 0 & \rho A\omega_b \ell/3 & 0 \\
0 & 0 & 0 & 0 & 0 & 0 \\
0 & -\rho A\omega_b \ell/3 & 0 & 0 & -2\rho A\omega_b \ell/3 & 0 \\
\rho A\omega_b \ell/3 & 0 & 0 & 2\rho A\omega_b \ell/3 & 0 & 0 \\
0 & 0 & 0 & 0 & 0 & 0
\end{bmatrix}
$$

Figure 45. Planar Element Coriolis Matrix

$$
\begin{bmatrix}
AE/\ell & 0 & 0 & -AE/\ell & 0 & 0 \\
0 & k_t A\Upsilon/\ell & k_t A\Upsilon/2 & 0 & -k_t A\Upsilon/\ell & k_t A\Upsilon/2 \\
0 & k_t A\Upsilon/2 & \begin{matrix} EI_y/\ell \\ + \\ k_t A\Upsilon\ell/4 \end{matrix} & 0 & -k_t A\Upsilon/2 & \begin{matrix} -EI_y/\ell \\ + \\ k_t A\Upsilon\ell/4 \end{matrix} \\
-AE/\ell & 0 & 0 & AE/\ell & 0 & 0 \\
0 & -k_t A\Upsilon/\ell & -k_t A\Upsilon/2 & 0 & k_t A\Upsilon/\ell & -k_t A\Upsilon/2 \\
0 & k_t A\Upsilon/2 & \begin{matrix} -EI_y/\ell \\ + \\ k_t A\Upsilon\ell/4 \end{matrix} & 0 & -k_t A\Upsilon/2 & \begin{matrix} EI_y/\ell \\ + \\ k_t A\Upsilon\ell/4 \end{matrix}
\end{bmatrix}
$$

Figure 46. Planar Element Conventional Stiffness Matrix

$$
\begin{bmatrix}
-\rho A \omega_b^2 \ell/3 & -\rho A \alpha_b \ell/3 & 0 & -\rho A \omega_b^2 \ell/6 & -\rho A \alpha_b \ell/6 & 0 \\
\rho A \alpha_b \ell/3 & -\rho A \omega_b^2 \ell/3 & 0 & \rho A \alpha_b \ell/6 & -\rho A \omega_b^2 \ell/6 & 0 \\
0 & 0 & 0 & 0 & 0 & 0 \\
-\rho A \omega_b^2 \ell/6 & -\rho A \alpha_b \ell/6 & 0 & -\rho A \omega_b^2 \ell/3 & -\rho A \alpha_b \ell/3 & 0 \\
\rho A \alpha_b \ell/6 & -\rho A \omega_b^2 \ell/6 & 0 & \rho A \alpha_b \ell/3 & -\rho A \omega_b^2 \ell/3 & 0 \\
0 & 0 & 0 & 0 & 0 & 0
\end{bmatrix}
$$

Figure 47. Planar Element Base-Motion Stiffness Matrix

$$
\left\{ \begin{array}{c}
\rho A\ell(\omega_b^2(2s_1+s_2)/6-a_{b_z}/2)+f_z\ell/2 \\
-\rho A\ell(\alpha_b(2s_1+s_2)/6+a_{b_x}/2)+f_x\ell/2 \\
-\rho I_y\alpha_b\ell/2 \\
\rho A\ell(\omega_b^2(s_1+2s_2)/6-a_{b_z}/2)+f_z\ell/2 \\
-\rho A\ell(\alpha_b(s_1+2s_2)/6+a_{b_x}/2)+f_x\ell/2 \\
-\rho I_y\alpha_b\ell/2
\end{array} \right\}
$$

Figure 48. Planar Element Force Vector

APPENDIX B

ELEMENT MATRICES FOR SPATIAL MANIPULATORS

APPENDIX B

ELEMENT MATRICES FOR SPATIAL MANIPULATORS

The elemental matrices for the case of spatial manipulators are easily defined using the following sub-matrices and vectors. Let us define:

$$[A]_{3X3} = \begin{bmatrix} A & 0 & 0 \\ 0 & A & 0 \\ 0 & 0 & A \end{bmatrix} \qquad [I]_{3X3} = \begin{bmatrix} I_{xx} & -I_{xy} & -I_{xz} \\ -I_{yx} & I_{yy} & -I_{yz} \\ -I_{zx} & -I_{zy} & I_{zz} \end{bmatrix}$$

$$[\omega_b]_{3X3} = \begin{bmatrix} 0 & \omega_{z_b} & -\omega_{y_b} \\ -\omega_{z_b} & 0 & \omega_{x_b} \\ \omega_{y_b} & -\omega_{x_b} & 0 \end{bmatrix} \qquad [\alpha_b]_{3X3} = \begin{bmatrix} 0 & \alpha_{z_b} & -\alpha_{y_b} \\ -\alpha_{z_b} & 0 & \alpha_{x_b} \\ \alpha_{y_b} & -\alpha_{x_b} & 0 \end{bmatrix}$$

$$[\Psi]_{3X3} = [\omega_b]\,[\omega_b] + [\alpha_b]$$

$$\{r_\omega\} = [r_{\omega_x} \quad r_{\omega_y} \quad r_{\omega_z}]^T = [I]\,\{\alpha_b\} + [\omega_b]\,[I]\,\{\omega_b\}$$

Let $[\Omega]_{3X3}$ be derived from:

$$[\Omega]\,\{\omega_r\} = [\,[I]\,[\omega_b] + [\omega_b]\,[I]\,]\,\{\omega_r\} + [\omega_r]\,[I]\,\{\omega_b\}$$

where, $\{\omega_r\}$ is the vector of angular deformational velocities.

Using the above definitions, the element matrices for the spatial manipulators are shown in figures 49-53.

$$
\begin{bmatrix}
(\rho\ell/3)[A]_{3X3} & [0]_{3X3} & (\rho\ell/6)[A]_{3X3} & [0]_{3X3} \\
[0]_{3X3} & (\rho\ell/3)[I]_{3X3} & [0]_{3X3} & (\rho\ell/6)[I]_{3X3} \\
(\rho\ell/6)[A]_{3X3} & [0]_{3X3} & (\rho\ell/3)[A]_{3X3} & [0]_{3X3} \\
[0]_{3X3} & (\rho\ell/6)[I]_{3X3} & [0]_{3X3} & (\rho\ell/3)[I]_{3X3}
\end{bmatrix}
$$

Figure 49. Spatial Element Inertia Matrix

$$
\begin{bmatrix}
(2\rho A\ell/3)[\omega_b]_{3X3} & [0]_{3X3} & (\rho A\ell/3)[\omega_b]_{3X3} & [0]_{3X3} \\
[0]_{3X3} & (\rho\ell/3)[\Omega]_{3X3} & [0]_{3X3} & (\rho\ell/6)[\Omega]_{3X3} \\
(\rho A\ell/3)[\omega_b]_{3X3} & [0]_{3X3} & (2\rho A\ell/3)[\omega_b]_{3X3} & [0]_{3X3} \\
[0]_{3X3} & (\rho\ell/6)[\Omega]_{3X3} & [0]_{3X3} & (\rho\ell/3)[\Omega]_{3X3}
\end{bmatrix}
$$

Figure 50. Spatial Element Coriolis Matrix

$$
\begin{bmatrix}
k_tA\gamma/\ell & 0 & 0 & 0 & k_tA\gamma/2 & 0 & -k_tA\gamma/\ell & 0 & 0 & 0 & k_tA\gamma/2 & 0 \\
0 & k_tA\gamma/\ell & 0 & -k_tA\gamma/2 & 0 & 0 & 0 & -k_tA\gamma/\ell & 0 & -k_tA\gamma/2 & 0 & 0 \\
0 & 0 & AE/\ell & 0 & 0 & 0 & 0 & 0 & -AE/\ell & 0 & 0 & 0 \\
0 & -k_tA\gamma/2 & 0 & \begin{matrix} EI_{xx}/\ell \\ + \\ k_tA\gamma\ell/4 \end{matrix} & 0 & 0 & 0 & k_tA\gamma/2 & 0 & \begin{matrix} -EI_{xx}/\ell \\ + \\ k_tA\gamma\ell/4 \end{matrix} & 0 & 0 \\
k_tA\gamma/2 & 0 & 0 & 0 & \begin{matrix} EI_{yy}/\ell \\ + \\ k_tA\gamma\ell/4 \end{matrix} & 0 & -k_tA\gamma/2 & 0 & 0 & 0 & \begin{matrix} -EI_{yy}/\ell \\ + \\ k_tA\gamma\ell/4 \end{matrix} & 0 \\
0 & 0 & 0 & 0 & 0 & \gamma I_{zz}/\ell & 0 & 0 & 0 & 0 & 0 & -\gamma I_{zz}/\ell \\
-k_tA\gamma/\ell & 0 & 0 & 0 & -k_tA\gamma/2 & 0 & k_tA\gamma/\ell & 0 & 0 & 0 & -k_tA\gamma/2 & 0 \\
0 & -k_tA\gamma/\ell & 0 & k_tA\gamma/2 & 0 & 0 & 0 & k_tA\gamma/\ell & 0 & k_tA\gamma/2 & 0 & 0 \\
0 & 0 & -AE/\ell & 0 & 0 & 0 & 0 & 0 & AE/\ell & 0 & 0 & 0 \\
0 & -k_tA\gamma/2 & 0 & \begin{matrix} -EI_{xx}/\ell \\ + \\ k_tA\gamma\ell/4 \end{matrix} & 0 & 0 & 0 & k_tA\gamma/2 & 0 & \begin{matrix} EI_{xx}/\ell \\ + \\ k_tA\gamma\ell/4 \end{matrix} & 0 & 0 \\
k_tA\gamma/2 & 0 & 0 & 0 & \begin{matrix} -EI_{yy}/\ell \\ + \\ k_tA\gamma\ell/4 \end{matrix} & 0 & -k_tA\gamma/2 & 0 & 0 & 0 & \begin{matrix} EI_{yy}/\ell \\ + \\ k_tA\gamma\ell/4 \end{matrix} & 0 \\
0 & 0 & 0 & 0 & 0 & -\gamma I_{zz}/\ell & 0 & 0 & 0 & 0 & 0 & \gamma I_{zz}/\ell
\end{bmatrix}
$$

Figure 51. Spatial Element Conventional Stiffness Matrix

$$
\begin{bmatrix}
(\rho A\ell/3)[\Psi]_{3X3} & [0]_{3X3} & (\rho A\ell/6)[\Psi]_{3X3} & [0]_{3X3} \\
[0]_{3X3} & [0]_{3X3} & [0]_{3X3} & [0]_{3X3} \\
(\rho A\ell/6)[\Psi]_{3X3} & [0]_{3X3} & (\rho A\ell/3)[\Psi]_{3X3} & [0]_{3X3} \\
[0]_{3X3} & [0]_{3X3} & [0]_{3X3} & [0]_{3X3}
\end{bmatrix}
$$

Figure 52. Spatial Element Base-Motion Stiffness Matrix

$$\left\{\begin{array}{c}
-\rho A\ell a_{b_x}/2 + f_x\ell/2 - \rho A\ell(2s_1+s_2)\Psi_{13}/6 \\
-\rho A\ell a_{b_y}/2 + f_y\ell/2 - \rho A\ell(2s_1+s_2)\Psi_{23}/6 \\
-\rho A\ell a_{b_z}/2 + f_z\ell/2 - \rho A\ell(2s_1+s_2)\Psi_{33}/6 \\
-\rho\ell r_{\omega_x}/2 \\
-\rho\ell r_{\omega_y}/2 \\
-\rho\ell r_{\omega_z}/2 \\
-\rho A\ell a_{b_x}/2 + f_x\ell/2 - \rho A\ell(s_1+2s_2)\Psi_{13}/6 \\
-\rho A\ell a_{b_y}/2 + f_y\ell/2 - \rho A\ell(s_1+2s_2)\Psi_{23}/6 \\
-\rho A\ell a_{b_z}/2 + f_z\ell/2 - \rho A\ell(s_1+2s_2)\Psi_{33}/6 \\
-\rho\ell r_{\omega_x}/2 \\
-\rho\ell r_{\omega_y}/2 \\
-\rho\ell r_{\omega_z}/2
\end{array}\right\}$$

Figure 53. Spatial Element Force Vector

APPENDIX C

FLEXIBLE LINK EXPERIMENT CONTROL PROGRAM

```
;============================================================
;       SOURCE CODE FOR FLEXIBLE LINK CONTROL PROGRAM
;    FOR STEPPER MOTOR CONTROL & STRAIN DATA COLLECTION
;                     ON APPLE-II PLUS
;============================================================
BUF      EQU   $0200          ;APPLE INPUT BUFFER
HMEMLO   EQU   $50            ;HIMEM_LO VALUE
HMEMHI   EQU   HMEMLO+1       ;HIMEM_HI VALUE
HIMEM    EQU   $F299          ;HIMEM_SETUP ROUTINE
SAVE     EQU   $FF4A          ;SAVE REGISTERS ROUTINE
RESTO    EQU   $FF3F          ;RESTORE REGISTERS ROUTINE
COUT1    EQU   $FDF0          ;OUT CHAR TO SCREEN
PRBYTE   EQU   $FDDA          ;PRINT 'A' AS HEX BYTE
PRNTAX   EQU   $F941          ;PRINT 'A' & 'X'
CROUT1   EQU   $FD8B          ;PRINT <CR> & CLEAR TO <EOL>
GETLN    EQU   $FD6A          ;GET AN INPUT LINE
RDKEY    EQU   $FD0C          ;READ THE KEYBOARD
KEYIN    EQU   $FD1B          ;DETECT KEYIN
HOME     EQU   $FC58          ;CLEAR SCREEN & HOME
AI13     EQU   $C0C0          ;A/D ADDRESS FOR SLOT 4
MOPORT   EQU   $C0B0          ;MOTOR PORT LOCATION
WAIT     EQU   $FCA8          ;APPLE'S WAIT ROUTINE
STORLO   EQU   $06            ;STORAGE ADDRESS
STORHI   EQU   STORLO+1       ;BYTES
RISRET   EQU   $08            ;RISE OR RETURN FLAG
ADGAIN   EQU   $09            ;A/D GAIN VALUE
ADSTOR   EQU   $19            ;UNUSED ON ZERO PAGE?
STPPTR   EQU   $1A            ;STEPPER TABLE POINTER
DLYADL   EQU   $D0            ;CURRENT DELAY VALUE
DLYADH   EQU   DLYADL+1       ;ADDRESS (INDIRECT)
DLYPLO   EQU   $FA            ;DELAY TABLE
DLYPHI   EQU   DLYPLO+1       ;POINTERS
;============================================================
         ORG   $9100
;============================================================
START    JMP   START1         ;START CODE EXECUTION HERE
START1   LDA   #>RESULT       ;AUTOMATICALLY SETS UP
         STA   HMEMLO         ;HIMEM DURING 'BRUN'
         LDA   #<RESULT
         STA   HMEMHI
         JSR   HIMEM
         LDA   #>BEGIN
         STA   START+1
         LDA   #<BEGIN
         STA   START+2
         RTS
STEPFU   DFB   $01,$02,$04,$08 ;FULL STEP PHASE VALUES
STEPHF   DFB   $0C,$08,$09,$01 ;HALF STEP PHASE VALUES
         DFB   $03,$02,$06,$04
STPTAB   DFB   $0C,$08,$09,$01 ;STEPPER TABLE HERE
         DFB   $03,$02,$06,$04
STPSIZ   DFB   $04             ;HALF OR FULL STEP FLAG
ADCHNL   DFB   $00             ;A/D CHANNEL VALUE
MAXTIM   DFB   $00             ;# OF SWEEPS
```

```
POSTRD  DFB    $F0              ;# OF POST-READINGS
;============================================================
BEGIN   EQU    *                ;MOTOR CONTROL CODE BEGINS
        JSR    SAVE             ;SAVE REGISTERS
        LDA    #$00             ;FREE MOTOR PHASES
        STA    MOPORT
        NOP
        JSR    HOME             ;CLEAR SCREEN
        LDA    #>LABEL1         ;LEGEND FOR A/D CHANNEL #
        STA    STORLO
        LDA    #<LABEL1
        STA    STORHI
        JSR    GETDAT           ;PROMPT & RETURN DATA IN 'A'
        STA    ADCHNL
        LDA    #>LABEL2         ;A/D GAIN
        STA    STORLO
        LDA    #<LABEL2
        STA    STORHI
        JSR    GETDAT           ;PROMPT & RETURN DATA IN 'A'
        STA    ADGAIN
        LDA    #$4C
        STA    STEPO1
        LDA    #>LABEL3         ;LEGEND FOR # PRINT-OUT
        STA    STORLO           ;OPTION
        LDA    #<LABEL3
        STA    STORHI
        JSR    GETCHR
        CMP    #$D9             ;IF YES
        BEQ    BEGIN1
        LDA    #$60
        STA    STEPO1
BEGIN1  LDA    #$04             ;HALF OR FULL STEP
        STA    STPSIZ
        TAX
BEGIN2  DEX
        CPX    #$FF
        BEQ    BEGIN3
        LDA    STEPFU,X
        STA    STPTAB,X
        JMP    BEGIN2
BEGIN3  LDA    #>LABEL4
        STA    STORLO
        LDA    #<LABEL4
        STA    STORHI
        JSR    GETCHR
        CMP    #$C8             ;IF = 'H'
        BNE    BEGIN5
        LDA    #$08
        STA    STPSIZ
        TAX
BEGIN4  DEX
        CPX    #$FF
        BEQ    BEGIN5
        LDA    STEPHF,X
```

```
         STA    STPTAB,X
         JMP    BEGIN4
BEGIN5   LDA    #>LABEL5       ;STORE A/D DATA?
         STA    STORLO
         LDA    #<LABEL5
         STA    STORHI
         LDA    #$01           ;DEFAULT IS TO STORE
         STA    ADSTOR
         JSR    GETCHR
         CMP    #$D9           ;IF YES?
         BEQ    BEGIN6
         DEC    ADSTOR
BEGIN6   LDA    #>LABEL6       ;MAX SWEEPS
         STA    STORLO
         LDA    #<LABEL6
         STA    STORHI
         JSR    GETDAT         ;PROMPT & RETURN DATA IN 'A'
         STA    MAXTIM
         LDA    ADSTOR
         BEQ    BEGIN7
         LDA    MAXTIM
         CMP    #$03           ;IF MAX SWEEPS > 2 ?
         BCC    BEGIN7
         LDA    #$02           ;RESET MAX SWEEPS = 2
         STA    MAXTIM
         LDA    #>LABE6A       ;MAX SWEEPS
         STA    STORLO
         LDA    #<LABE6A
         STA    STORHI
         JSR    PROMPT         ;MESSAGE FOR MAX VALUE
BEGIN7   LDA    #>LABEL7       ;MAX SWEEPS
         STA    STORLO
         LDA    #<LABEL7
         STA    STORHI
         JSR    GETDAT         ;PROMPT & RETURN DATA IN 'A'
         STA    POSTRD
         LDA    #>LABEL8       ;CONTINUE ?
         STA    STORLO
         LDA    #<LABEL8
         STA    STORHI
         JSR    PROMPT
         JSR    KEYIN          ;READ A KEY
         PHA
         JSR    CROUT1
         PLA
         CMP    #$9B           ;IF 'ESC'
         BEQ    QUIT           ;YES -- ABORT
         NOP
         NOP
         NOP
;=============================================================
RUNPRG   JSR    CLEAN          ;CLEAN STORAGE SPACE
         LDA    #>RESULT       ;INITIALIZE LOCATIONS
         STA    STORLO
```

```
         LDA    #<RESULT
         STA    STORHI          ;STARTING LOCATIONS FOR STORING RESULTS
         SEC                    ;FULL/HALF STEP PARAMETERS
         LDA    STPSIZ
         STA    TEMP1+1
         SBC    #$01
         STA    TEMP2+1
         LDA    #$01            ;SET TO RISE
         STA    RISRET          ;
         LDA    ADGAIN
         AND    #$0F
         ASL    A               ;MULTIPLY GAIN BY 16
         ASL    A
         ASL    A
         ASL    A
         CLC
         ADC    ADCHNL          ;ADD IT TO CHANNEL #
         STA    ADGAIN          ;VALUE TO POKE IN AI13
         LDA    #$FF            ;INITIALIZE POINTERS
         STA    STPPTR          ;STEPPER TABLE POINTER
         LDA    #$00            ;INITIALIZE POINTERS
         STA    DLYPLO          ;DELAY TABLE POINTER
         STA    DLYPHI
LOOP1    JSR    STEP            ;STEP THE MOTOR
         LDA    ADSTOR          ;IF READ A/D ?
         BEQ    SLEEP
         JSR    READAD          ;READ A-D & STORE
SLEEP    LDY    #$00
         LDA    (DLYADL),Y      ;CURRENT DELAY VALUE BYTE
         JSR    WAIT            ;APPLE'S WAIT ROUTINE
         LDA    MAXTIM          ;IF ALL SWEEPS DONE?
         BNE    LOOP1           ;NO --> GO & STEP
DMPOUT   LDA    #>RDONLY        ;READ DAMPENING VIBRATIONS
         STA    STORLO
         LDA    #<RDONLY
         STA    STORHI
LOOP2    LDA    #60             ;APP. 10 MILLISEC WAIT
         JSR    WAIT
         JSR    READAD          ;READ A-D & STORE
         DEC    POSTRD          ;CHECK # OF POST-READS
         BNE    LOOP2           ;IF 0, RETURN TO BASIC
QUIT     LDA    #>LABEL9        ;PAUSE TO FREE MOTOR
         STA    STORLO
         LDA    #<LABEL9
         STA    STORHI
         JSR    PROMPT
         JSR    KEYIN           ;READ A KEY
         JSR    CROUT1
         LDA    #$00            ;FREE THE MOTOR
         STA    MOPORT
         JMP    RESTO           ;RESTORE REGISTERS &
                                ;RETURN TO BASIC
;=============================================================
GETDAT   JSR    LEGEND
```

```
        LDA    STPPTR          ;GET DEFAULT VALUE
        CPX    #$FF
        BEQ    DATEND
        JSR    NUMBER
        STA    RISRET          ;USE 'RISRET' AS TEMPORARY
        DEX                    ;LOCATION
        CPX    #$FF
        BEQ    DATEND
        JSR    NUMBER
        ASL    A
        ASL    A
        ASL    A
        ASL    A
        ORA    RISRET
DATEND  RTS
;==============================================================
;CONVERTS AN ASCII INPUT TO A NUMERIC VALUE
NUMBER  LDA    BUF,X
        CMP    #$BA            ;IF <=9
        BCS    DATHEX          ;IF NOT, THEN HEX
        JMP    NUMEND
DATHEX  SEC
        SBC    #$B7
NUMEND  AND    #$0F
        RTS
;==============================================================
;PROMPT THE USER WITH THE TITLE
PROMPT  LDY    #$00
        LDA    (STORLO),Y
        STA    STPPTR          ;DEFAULT VALUE
        INY
PROMP1  LDA    (STORLO),Y
        CMP    #$C0            ;IF  '@' THEN QUIT
        BEQ    PROMP2
        JSR    COUT1           ;OUTPUT A CHARACTER
        INY
        JMP    PROMP1
PROMP2  RTS
;==============================================================
;CALL SUBROUTINE PROMPT,GET THE HEX DATA, & ISSUE <CR>
LEGEND  JSR    PROMPT
        LDA    #$A0            ;NORMAL SPACE AS CURSOR
        STA    $33
        JSR    GETLN
        DEX
        TXA
        PHA
        JSR    CROUT1
        PLA
        TAX
        RTS
;==============================================================
;PROMPT, GET A CHARACTER & DISPLAY
GETCHR  JSR    PROMPT
```

```
        JSR   RDKEY
        CMP   #$8D          ;IF = CR ?
        BNE   GETCH1
        LDA   STPPTR        ;IF <CR>, THEN DEFAULT VALUE
GETCH1  PHA
        JSR   COUT1
        JSR   CROUT1
        JSR   CROUT1
        PLA
        RTS
;===============================================================
;NULLS THE STORAGE LOCATIONS
CLEAN   LDY   #$00
        LDA   #>RESULT      ;USE STORAGE LOCATIONS
        STA   STORLO        ;FOR INDIRECT ADDRESSING
        LDA   #<RESULT
        STA   STORHI
CLEAN1  TYA
        STA   (STORLO),Y
        JSR   INCSTO
        LDA   STORHI
        CMP   #<MAXPLO
        BNE   CLEAN1
        LDA   STORLO
        CMP   #>MAXPLO
        BCC   CLEAN1
        RTS
;===============================================================
;STEP THE MOTOR AFTER CHECKING DIRECTIONS
STEP    LDA   RISRET        ;IF RISE OR RETURN?
        BEQ   RETUN1        ;IF 0, THEN RETURN
        LDA   DLYPHI        ;CHECK IF END OF RISE
        CMP   MAXPHI
        BCC   RISE1         ;IF < NOT YET AT THE END OF RISE
        LDA   DLYPLO        ;CHECK LOW BYTE
        CMP   MAXPLO
        BCC   RISE1         ;IF <, NOT YET
        LDA   #$00          ;IF END, REVERSE
        STA   RISRET        ;WITH CURRENT DELAY POINTER
        JMP   DRIVE1
RISE1   CLC                 ;IF RISE TO CONTINUE,
        LDA   DLYPLO        ;INCREMENT POINTER ON DELAY
        ADC   #$01          ;TABLE
        STA   DLYPLO
        BCC   RISE2
        INC   DLYPHI
RISE2   JMP   DRIVE1        ;& MOVE FORWARD
RETUN1  LDA   DLYPHI        ;WHERE AT REVERSE?
        BNE   RETUN2        ;THEN CONTINUE RETURN
        LDA   DLYPLO        ;CHECK IF END OF RETURN
        CMP   #$02
        BCS   RETUN2        ;NOT YET THERE
        DEC   MAXTIM        ;CHECK # OF SWEEPS
        BEQ   DONE          ;IF 0, NO MORE STEPPING
```

```
        LDA     #$01            ;OTHERWISE, RISE AGAIN
        STA     RISRET
        JMP     DRIVE1          ;START RISE WITH CURRENT PTR.
RETUN2  SEC                     ;DECREMENT DELAY POINTER
        LDA     DLYPLO
        SBC     #$01
        STA     DLYPLO
        BCS     DRIVE1
        DEC     DLYPHI
DRIVE1  CLC                     ;GET NEW DELAY VALUE ADDRESS
        LDA     #>DLYTAB        ;COMPUTE CURRENT DELAY
        ADC     DLYPLO          ;ADDRESS
        STA     DLYADL
        LDA     #<DLYTAB        ;HIGH BYTE
        ADC     DLYPHI
        STA     DLYADH
        LDX     STPPTR          ;PTR. TO STEPPER PHASE TABLE
        LDA     RISRET          ;IF FORWARD OR REVERSE ?
        BEQ     REVERS          ;IF 0, REVERSE
        INX                     ;MOVE UP IN THE TABLE
TEMP1   CPX     #$04            ;IF FORWARD, IF TABLE-END?
        BNE     STEPON          ;IF NOT, MOVE ON
        LDX     #$00            ;IF END OF TABLE, THEN RESET POINTER
        JMP     STEPON
REVERS  DEX                     ;DECREMENT SEQUENCE
        CPX     #$FF            ;IF BOTTOM OF TABLE?
        BNE     STEPON
TEMP2   LDX     #$03            ;RESET, IF NEEDED
STEPON  LDA     STPTAB,X
        STA     MOPORT          ;STEP THE MOTOR
        STX     STPPTR          ;SAVE CURRENT POINTER
STEPO1  JMP     DISPLY          ;PRINT DATA
DONE    RTS                     ;STEP DONE
;=============================================================
;DISPLAYS MAXTIM,RISRET,DLYPTR,DLYVAL,STPPTR,PHASE-VALUE
DISPLY  LDA     MAXTIM
        JSR     PRINT
        LDA     RISRET
        JSR     PRINT
        LDA     DLYPHI
        LDX     DLYPLO
        JSR     PRNTAX          ;PRINT DELAY POINTER (2 BYTES)
        JSR     PRINT1
        LDY     #$00
        LDA     (DLYADL),Y      ;DELAY VALUE
        JSR     PRINT
        LDA     STPPTR
        JSR     PRINT
        LDX     STPPTR
        LDA     STPTAB,X
        JSR     PRBYTE
        JMP     CROUT1
;=============================================================
;PRINT A BYTE & THEN SPACE
```

```
PRINT   JSR   PRBYTE
PRINT1  LDA   #$A0           ;PRINT A SPACE
        JMP   COUT1
;==============================================================
;READS A-D & STORES IN THE MEMORY USING POINTERS
READAD  LDA   ADGAIN         ;POKE VALUE IN AI13
        STA   AI13
        PHA                  ;DELAY    FOR CONVERSION
        LDY   #$00
        PLA
        LDA   AI13+1         ;HI-BYTE IN 'A'
        AND   #$0F           ;MASK OFF HIGH NIBBLE
        PHA                  ;SAVE HI-BYTE ON STACK
        LDA   AI13           ;LSB IN 'A'
        STA   (STORLO),Y     ;STORE LSB FIRST
        JSR   INCSTO         ;INCREMENT MEMORY LOCATION
        PLA                  ;RETRIEVE HI-BYTE FROM STACK
        STA   (STORLO),Y     ;SAVE HI-BYTE IN MEMORY
        JSR   INCSTO         ;UPDATE STORAGE FOR NEXT READING
READA1  RTS
;==============================================================
;INCREMENTS STORAGE LOCATIONS
INCSTO  CLC
        LDA   STORLO
        ADC   #$01
        STA   STORLO
        BCC   INCST1
        INC   STORHI
INCST1  LDY   #$00
        RTS
;==============================================================
MAXPLO  EQU   START-$0F00  ;ALLOCATE 15 PAGES
MAXPHI  EQU   MAXPLO+1
DLYTAB  EQU   MAXPHI+1
RDONLY  EQU   MAXPLO-$0200 ;2 PAGES FOR POST-READINGS
RESULT  EQU   RDONLY-$4000
;==============================================================
LABEL1  DFB   $00,$8D,$8D
        ASC   'A/D CHANNEL # --------------('
        DFB   $30
        ASC   ')-> $@'
LABEL2  DFB   $04
        ASC   'A/D GAIN    # --------------('
        DFB   $34
        ASC   ')-> $@'
LABEL3  ASC   'NOUTPUT PARAMETERS TO SCREEN (Y/'
        DFB   $0E
        ASC   ')   @'
LABEL4  ASC   'HHALF ('
        DFB   $08
        ASC   ') OR FULL (F) STEPPING  ?    @'
LABEL5  ASC   'NLIKE TO STORE A/D DATA ?    (Y/'
        DFB   $0E
        ASC   ')   @'
```

```
LABEL6  DFB    $0A
        ASC    'IF YOU CHOOSE TO STORE A/D DATA, THEN,'
        DFB    $8D
        ASC    'THE MAXIMUM # OF SWEEPS ALLOWED = $ 02'
        DFB    $8D,$8D
        ASC    'ENTER MAXIMUM # OF SWEEPS ('
        DFB    $24,$30,$01
        ASC    ')   $@'
LABE6A  DFB    $A0,$87
        ASC .  '*** (MAX SWEEPS = 2) ***'
        DFB    $8D,$8D,$C0
LABEL7  DFB    $01
        ASC    '# OF POST-READINGS (MAX=$FF) ('
        DFB    $24,$30,$31
        ASC    ')$@'
LABEL8  DFB    $A0,$8D
        ASC    'PRESS <RET> TO PROCEED / <ESC> TO ABORT@'
LABEL9  DFB    $A0,$8D
        ASC    'PRESS ANY KEY TO FREE MOTOR@'
```

2 copy

VITA

Ganapathy Naganathan

Candidate for the Degree of

Doctor of Philosophy

Thesis: NONLINEAR MODELING OF FLEXIBILITY EFFECTS IN MANIPULATOR DESIGN

Major Field: Engineering

Biographical:

Personal Data: Born in Kumbakonam, Tamil Nadu, India, May 4, 1956, the son of Mr. & Mrs. Ganapathy Sastri

Education: Received Bachelor of Engineering (Honours) in Mechanical Engineering from University of Madras, India in 1978; Master of Science in Mechanical & Industrial Engineering from Clarkson University (previously, Clarkson College of Technology), Potsdam, New York, U.S.A. in 1981; completed requirements for the Doctor of Philosophy degree at Oklahoma State University in December, 1986.

Professional Experience: Design Engineer, Ashok Leyland Motors, Madras, India, 1978-79; Graduate Teaching Assistant, Department of Mechanical & Industrial Engineering, Clarkson University, 1979-80; Graduate Research Associate, School of Mechanical & Aerospace Engineering, Oklahoma State University, 1981-86.